NMR STUDIES OF MEMBRANE ASSOCIATING PEPTIDES AND IMPLICATIONS IN AUTOTRANSPORTER FUNCTION

A Dissertation

by

GIRIDHAR SEKAR

Submitted to the Office of Graduate and Professional Studies of
Texas A&M University
in partial fulfillment of the requirements for the degree of

DOCTOR OF PHILOSOPHY

Chair of Committee,	Christian Hilty
Co-Chair of Committee,	Ryland Young
Committee Members,	Pingwei Li
	James Sacchettini
Head of Department,	Gregory Reinhart

December 2014

Major Subject: Biochemistry

ABSTRACT

Membrane associating peptides such as antimicrobial peptides and viral fusion peptides are involved in a diverse set of physiological processes. Their functions often require a change in the structure of the peptide, caused by interactions between the peptide and the biological membrane. This change in structure can be investigated in vitro, by performing circular dichroism (CD) and nuclear magnetic resonance (NMR) spectroscopy experiments with peptide solutions in membrane mimetic such as detergent micelles and in organic solvents. NalP is an outer membrane autotransporter protein from *N. meningitidis* that transports its serine protease passenger domain across the outer membrane of the cell. The secondary structure of a linker peptide from this protein was determined in an aqueous medium, in sodium dodecyl sulfate (SDS) detergent micelles and in trifluoroethanol (TFE). The peptide exhibits a random coiled secondary structure in the aqueous medium and has a partial helical character in SDS detergent micelles. In TFE, the peptide has an α-helical secondary structure, and this structure was determined by NMR spectroscopy. The difference in structure of the peptide in the detergent micelle and in the hydrophobic organic solvent, when compared to the aqueous medium, suggests that the linker might interact with the biological membrane during the protein transport event.

The stability of the α-helix formed by this peptide in TFE was determined by investigating the overall and residue specific effects of temperature on the secondary structure of the peptide. Partial loss of secondary structure is observed when the peptide is heated to a temperature of 348 K. Nuclear Overhauser Effect (NOE) crosspeaks that had high relative intensities at elevated temperatures were observed on a stretch of residues located in the middle of the α-helix, suggesting that this region of the α-helix is comparatively more stable and that the unfolding is initiated at both termini of the helix.

The effect of electrostatic interactions on thermally induced unfolding of charged helical peptides was determined in detergent micelles of different charge. In the presence of a similar charge on the peptide and the micelle, the antimicrobial peptide Magainin2 and a mutant of the viral fusion peptide HA G1V showed a greater curvature in the temperature dependence of CD signal at 222 nm, suggesting an increased co-operativity in the helix coil transition of the peptide. The residue specific effects of electrostatic interactions were also determined by measuring the temperature dependence of chemical shifts and NOE intensities of Magainin2 peptide in SDS and dodecylphosphocholine (DPC) detergent micelles.

DEDICATION

"Ancora Imparo."

Yet still I learn.

The human endeavor is driven by curiosity. If my desire to learn does not diminish with my age, I would consider that I have lived my life well. I dedicate this work to all the curious minds and the students of science who toil away into the night, pushing the boundaries of knowledge and grappling with the limits of feasibility, to unearth what is yet unknown.

ACKNOWLEDGMENTS

I thank my advisor, Dr. Christian Hilty for supporting me and guiding me at all stages of my graduate education. He has always shown the utmost concern for my welfare as a student and has been extremely patient with me, even at times when I have been difficult. I thank my co-chair Dr. Ryland Young and members of my committee Dr. Pingwei Li and Dr. James Sacchettini for their constructive input and discussion during all my committee meetings. I remember leaving many such meetings with new ideas and the motivation to try out new things in my research.

I thank my colleague and friend Mukundan Ragavan for the countless scientific discussions that we have had over the last few years. I particularly enjoyed talking not only about research, but also about the philosophy of research with him. He has also helped me with everything related to computers and has written some scripts for me that I have used in data processing. I thank other current and former members of the Hilty research group, I have learned a lot by merely observing some of your work. I thank Dr. Donghan Lee for his invaluable input in the NalP project. I thank former undergraduate students Bianca Coria and Chris Berger who worked on the thermal denaturation of NalP linker peptide and the thermal denaturation of magainin2 projects, some of their work has been reported in this thesis. I would also like to thank other undergraduate student workers who have collectively put in many fruitless hours into the NalP autotransporter project. While their work did not give us any publishable results, I really appreciate the effort they put in. I thank my chemistry teacher Ms. Padmini Iyer and my biology teacher Mrs. Visalam Vivekanandan from my high-school. I am very grateful that they were keen on educating me rather than preparing me to attend an exam. They were the first teachers that motivated me to pursue a career in science.

I thank my mother, who once asked me if I thought I would win the Nobel prize and I am often driven only by the faith that she has in me. I thank my father who has always put every need of mine in front of his own, and I realize today how much courage this takes. In doing so he has become my greatest hero and inspiration. I would like to thank my little sister, who has grown up so fast. She is very supportive of my ambitions, but I sometimes wish we could get back to being kids and fight over ice-cream. I would like to thank my late grandmother, to whose iron willed effort I owe every fiber of health in my body. I would also like to thank all my friends, but I think they all would prefer that I throw them a good party rather than waste my words here.

TABLE OF CONTENTS

Page

LIST OF FIGURES

FIGURE Page

LIST OF TABLES

1. INTRODUCTION

Membrane proteins constitute about 20-30% of cellular proteins and have diverse functions in the cell including physiologically important processes such as signal transduction, respiration, photosynthesis, transport [1, 2]. 60-70% of drug targets are estimated to be membrane proteins [3, 4]. Despite their importance, the number of known structures of transmembrane proteins is very limited when compared to soluble proteins. At the date of writing this manuscript, 2.5% of high resolution protein structures from the Protein Data Bank (PDB) belong to integral membrane or membrane associated proteins [5]. The challenge in performing in vitro biochemical studies with membrane proteins and solving their structures stems from their poor solubility in aqueous media. Obtaining soluble protein of high concentration is a requisite for crystallization of the proteins for X-ray crystallography or structure determination by NMR spectroscopy.

While it is possible to solubilize these proteins in denaturing conditions, such as in the presence of high concentrations of chaotropic agents like urea or guanidium hydrochloride, this approach is limited in its utility because the native fold of the protein is not preserved under these conditions. Common approaches to get soluble proteins having native folds for biochemical experiments include using ordered lipid structures, such as detergent micelles, bicelles, vesicles and liposomes, or alternatively using organic solvents or chaotropes under partially denaturing conditions [6, 7, 8, 9, 10, 11]. The strategies for obtaining soluble protein still largely is based on a trial and error approach and acts as a bottle neck for progress in this field.

An important method for observation of membrane proteins and membrane associating peptides in solution is NMR spectroscopy. Structures of membrane proteins and peptides can be determined to atomic resolution using NMR. It is additionally possible to study in-

teractions of the target macromolecule with the ordered lipid structures, orientation of the macromolecule and chemical exchange between different conformations or states. While membrane proteins are interesting targets to study using NMR spectroscopy, the quality of data obtained from NMR experiments depends on the size of the molecule. Larger proteins have more resonances which overlap in the NMR spectra and it is challenging to resolve and assign these resonances unambiguously. The larger size also increases the correlation time of the protein in solution leading to broader lines in spectra and detrimental effects from spin diffusion. An additional strategy to investigate a membrane protein, is to observe a peptide which is a part of a larger protein, in isolation [12]. Viral fusion peptides and isolated transmembrane α-helices from integral membrane protein existing as helical bundles, have been studied by this approach [12, 13, 14, 15]. The use of small peptides is advantageous because the smaller peptides are easier to solubilize in organic solvents and detergent micelles, while preserving their secondary structure, when compared to larger proteins. Using this approach, it is often possible to determine processes that may be relevant to the biochemical function of the full length protein. Similar molecules that are also of intrinsic biochemical interest are peptides that associate with the membrane, such as antimicrobial peptides and cell penetrating peptides.

The subsequent portions of this chapter give a general description of the different structural and biochemical aspects of membrane proteins and membrane associating peptides, including the ones studied in this manuscript. A description of NMR methods to study these systems is also provided.

In chapter 2, a small linker peptide which is found in the autotransporter protein NalP from *Neisseria meningitidis* is observed in isolation. The structure of the peptide in an aqueous medium, a detergent micelle and an organic solvent are determined using circular dichroism (CD) and NMR spectroscopy. The linker peptide shows different structure in each medium and the observations are used as a basis to suggest a role for the linker region

in the transport function exhibited by the full length autotransporter.

In chapter 3, the linker peptide from NalP in the organic solvent 2,2,2-trifluoroethanol (TFE) is subject to a thermally induced unfolding. The overall and residue specific loss of secondary structure are observed by CD and NMR spectroscopy.

In chapter 4, the antimicrobial peptide magainin2 and a mutant of a viral fusion peptide HA G1V are observed in detergent micelles of differing charges using CD and NMR spectroscopy. The overall and residue-specific effects of the electrostatic interactions upon thermal denaturation of the peptide is investigated.

1.1 Structural Motifs in Transmembrane Proteins

Membrane proteins perform many physiologically important functions, including signal transduction, respiration, cell adhesion and other enzymatic functions. Apart from the interest generated by their physiological importance, it is of additional interest to study the determinants of folding in membrane associating proteins. The interactions that affect protein folding in the membrane are expected to be different from that of soluble proteins due to the hydrophobic nature of the biological membrane. For example, hydrophobic interactions in the core of the protein which are believed to be critical to the stability of soluble proteins may not have as significant a role in membrane proteins. Instead interactions among polar residues and strong inter-helical hydrogen bonds are believed to play a larger role in the structures of these proteins [16, 17].

The fold of transmembrane proteins can be classified under two main categories. Proteins with α-helical bundles are found on the plasma membrane and the endoplasmic reticulum [18]. β-barrel proteins are predominantly found in the outer membrane of Gram negative bacteria and the membranes of the mitochondria and the chloroplast [19, 20]. Members of each family of membrane protein, despite having varied functions, are unified by many conserved structural themes.

1.2 Structural Themes in β-barrel Proteins of the Outer Membrane

In bacteria, membrane associated β-barrels are found on the outer membrane. The outer membrane of Gram negative bacteria is different from the inner membrane in its composition. While the inner membrane is symmetric and is composed of phospholipids, the outer membrane is asymmetric. The inner leaf is composed of phospholipids and the outer leaf contains lipopolysaccharides [21]. β-barrel outer membrane proteins (OMPs) fall under a variety of functional families including adhesins, peptidases, autotransporters, general and substrate specific porins. Structures for many β-barrel proteins have been solved using X-ray crystallography and NMR spectroscopy. In Table 1.1, some representative β-barrel proteins, covering different sizes and functions, for which structures have been solved are listed.

The β-barrel motif consists of an anti-parallel β-sheet wrapped around in the shape of a cylinder. Known proteins of this family have between 8 and 22 β-strands and the number of strands in most cases is an even number. The first and last strands of the barrel are anti-parallel and both termini of the folded protein are on the periplasmic side of the membrane [20, 19]. A notable exception are the VDAC family of proteins from mammalian mitochondria. These proteins are reported to have 19 β-strands and the interface of the first and last strands is parallel [22, 23, 24]. In mammalian β-barrels, the protein synthesis happens in the cytoplasm and the polypeptide is delivered from the exterior surface of the membrane bound organelle.

The β-strands of OMPs are typically rich in glycine and have alternating hydrophobic and hydrophilic residues [25]. The hydrophobic residues face outwards into the membrane bilayer and the hydrophilic residues face the interior of the β-barrel. Thee rim of the barrel, which is located in the interface of the lipid bilayer is rich in tryptophan and tyrosine residues [26]. The aromatic residues present in the β-barrel fold into 2 girdle like structures

Table 1.1: List of outer membrane proteins discussed in this chapter.

Name	**Organism**	**Strands**	**PDB-ID**	**Function**
OmpX	*E. coli*	8	1QJ8	Binding targets in host defense
OmpA	*E. coli*	8	1QJP	Structural protein
OmpW	*E. coli*	8	2F1V	Putative transporter of small hydrophobic molecules
NspA	*N. meningitidis*	8	1P4T	Adhesin
OmpT	*E. coli*	10	1I78	Protease
OMPLA	*E. coli*	10	1QD6	Phospholipase
OpcA	*N. meningitidis*	10	1K24	Adhesin
OmpG	*E. coli*	14	2F1C	General porin
Tsx	*E. coli*	12	1TLY	Substrate specific porin
FadL	*E. coli*	14	1T16	Substrate specific porin
OmpF	*E. coli*	16	2OMF	General porin
OmpC	*E. coli*	16	2J1N	General porin
PhoE	*E. coli*	16	1PHO	General porin
LamB	*E. coli*	18	1MAL	Substrate specific porin for maltose
Maltoporin	*S. thyphimurium*	18	2MPR	Substrate specific porin for maltose
BtuB	*E. coli*	22	1NQE	TonB dependent cobalamin transporter
FhuA	*E. coli*	22	2FCP	TonB dependent iron transporter
FepA	*E. coli*	22	1FEP	TonB dependent iron transporter
FecA	*E. coli*	22	1KMO	TonB dependent iron transporter

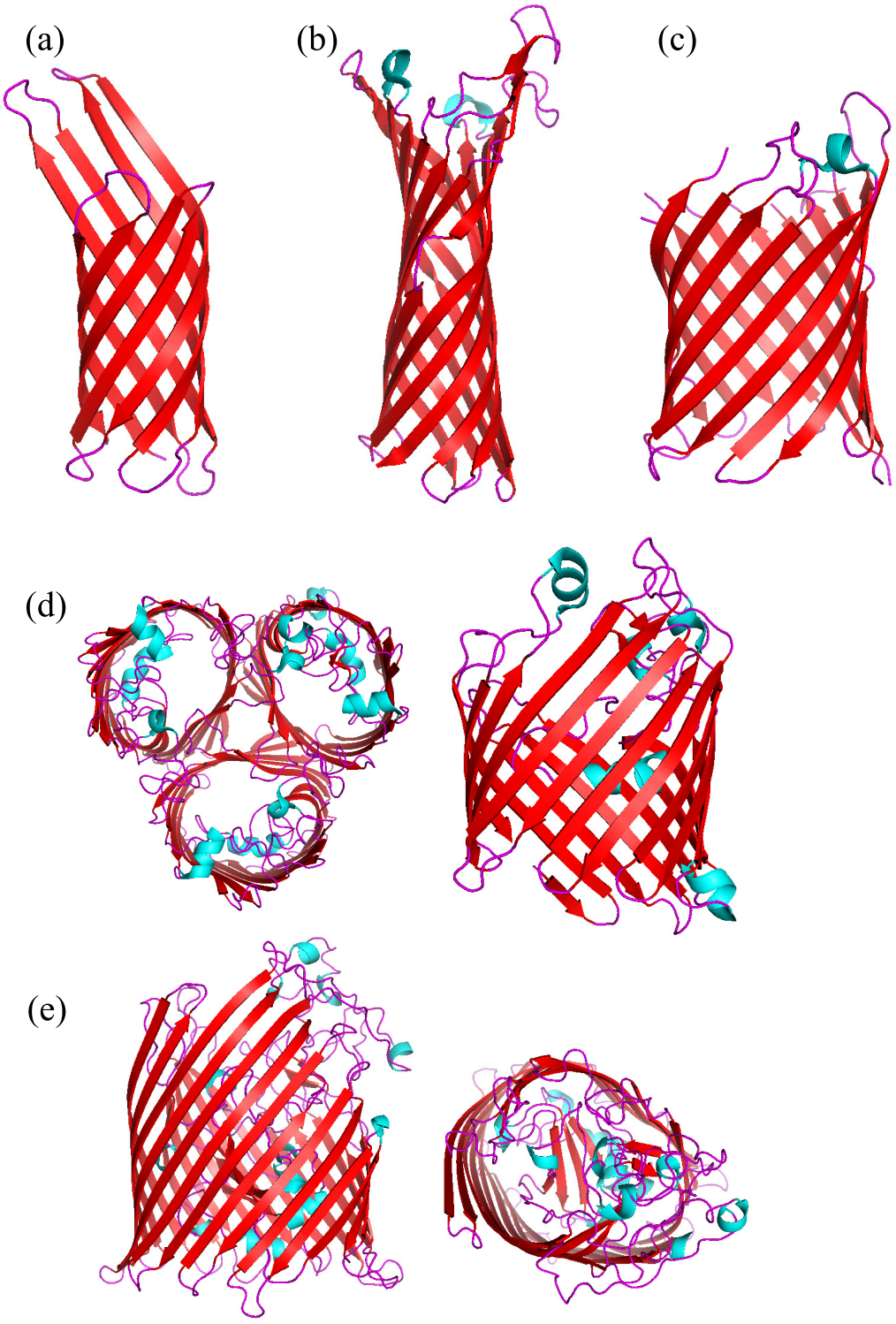

Figure 1.1: The structures of a) OmpX, b) OmpW, c) OmpT, d) OmpC e) FhuA are shown. The PDB ID of the structures are as shown in Table 1.1. Figures are rendered such that the extracellular side of the protein is in the top and the periplasmic side is in the bottom

and contribute strongly to the stability of the barrel [27]. In the periplasmic side, the strands of the β-barrel are joined by tight turns. In the extracellular end they are joined loops that are longer in comparison, as seen in the structure of OmpX (Figure 1.1 a) [28, 29]. In some OMPs, like in the outer membrane protease OmpT (Figure 1.1 b), a β-sheet structure is formed that extends far above the lipid head groups in the extracellular side of the barrel. This extended sheet structure acts as the catalytic site of the protein [30].

The β-barrels of OMPs are distinctly from those found in soluble proteins in the feature that the β-barrels of soluble proteins have a closely packed hydrophobic core and typically have lesser number of strands in the barrel. On the other hand, the interiors of OMP β-barrels, even in the ones that do not have a continuous pore, are predominantly hydrophilic in nature [31]. The barrel interior exists in many different configurations. In small OMPs such as OmpX (Figure 1.1 a), the interior of the barrel is hydrophilic but not large enough to form a continuous pore. The interior of the barrels formed by these proteins have been described to have pockets of water and a network of ionic interactions and hydrogen bonds. In larger OMPs like the monomeric porin OmpG (Figure 1.1c) and the trimeric porin OmpC (Figure 1.1d) from *E. coli*, a larger pore is present. They form pores of about 15 Å and 20 Å respectively and enable the permeation of molecules through these pores. OmpG non-specifically transports small sugar molecules [32] and OmpC preferentially transports cations. In the large 22 stranded TonB-dependent transporters like FhuA (Figure 1.1e), a globular N-terminal domain plugs the pore of the β-barrel. This plug is rigidly held in the interior with many hydrogen bonds and salt bridges [33].

1.3 Type V_a Autotransporters

Protein transport across the biological membrane is a ubiquitous event in Gram negative bacteria. The ability to present proteins on the extracellular surface and to secrete them is relevant to the lifestyle and pathogenicity of the bacteria. Concomitant to this,

a large number of secreted proteins in bacteria are important markers of pathogenicity [34]. In Gram negative bacteria, the process of secreting a protein involves traversing both the inner and the outer membranes. Bacteria have evolved a diverse set of pathways (Types I-VIII, and additionally the chaperone-usher pathway) to accomplish this process [35]. Seemingly the most minimal of these systems is the type V autotransporter. Type V autotransporters were initially termed as such because it was believed (a notion that is no longer considered accurate) that they were independently capable of transporting a passenger domain across the outer membrane. Type V autotransporters are categorized into 3 groups, the type V_a, V_b and V_c autotransporters. Type V_b autotransporters are the two-partner systems such as TpsB from *N. meningitidis* and Type V_c are the trimeric autotransporters such as the Hia from *H. influenzae* [36]. For the sake of relevance, these two groups are not covered in detail here. The type V_a autotransporter is considered to be the classical autotransporter and the term 'autotransporter' is used in this document to refer to this category of proteins.

The autotransporter protein has an N-terminal signal sequence and a soluble passenger domain that is transported across the membrane. The C-terminal translocator domain, which forms a β-barrel, is essential for transport of the passenger domain across the outer membrane. The mechanism of autotransporter function is poorly described [37].

1.3.1 Structure of Autotransporter Domains

The C-terminal domain of the autotransporter protein is called the translocator domain and it folds into a β-barrel. The first high resolution structure determined for the translocator domain of an autotransporter was that of NalP from *N. meningitidis* [38]. Subsequently, the structures of the translocator domains of EspP [39] and Hbp from *E. coli* [40] and BrkA from *B. pertussis* [41] were solved. Additionally, the structure of the full length autotransporter EstA from *P. aeruginosa* has been determined [42]. Despite low sequence

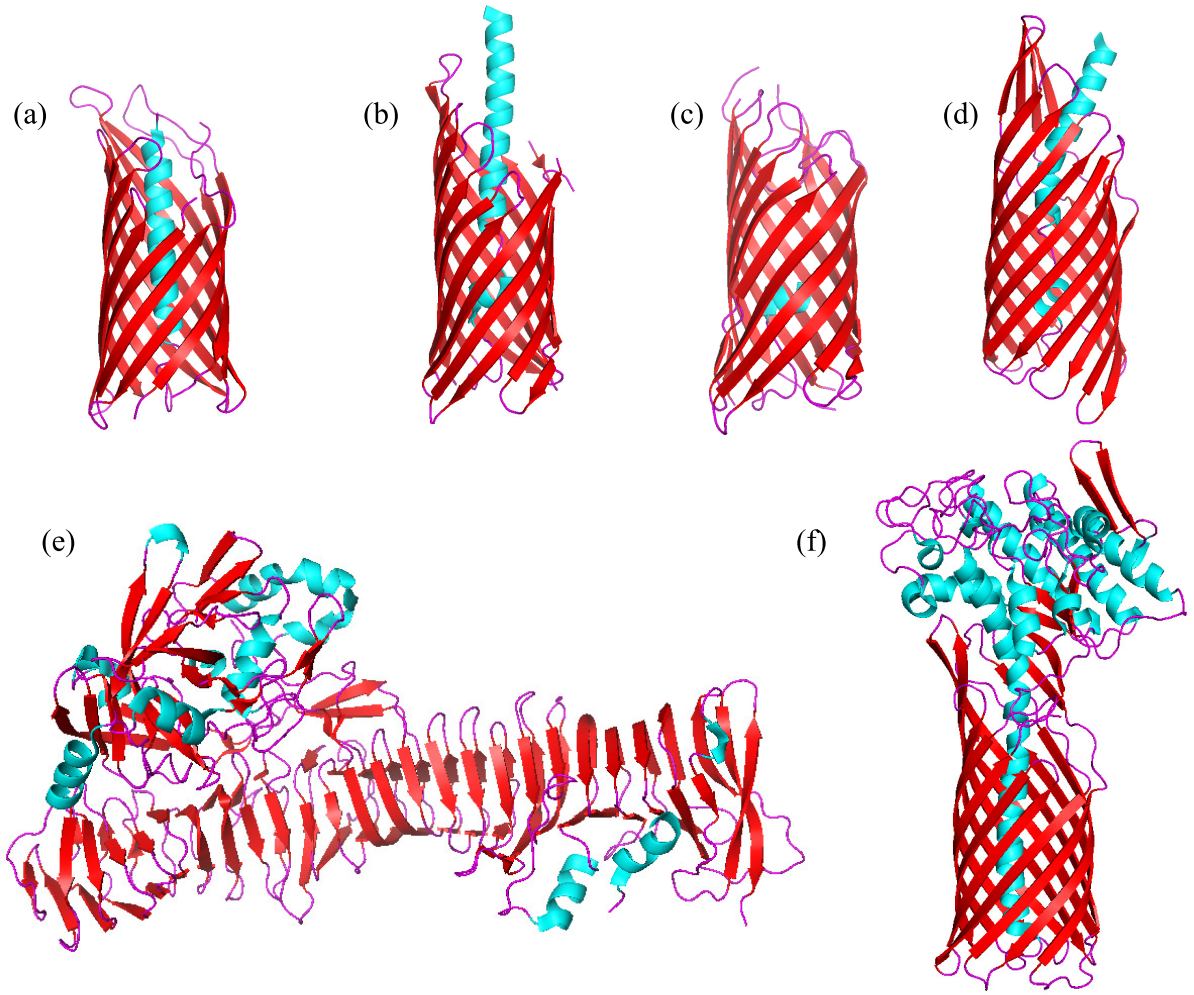

Figure 1.2: The structures of the translocator domains of a) NalP , b) Hbp, c) EspP, d) EspP N1023A, e) passenger domain of EspP, and f) full length EstA. The PDB ID of the structures are as shown in Table 1.2.

Table 1.2: Restricted list of structures solved for different functional domains of autotransporter proteins.

Name	Organism	PDB-ID
Translocator Domain		
NalP	*N. meningitidis*	1UYN
EspP	*E. coli*	2QOM
EspP (N1023A)	*E. coli*	3SLJ
BrkA	*B. pertussis*	3QQ2
Hbp (N1191D)	*E. coli*	3AEH
Passenger Domain		
EspP	*E. coli*	3SZE
Pet	*E. coli*	4OM9
Pertactin	*B. pertussis*	1DAB
VacA	*H. pylori*	2QV3
Hap	*H. influenzae*	3SYJ
IgaP	*H. influenzae*	3H09
Full length		
EstA	*P. aeruginosa*	3KVN

similarity, the size and shape of β-barrel domains are comparable. A list of autotransporter domains for which have been determined are listed in Table 1.2, and representative structures for the proteins discussed are given in Figure 1.2. In all these structures, the β-barrel is composed of 12 anti-parallel strands and has a pore of $\sim$12 Å diameter. Like in the other smaller OMPs, the periplasmic side exhibits tight turns whereas the extracellular side has long turns. The β-strands are variable in length and may contain approximately between 10 and 25 residues. The height of the β-barrel is $\sim$70 Å which is only slightly larger than the thickness of the bacterial membrane.

The presence of an even number of strands implies that the N and the C termini of the barrel would face the periplasmic side of the membrane. This arrangement presents a topological challenge, given that the passenger domain is to be presented in the extracellular side of the membrane. In all known autotransporters, immediately upstream to the

translocator domain is a linker region that connects the β-barrel to the passenger domain of the autotransporter. In the crystal structures of various autotransporters, this linker is located in the pore of the barrel. This configuration would enable presenting the passenger domain on the extracellular surface. In NalP, the linker region is an α-helix that is 30 residues long. The construct containing the linker and the β-barrel is believed to represent the autotransporter after cleavage of the passenger domain has occurred. In EspP, the crystal structure (PDB ID: 2QOM) represents the post cleavage state of the autotransporter [43]. In this structure, the linker region retained after cleavage is much smaller than in NalP and is only 15 residues long. The linker is folded as a single turn of a helix and is tilted such that it is almost perpendicular to the axis of the barrel (Figure 1.2 c). A structure has also been solved for the N1023A mutant of EspP which is cleavage resistant (PDB ID: 3SLJ) [43]. The construct used in the crystal structure determination, contains 25 additional residues from the passenger domain in the N-terminus of the translocator domain. This additional region is folded as an α-helix and extends outwards towards the extracellular side from the pore of the barrel (Figure 1.2 d). The crystal structure has been reported for a cleavage resistant N1191D mutant of the Hbp autotransporter [40]. The crystal structure of this mutant is similar to that of EspP N1023A. The difference between the two structures is that the helix from the passenger domain in the EspP is kinked and is tilted with respect to the axis of the β-barrel, whereas in Hbp, the helix from the passenger domain is nearly parallel to the axis of the barrel. The secretion of the passenger domain is affected by mutations to the linker region [44].

The structure of the β-barrels of these monomeric autotransporters is also comparable to that of the trimeric autotransporer Hia [41]. Like in the monomeric autotransporters, Hia forms a barrel of 12 anti-parallel β-strands. In this case, 4 strands are contributed by each monomer. There are three helices, one contributed by each monomer, that are located in the central pore of the β-barrel and the pore diameter is comparable to that of

the monomeric autotransporters.

The passenger domains of autotransporters vary more in their size when compared to the translocator domains, but they have some common features in their structures. Crystal structures have been determined for the passenger domains of various autotransporters including those of EspP [45], Hbp and Pet from *E. coli* [46, 47], pertactin from *B. pertussis* [48], VacA from *H. pylori* [49], Hap and IgaP from *H. influenzae* [50, 51]. These soluble domains range between 45-110 kDa, but they all have a characteristic right handed β-helix structure (Figure 1.2 e). The β-helix is constituted of many parallel β-sheets that form a curved β helix spine. In IgaP and pertactin, the β-helix is made up of three distinct β-sheets. In the larger passenger domains such as Hbp, IgaP some additional loop and helical regions exist in N-terminus and they act as the enzymatically active domain of the protein [51, 52].

A crystal structure has also been determined for the full length autotransporter EstA from *P. aeruginosa* (Figure 1.2 f). The β-barrel domain of the protein is very similar to that found in the other autotransporters described above. The pore of the barrel is traversed by a long curved helix that links the passenger domain in the extracellular region to the barrel. The passenger domain of EstA is unusually small compared to that of other autotransporters and it does not have the long β-helix spine that is found in the other autotransporter proteins. Instead in this protein there is small single parallel β-sheet located in the center of the domain. The structure of EstA represents the final folded conformation of the autotransporter. The structure establishes that the linker helix of the autotransporter is indeed located inside the β-barrel in its final folded state and that the interior of the barrel is likely to be the conduit for the transport process.

1.3.2 Models for Autotransporter Function

After translation of the protein in the ribosome, the autotransporter is translocated across the inner membrane in to the periplasm. A cleavable signal sequence in the N-terminus of the autotransporter enables the transport across the inner membrane using the SecYEG translocon. The signal peptide which is typically about 30 residues long and has a cationic N-terminus. The C terminus of the signal peptide acts as the recognition sequence for the signal peptidase that cleaves this signal peptide. The middle of the signal peptide is hydrophobic and it is believed that this part of the peptide interacts with the cell membrane to enable the recruitment of the translocon machinery [53]. Once the autotransporer is secreted across the inner membrane, it interacts with periplasmic chaperones. The binding of periplasmic chaperones SurA and DegP to both the translocator and passenger domains of EspP has been demonstrated using surface plasmon resonance analysis [54]. DegP not only binds the unfolded OMP in the periplasm, but also acts as a protease to degrade modified or misfolded autotransporters that are incapable of insertion into the outer membrane [55].

Multiple models have been proposed to describe the transport process in autotransporters. Some of these models have gained disfavor over time due to subsequent discoveries. The multimer model (Figure 1.3 a), which suggests a large pore formed by multimerization of the β-barrel on the membrane [56] is no longer favored because as the number of identified autotransporters increased, it was observed that many of these proteins do not have any identified multimeric states. Among the earlier models, the secretion function of autotransporters was described using the threading (Figure 1.3 b)and the hairpin threading models (Figure 1.3 c) [57, 58, 59]. The threading model suggests that the passenger domain is threaded into the pore such that the N-terminal is transported first through the pore of the barrel. On the other hand, the hairpin threading model suggests that the transport

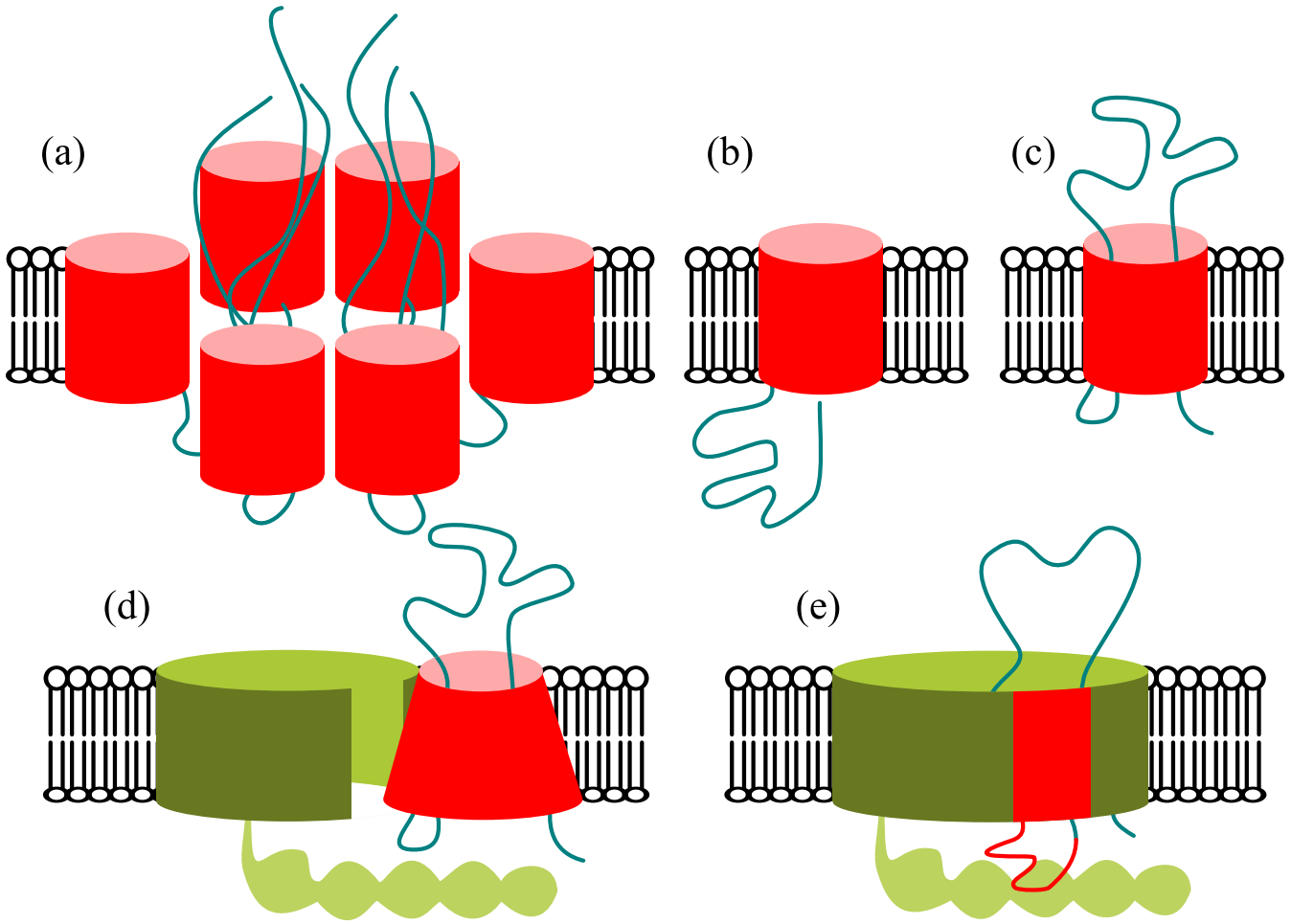

Figure 1.3: Models to describe autotransporter functions a) threading model, b) hairpin threading model, c) multimer model, d) Omp85 associated concerted folding model, and e) Omp85 associated hybrid barrel model.

is initiated from the C-terminus of the passenger domain and proceeding such that the N-terminus is the last part to exit the pore of the barrel. These two models have subsequently been improved, with subtle but important changes being proposed to the model.

Initial versions of these models were proposed with the passenger domain being fully unfolded and in an extended configuration because the size of the pore of the β-barrel is only $\sim$12 Å. The passenger would have to be fully unfolded to be able to fit into the pore of the fully formed β-barrel. However, it was later shown that recombinant autotransporters, with passenger domains composed of antibody fragments that were expected to be fully folded, were capable of efficient transport of their cargo [56]. In EspP, cysteine mutants were used to create small loops in the passenger domain. The efficiency of the transport process was not affected significantly by these structures. But introduction of larger loops resulted in a reduction in efficiency of the transport process. Intolerance to folded structure was demonstrated in a hybrid autotransporter where one domain of the passenger was replaced with calmodulin. The folded state of calmodulin was controlled by the changing the concentration of Ca^{2+} in solution. It was demonstrated that in the presence of a calcium chelator, there was efficient secretion of the passenger domain, whereas the presence of Ca^{2+} in solution eliminated the secretion process [55]. These observations suggest that there is a limited tolerance for folded structures in the passenger domain during the transport process. The size of these folded structures would be incompatible with transport through the pore of the β-barrel if the barrel was fully folded. Thus the simple threading and hairpin models, where the β-barrel is fully folded prior to translocation, are unlikely to be correct. It is still possible that the interior of the β-barrel is the conduit for transport, provided the transport occurs when the β-barrel is not in its final folded state.

More recent models favor a simultaneous mechanism where the folding of the barrel and the transport of the passenger domain occurring at the same time [60, 61]. Corroborating this view, the diameter of the active translocation pore of Hbp autotransporter was

measured to be $\sim$1.7 nm which is much larger than the pore size of about $\sim$1.2 nm in the folded β-barrel domain of the autotransporter [62]. Also an it was demonstrated that mutants of Hbp, that stalled during translocation event, copurified along with the membrane chaperone Bam (Omp85) [60]. Currently favored models of autotransporter function suggest that the folding and transport process occur in a concerted fashion and that the process is mediated by Omp85 (Figure 1.3 d and e) or equivalent membrane chaperones to be critical to the transport process [63].

One additional aspect of interest in autotransporter function is that the energetic driving force for the transport process has not been established yet. The outer membrane does not have an ion-gradient, and the periplasm does not have any significant concentration of ATP. One theory is that the energy for the process comes from the folding of the large β-helix spine of the passenger domain [64, 65, 66]. It has been demonstrated using mutants of pertactin that form stalled intermediates, that the C-terminus gets transported across the outer membrane first, followed by the N-terminus [66]. Based on this observation it has been suggested that the folding of the passenger domain happens in a vectorial fashion and that this directionality is required for successful transport of the domain. However, mutations that severely affect the folding of the β-helix spine of the passenger domain only affect the secretion efficiency moderately [67]. This leads to the counter argument that while the free energy from the folding of the passenger domain can add to the efficiency of the transport process, the primary energetic driving force is derived from elsewhere.

1.3.3 Assembly of OMPs and Autotransporters

Smaller β-barrel proteins assemble readily into membrane mimetics such as detergent micelles in vitro. Initial protocols for preparation of β-barrel proteins involved the expression of the protein without the signal sequence. Protein expressed in this fashion form inclusion bodies. The protein is unfolded from the inclusion bodies using denaturants

such as urea or guanidium hydrochloride and is folded by rapid dilution into a solution containing detergent micelles [68, 19]. While, in vivo, it is expected that the assembly of β-barrels and autotransporters is assisted by Omp85 and related membrane chaperones, a description of their in vitro folding is still useful.

In the presence of 8 M urea or 6 M guanidium hydrochloride, β-barrel proteins do not possess a global fold, but retain some residual non-random structure. In OmpX, two such hydrophobic clusters were identified with local structure. These clusters were situated around the two tryptophan residues in the protein [69]. Mutation of these tryptophan residues causes a loss of the local residual structure of the hydrophobic cluster. In OmpX, the loss of residual structure by mutation in one cluster does not alter the other one significantly, suggesting an absence of tertiary interactions. However, it is possible that such tertiary interactions exist in other OMPs. These hydrophobic clusters also interacted specifically with detergent micelles at concentrations above the critical micelle concentration. These hydrophobic clusters have been suggested to be putative sites for initial contact with the biological membrane [70].

The in vitro assembly of β-barrel proteins into membranes is reviewed by Tamm et al. [71, 72]. Folding intermediates in the assembly of OmpA were identified using time-resolved distance determination by tryptophan fluorescence quenching method [73]. The method detects the fluorescence signal from tryptophan residues as they go from the solution into the membrane. The position of the tryptophan with respect to the membrane is determined by quenching of fluorescence signals by quenchers located at different depths in the bilayer. Using this method kinetically resolved intermediates were identified for the in vitro folding of OmpA. It was found in OmpA that the individual β-hairpins traverse the membrane at similar rates leading to a concerted model of β-barrel formation, where the hydrogen bonds that determine the formation of the β-sheet occur as the protein is inserted into the membrane [74] [75]. In this model, the unfolded state (Figure 1.4 a) undergoes

hydrophobic collapse to form a collapsed intermediate (Figure 1.4 b). The collapsed intermediate localizes to the surface of the membrane to form an intermediate where the reporter tryptophan residues are still not ordered, possibly because the intermediate does not have a well defined β-sheet secondary structure. The intermediate has been described as a molten disk at this stage (Figure 1.4 c). From this stage, the protein proceeds to a molten globule state (Figure 1.4 d), which is characterized by further penetration into the membrane all the way to the center of the lipid bilayer. In the molten globule state, some secondary structure is believed to be formed already. Long range tertiary contacts are still not observed at this stage. Finally, the protein is folded into the native state that has fully formed tertiary contacts (Figure 1.4 d). At this stage, the tryptophan residues have been measured to be located $\sim$10Å from the center of the lipid bilayer and this position agrees with their position in the crystal structure of the folded protein. While this model is applicable for small OMPs like OmpX and OmpA, the larger β-barrel like that of NalP or EspP can possibly have further complications. For example, the position of the linker peptide is not defined during the membrane insertion process. It is not established whether the linker region of the autotransporter interacts with the membrane in the initial stages of barrel formation. It would also be relevant to know if the linker traverses the membrane simultaneously with the rest of the barrel, or whether it precedes or succeeds it. Being able to define these events would help develop a better model to describe the role played by the linker during autotransporter function.

In vivo, the folding and membrane insertion of OMPs is assisted by many chaperone proteins. Periplasmic chaperones such as SurA, Skp, DegP and DegQ interact with the protein in the periplasm, in its non-native state. The extent of fold attained in the periplasm is still ambiguous [76, 77]. In *E. coli*, BamA is the primary membrane chaperone that aids the membrane insertion of all OMPs. Additionally, the protein TamA, which is closely related to BamA, enables the membrane insertion of a specific subset of auto-

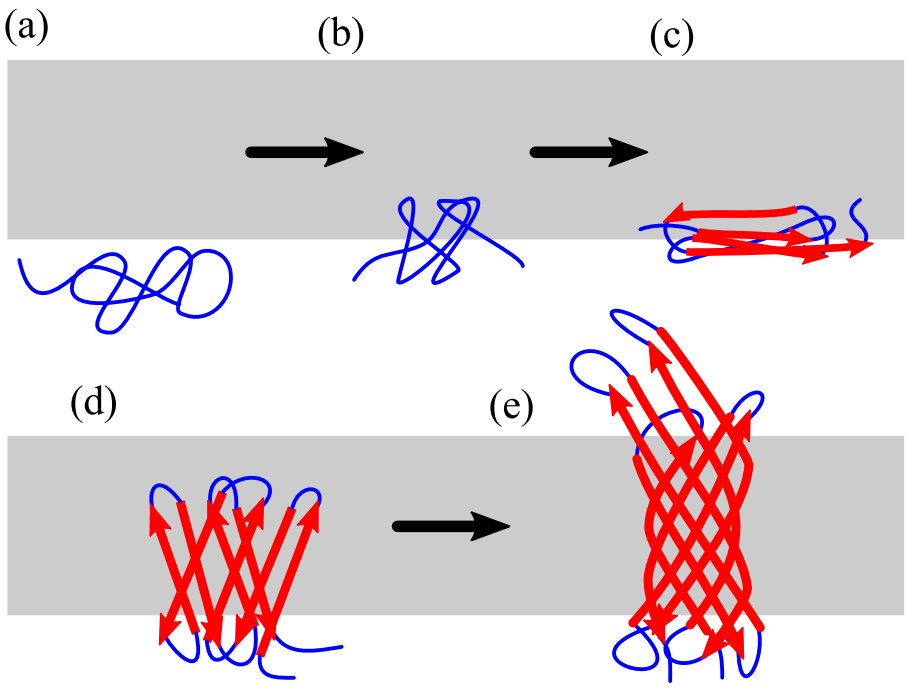

Figure 1.4: The in vitro folding and assembly model of outer membrane β-barrels. The 5 kinetically resolved states are given as a) unfolded state, b) hydrophobically collapsed intermediate, c) molten disk intermediate, d) molten globule intermediate, and e) final folded state. The membrane is represented with the outer leaf facing the top.

transporters [78]. BamA is constituted of a 16 stranded β-barrel transmembrane domain and 5 periplasmic domains. The periplasmic domains are called polypeptide translocation associated (POTRA) domains. BamA functions as a complex constituted of BamA, B, C, D, E proteins. Of these, BamB, C, D, E are membrane associated and are anchored to membrane on the periplasmic side [79, 80]. The complex is held together by interactions of BamB, C, D, E with each other and with the POTRA domain acting as a scaffold to make the complex [81]

While the structures of BamB, C, D, E and the POTRA domains were determined earlier, structures were determined for the transmembrane β-barrel domains of BamA only recently [82, 61]. These structures suggest models for membrane insertion of OMPs including autotransporters. Noinaj et al. solved the crystal structures of two BamA proteins from *H. ducreyi* (a deletion mutant lacking the first three POTRA domains) and *N. gonorrhoeae* (full length) and Gruss et al. solved the structure for the full length TamA protein. TamA has only 3 POTRA domains, compared to the 5 POTRA domains of BamA. There are some common conserved features among the structures determined. Both TamA and the BamA proteins form 16-stranded β-barrels. In the deletion mutant of BamA described above, the POTRA domains extend away from the barrel representing a configuration in which the pore of the barrel is open and accessible to the periplasm. The wild type BamA from *N. gonorrhoeae* has all the POTRA domains intact. In this structure, POTRA5 which is the domain closest to the barrel occludes the pore and restricts access from the periplasm. In the structure of TamA, the POTRA domains adopt a conformation that is similar to the open conformation seen in the BamA deletion mutant. In molecular dynamics simulations, based on the structure of BamA,it has been predicted that at the interface between strand 16 and 1 the membrane is thinner and has poor ordering of lipid molecules. This region has been hypothesized to be a site for membrane insertion for target OMPs [82, 61]. Also in both TamA and BamA, strands 16 and 1 have a relatively small interface of contact.

This has been proposed to be a site of a lateral opening mechanism that can facilitate the binding of the target OMP to the chaperone. Simulations also suggest that the interface is unstable and is amenable to the opening of the barrel [82].

It has been suggested that the mechanism of OMP insertion may involve recruitment of the nascent OMPs to the site of insertion by the POTRA domains, followed by a conformational switch involving the periplasmic domains and loop 6 of BamA enabling access to the pore [82, 83]. After recruitment, the smaller OMPs may insert into the locally destabilized membrane directly. For larger OMPs, it has been suggested that the OMPs may use the laterally opened BamA barrel as a template to form additional strands in the barrel enabling formation of secondary structure and insertion into the outer membrane (Figure 1.3 e). In the case of autotransporters, it is not yet clear whether a large hybrid barrel is formed involving the chaperone and the autotransporter. If such a barrel is formed, it can be considered as a conduit for the transport of the passenger domain as it would form a large pore. The formation of a hybrid barrel would explain easily how the linker gets located in the center of the barrel. Alternatively, it has also been suggested that the linker may simply insert into the membrane and diffuse across it at a site near the site of insertion of the β-barrel of the translocator domain.

1.4 NMR Spectroscopy of Membrane Proteins

Along with X-ray crystallography, NMR spectroscopy is one of the primary methods for structure determination in proteins. Apart from giving the structure, NMR spectroscopy has the added advantage in being able to study chemical exchange events and backbone dynamics in proteins. Added to the general limitations in size due to overlap of resonances and longer correlation time in solution of large proteins, membrane proteins suffer some additional setbacks when compared to soluble proteins. Since the native environment of membrane protein is in the hydrophobic lipid bilayer, such proteins usually are

not readily soluble in aqueous media. Special folding or extraction strategies are required to obtain membrane protein samples that are in their native states. For this purpose, choice of solvent or membrane mimetic is important. Also ^{15}N and ^{13}C isotopic labeling of the proteins is required for assignment of chemical shifts using triple resonance experiments. It is also of additional consideration that a for a membrane protein, the added size from the detergent micelle gives rise to a much larger apparent size. Thus observation of membrane proteins by NMR spectroscopy requires the deuteration of side-chain proton resonances and TROSY (transverse relaxation optimized spectroscopy) experiments.

1.4.1 Protein Expression and Isotopic Labeling

The most convenient strategy for over-expression of protein is in bacterial systems because of their robust nature, low cost for both initial set up and for running, and high yields obtained from recombinant systems employing viral T7 promoters in *E. coli*. Recombinant expression using *E. coli* is relatively straight-forward for small sized bacterial OMPs. This is because they refold spontaneously into detergent micelle solutions. This strategy has been used in structure determination studies of outer membrane proteins such as OmpA, OmpX and PagP [84, 28, 85]. Inclusion bodies are expressed to very high intracellular concentrations when compared to proteins expressed on the membrane, giving high yields of the proteins. A similar inclusion bodies based approach also has been used for over-expressing and folding the much larger mitochondrial outer membrane protein hVDAC (human voltage dependent anion channel) [22, 86]. The additional challenge in expressing such eucaryotic proteins is that a cDNA template has to be used to express these proteins. Furthermore, codon optimization of the template and/or using host organisms that have been engineered to optimally use tRNA that are frequently used in eukaryotes [87, 88].

The method using inclusion bodies is not typically useful for helical membrane proteins of the inner membrane. While refolding of these proteins has been demonstrated

for smaller constructs that contain only 2 helical segments, refolding from inclusion bodies is not common for larger proteins. One notable expression is the chemokine receptor CXCR1, which was cloned as a fusion protein, expressed as inclusion bodies and finally folded in detergent micelles to prepare the samples for structure determination [89]. Many α-helical membrane proteins for which structures were determined using NMR spectroscopy, such as DsBB, DAGK, Rhodopsin II and Mistic, were targeted to the biological membrane using either their native or recombinant signal sequences and washed from the membrane fraction using detergent micelle solutions [90, 91, 92, 93]. An alternate and newly emerging strategy is to use cell free expression systems, as it was used in the case of proteorhodopsin and the histidine kinase receptors (ArcB, QseC and KdpD) [94, 95]. In these cases, the protein was expressed as a precipitate in the cell free expression medium and was solubilized by washing with a detergent solution. Mistic is a very unique membrane protein as it lacks any previously identified signal sequences. It targets independently to the bacterial membrane and can be extracted from the membranes using detergents. It has been proposed as a good candidate to make fusion proteins to target other membrane proteins to the membrane and effectively solubilize them [92].

As the size of protein molecules increase, there are two effects that can be observed. The spectra become very crowded making it difficult to resolve individual resonances. Also the transverse relaxation rate becomes higher causing a line-broadening effect and increases effects of spin diffusion making it difficult to observe nuclear Overhauser effect (NOE) crosspeaks. Incorporation of uniform ^{15}N and ^{13}C labels allows resolution of resonances using multidimensional experiments. The detrimental effects of transverse relaxation and spin diffusion also can be ameliorated by deuterating the proteins. Deuteration of proteins can also be achieved by growing the bacteria in $^{2}H_2O$. For very large proteins, uniform labeling is often not sufficient and more advanced strategies such as site specific labeling is employed [96, 97].

1.4.1.1 Choice of Membrane Mimetics and Optimizing Sample Conditions

Common mimetics of the lipid bilayer are ordered lipid structures composed of detergent molecules. Micelles, bicelles, vesicles and liposomes can be typically used to solubilize proteins. Of these, micelles and bicelles are most relevant for solution NMR because of their smaller relative size and more rapid tumbling in solution compared to vesicles and liposomes. One alternate strategy for studying membrane proteins is to use an organic solvent or mixtures of organic solvents and water. The structures of EmrE [98] and the subunit c of F_1F_0 ATP synthase [99] have been solved in mixtures of chloroform, methanol and water. The use of organic solvents comes with the advantage that they do not form ordered structures in solution and therefore result in rapid tumbling of the protein molecule. However since these conditions are different from the native conditions, they may not accurately reflect the native structure. Additionally, these structures are difficult to validate because functional assays which are typically used to verify enzyme activity may not be applicable in organic solvents [100, 101]. It has been shown that enzymes in organic solvents often do not retain their activity even when they do retain their native structure [102]. Trifluoroethanol (TFE) is a common helix stabilizing organic solvent that is used for studying membrane associating peptides [102].

Various detergents differing in properties such as charge, length of hydrophobic tail have been used for structure determination of membrane proteins. While the exact detergent of choice largely depends on the particular protein being studied, systematic folding studies using a large screen of detergents offers some useful insight [6, 103]. The detergents that emerge as preferred candidates are single chain (or in some case double chain) analogs of common phospholipids. Common choices include 1,2-diacyl phosphatidyl cholines, alkyl-dimethylamine-N-oxides, lysophosphatidyl cholines, lysophosphatidyl glycerols, phosphocholines, tetraoxyethyleneglycols, glucosides, maltosides, and

sulfobetaines. In the studies with OmpA [103], a minimum chain length of 10 carbon atoms in the alkyl chain (or seven in case of detergents with two alkyl chains) was required to obtain considerable yield of folded protein. To the contrary, the identity of the head group had minimal effect on the ability of OmpA to form folded protein. For the purpose of structure determination by NMR spectroscopy, detergent micelles of dodecylphosphocholine (DPC) and 1,2-dihexanoyl-sn-glycero-3-phosphocholine (DHPC) have been used for multiple structure determinations of small OMPs such as OmpA and OmpX [84, 28]. For α-helical membrane proteins, lysophosphatidyl glycerols such as 1-palmitoyl-2-hydroxy-sn-glycero-3-phospho-(1'-rac-glycerol) (LPPG) emerged as a broadly applicable candidate that produced high quality spectra for many protein systems tested [6]. Likewise, LPPG has been used to determine the structures of many helical membrane proteins [104, 105, 106].

Screening for the best choice of detergent for a specific target protein can be done by several approaches. For proteins that have enzymatic activity, this is often done using assays [93, 90]. Small OMPs (8-12 strands) that are folded correctly from inclusion bodies, show thermal stability and do not denature in the presence of SDS, which is often considered a harsh detergent for folding of OMPs. This property is used as an assay of the folded state. A change in mobility is observed for samples that are completely denatured by boiling, when compared to samples that are not boiled [103]. For screening suitable detergents for NMR, HSQC spectra (or TROSY spectra for larger proteins) is a good tool to evaluate sample quality. The prepared samples should show the expected number of peaks in the HSQC. The stability of the sample upon storage can also be evaluated by integrating the volume of the individual peaks in the HSQC and observing the appearance of newer peaks not present initially [6].

1.4.2 NMR Experiments for Studying Membrane Proteins

1.4.2.1 TROSY Based Experimental Methods

Even in perdeuterated proteins, the amide protons that are labile exchange effectively with the protons in the bulk solvent. This is especially very efficient for β-barrel proteins that can freely exchange with the solvent when unfolded from inclusion bodies. In membrane proteins that are retained in their fully folded conformation, it is possible that amide deuterons that are very deeply buried in the expressed protein do not exchange as readily. Having protonated amide residues, while retaining the deuteration in the side chains enables the performance of experiments where the amide protons are the origin of the magnetization. In implementation of these techniques, the effects of transverse relaxation can be further ameliorated by implementing the TROSY effect to obtain spectra with narrower linewidths. At high magnetic fields, the transverse relaxation is dominated by contributions from chemical shift anisotropy interactions and dipole-dipole interactions. In a two spin system, each component of the multiplet relaxes with different overall rate. This is because there is interference between the two relaxing mechanisms and the two mechanisms contribute with different signs to each component of the multiplet. In a HSQC spectrum that is not decoupled, you will see that 4 peaks appear in the spectrum for each ^{1}H-^{15}N correlation. Each peak in the quadruplet has a different linewidth. The TROSY spectrum observes the component in which the two interactions cancel each other out, to obtain spectra with narrow linewidths [107, 108].

TROSY versions of HNCA, HNCACB, HNCO, HNCACO and other carbon sidechain experiments are useful for obtaining chemical shift assignment of proteins. However, in perdeuterated proteins, carbon side-chain resonances will have to be measured using CC(CO)NH type experiments where the magnetization is obtained from the carbon side-chains and is detected using the amide protons. But a more efficient scheme would be

to use a protein sample where the methyl groups of leucine, isoleucine and valine alone are protonated. The magnetization originates in these methyl groups and is transferred along the carbon sidechain using an efficient ^{13}C-^{13}C TOCSY mechanism and is detected ultimately using the amide protons [109, 110]. The additional methyl-protons also will provide more NOEs for structure calculations. In a perdeuterated protein, the only observable NOEs are those between amide protons. So adding methyl protons is required to get more constraints for structure calculations. In a soluble protein these methyl protons are often buried in the hydrophobic core, so they can be very useful to get long distance information [97]. However, in membrane proteins, often the side-chains of hydrophobic residues are buried in the lipid bilayer, leading to speculation whether this strategy is useful in membrane proteins. However, in OmpX, a four-fold increase in NOE constraints was observed after selective protonation of methyl groups [110].

1.4.2.2 Paramagnetic Relaxation Enhanced NMR

While NOEs are the primary determinants of distance constraints for structure calculation using NMR, additional restraints can be obtained from paramagnetic relaxation enhanced (PRE) NMR experiments. It has been demonstrated that distance restraints obtained from PRE experiments alone can be used to determine structure to about 1.5 Å resolution [111]. This can be especially useful for helical membrane proteins where the amount of available NOE constraints can be very limited in the absence of special labeling schemes. Consequently PRE has been used to obtain distance restraints in the structure calculations of many helical membrane proteins [90, 94, 92, 93]. Paramagnetic spin labels can be introduced in proteins by engineering a reactive cysteine residue that can be reacted with a nitroxide spin radical that can react to this residue to act as a paramagnetic center [112]. Calculating intensity ratios of peaks in a HSQC spectrum between a paramagnetic sample and a diamagnetic sample that can be produced by quenching the nitroxide radical

can give a rough estimate of the distances of different resonances from the location of the spin radical. Accurate distance restraints however can be obtained by measuring observed transverse relaxation rates of the protons and obtaining distance information using the Solomon-Bloembergen equation [113].

1.4.2.3 Residual Dipolar Couplings

Anisotropic magnetic interactions such as dipole-dipole interactions get averaged out in solution due to random orientations of molecules. When the molecules in solution are weakly oriented to the magnetic field, these contributions do not get completely averaged out. The residual dipolar couplings (RDCs) can be used to obtain the orientation of the dipolar interaction vector with respect to the magnetic field. The use of RDCs has been shown to greatly improve the quality of structures obtained from calculations. Common media for obtaining alignment are stressed polyacrylamide gels, phage particles and bicelles [114, 115, 116]. Apart from protein in detergent micelles and bicelles, aligned samples have been produced with even more complicated membrane mimetics such as lipid nanodiscs [117].

1.4.2.4 Characterization of Interactions with Membrane Mimetic

It is often of interest to study the interactions of protein with the membrane mimetic of choice. The direct method of observing this is by measuring ^{15}N resolved NOESY spectra and observing NOEs from detergent spins to the amide protons [118, 119]. These NOEs were used to determine the orientation of the detergent molecules around the β-barrel of OmpX [118]. Alternatively, paramagnetic probes were used to determine the solvent exposed residues and buried residues in OmpX [120]. Three paramagnetic compounds Gd^{3+} chelated with tetraazacyclododecanetetraacetic acid (Gd(DOTA)), 16-doxyl stearic acid (16-DSA), and 5-doxyl stearic acid (5-DSA) can be used as paramagnetic probes to determine the interaction of the protein with the detergent micelles and to determine the solvent

exposed regions. Gd(DOTA) is a water soluble compound that does not interact with the detergent micelle. In the case of OmpX, Gd(DOTA) specifically causes the broadening of resonances predominantly from the loop regions which are expected to be solvent exposed. 5-DSA and 16-DSA form mixed micelles with the DHPC detergent that was used to solubilize OmpX. 16-DSA specifically broadens resonances from residues that are located deep in the interior of the micelle, along with broadening the methyl group of the detergent molecule itself. In 5-DSA, the doxyl group is present more towards the head group of the detergent, broadens residues that are both near the surface and to a certain extent the ones located in the interior of the barrel. In smaller peptides, the interaction of antimicrobial peptides such as MSI-594 and mellitin with lipopolysaccharide detergent micelles has been determined using saturation transfer difference (STD) NMR. Continuous wave irradiation of lipid resonances was done to identify residues on the peptide where the saturation was transferred, these residues are in close proximity to the detergent resonance being irradiated [121, 122].

1.5 Membrane Associating Peptides

Many biologically active peptides interact with the lipid bilayer membrane. These include small antimicrobial peptides, cell penetrating peptides, viral fusion proteins and transmembrane segments of helical membrane proteins. Depending on their activity, they may adopt many different configurations. They may form transmembrane helical bundles, or be oriented parallel to the lipid bilayer and located close to the lipid head group, or be inserted at an angle. These interactions are often critical to the biological activity of the peptides. The different categories of membrane associating peptides differ in their amino acid composition and the specific arrangement of these amino acids on the sequence. Thus, it is of interest to characterize how the sequences of these peptides and the properties of the different amino acids such as charge and hydrophobicity, determine the interaction of

the peptides with the membrane.

1.5.1 Antimicrobial Peptides

Antimicrobial peptides are present in a wide range of host organisms from bacteria to higher eukaryotes [123]. Different antimicrobial peptides have been attributed to function in a variety of ways including formation of pores, permeablization of the membrane or thinning the membrane by having a detergent effect, or traversing the membrane barrier to target internal metabolic pathways inside the cell [124, 125]. Antimicrobial peptides that target the membrane predominantly have two different constructions. They are either amphipathic peptides that form α-helices on the membrane like in the case of magainins, or alternatively they form a flat dimeric β-hairpin mediated by the formation of a disulphide bond [126].

Membrane associating antimicrobial peptides have many proposed modes of action. The "barrel-stave" model proposed for amphipathic helices suggests that a large pore is formed by multiple individual peptides [127]. According to the model, the individual peptides interact with the membrane to form α-helices [125]. Each helix, by virtue of its sequence has a hydrophobic face and a polar face. The individual helices arrange themselves like the staves of a barrel to form the pore. The hydrophobic residues of the amphipathic peptide interact with the lipid bilayer, and the charged and polar residues line the interior of the pore. The specific details of the model, such as how individual helices are recruited to the site of the pore are still under investigation. Prior to the formation of a pore, it is unlikely that each monomeric peptide would be inserted perpendicular to the membrane because of energetic considerations [128]. It is believed that it would be unfavorable for the hydrophobic interior of the lipid phase, due to its low dielectric constant and inability to form hydrogen bonds, to interact with the polar face of the peptide and that it would be more favorable for the peptide to orient itself parallel to the membrane

such that the polar face of the helix is exposed away from the membrane. Another model for the membrane interaction of antimicrobial peptides is the carpet model [129]. In this model, membrane associating peptides are oriented parallel to the lipid bilayer at all times. The membrane permeation occurs when a high local concentration of peptide on the lipid bilayer facilitates the formation of pore or internalization of the peptide by disruption of the membrane curvature.

A common category of antimicrobial peptides are cationic peptides. Their sequences are composed with $\sim$50% hydrophobic residues and they have a net positive charge at neutral pH due to the presence of multiple cationic residues. They are amphipathic in nature and are typically soluble in water. They exhibit a random coiled structure in aqueous media, but fold into an α-helical structure in the presence of suitable biological membranes or membrane mimetics. Despite their relatively simplistic design compared to larger proteins that act on specific receptors, cationic peptides have high levels of toxicity in bacteria, but do not have any measurable toxicity towards eucaryotic cells [130]. This selectivity has been attributed to their ability to interact with the membranes of bacteria and not with that of the host organism [131]. The idea that the selective toxicity of these peptides is an outcome of mere interaction with membrane lipid components and not due to an interaction with a specific protein target is corroborated by the observation that both D- and L-enantiomers of these peptides show nearly equally efficient antimicrobial action [132]. Eucaryotic and procaryotic membranes differ in composition [132]. Eucaryotic membranes have upto $\sim$25% cholesterol, are predominantly neutral and composed mainly of zwitterionic phospatidyl cholines [133]. Bacterial membranes on the other hand have a negative charge due to presence of upto 25% negatively charged lipids in the form of cardiolipn and phosphatidyl glycerol along with the zwitterionic phosphatidyl ethanol amine [134, 135]. The fact that the selective toxicity is due to the interaction with the biological membrane has some additional advantages that these peptides have a wide spectrum of action and

that resistance is not readily developed towards these peptides.

1.5.2 Viral Fusion Peptide

An important category of membrane interacting peptides are viral fusion peptides. These peptides are a part of a larger viral fusion protein that mediates the fusion of the viral membrane and the host membrane. Two separate mechanisms have been used to describe viral entry into the cell. In one model, viral fusion with host membrane occurs at the surface of the cell and in the other, the virus enters the cell by receptor mediated endocytosis and the viral fusion with the host membrane occurs from within the endosome. In either case, the fusion is mediated by a viral fusion protein [136]. Viral fusion proteins are diverse in their design and complexity but have one central theme. The fusion protein is constituted of 3 domains. The C-terminal domain is a transmembrane domain that is found on the viral membrane, the other domains are presented towards the exterior of the virus. The N-terminus is called the viral fusion peptide segment, which in the fusion competent state attaches to the host membrane and anchors the fusion protein to the membrane and in between these two domains is a helical hairpin bundle. In the fusion competent state, fusion proteins exist as trimers (or in some cases as dimers). Upon binding of the fusion peptide to the host membrane, the trimeric hairpin region bends into a hairpin to form a hexameric helical bundle to mediate the fusion process [136, 137].

Viral fusion peptides differ in composition compared to other transmembrane helices. They have an abnormally large content of alanine and glycine residues in their sequences [138]. It has been suggested that these peptides have large content of these residues because the fusion process requires conformational flexibility of the peptide and interaction with the membrane alone is not sufficient [139]. Viral fusion peptides have two distinct states, their native pre-fusion states and the membrane bound or active state. In the native state, the structures of these peptides are varied. They may in one of many configurations

including but not limited to being buried in a local hydrophobic pocket, being partially solvent exposed or interacting with other subunits of the fusion protein [137]. In the active membrane bound state, many fusion peptides are known to adopt helical structures. The peptides differ among themselves with respect to the depth of insertion, and the angle of insertion. In many cases, the helix is not continuous and may have loops and/or kinks [140, 15].

1.5.3 Characterization of Membrane Associating Peptides Using NMR Spectroscopy

NMR is a very powerful tool for the biophysical characterization of membrane associating peptides such as viral fusion peptides and antimicrobial peptides [141, 142, 140, 15]. Structures of many membrane interacting peptides of either category have been determined by NMR spectroscopy [143, 144, 145, 13]. The membrane mimetics used in these studies are typically either ordered lipid structures like detergent micelles or helix stabilizing organic solvents such as TFE. Apart from structures, NMR spectroscopy can be used to obtain the orientation of these peptides in the detergent micelles. The orientation of the peptides on the lipid bilayer is often a determinant of function [140, 146]. Common methods involve the use of paramagnetic probes [147] or observation of NOEs with the detergent molecule to get the depth of insertion of the peptide into the membrane mimetic. Residual dipolar couplings are also used to obtain the tilt and the angular orientation of the peptide in the detergent micelle [148].

2. STRUCTURAL STUDIES OF THE LINKER REGION OF NalP AUTOTRANSPORTER AND IMPLICATIONS IN FUNCTION

2.1 Introduction

Bacteria possess the ability to secrete and display proteins on the surface of their cell membranes. This ability commonly determines the virulence and pathogenicity of the bacteria. In Gram negative bacteria, the secretion of protein involves crossing both the inner and the outer membranes. The pathways involved in transport across these membranes vary both in complexity and in mechanism. The Type V secretion pathway includes autotransporter proteins, which were initially believed to be capable of transport across the outer membrane autonomously [149, 57, 36]. The autotransporter family has over a hundred members that have been identified using biochemical and computational methods [34]. Autotransporters are translocated across the inner membrane in an unfolded configuration by SecYEG translocon, using a cleavable signal sequence. Transport across the outer membrane involves the integration of a C-terminally located β-barrel domain into the outer membrane and presentation of the passenger domain towards the extra cellular space. The transport across the outer membrane does not require ATP hydrolysis or an ion gradient [59]. The passenger domains may either be released by cleavage, or be retained at the outer surface of the outer membrane. The passenger domains function as proteases, esterases and adhesins among others [36, 150]. Autotransporters are important targets for vaccines and drugs [58].

Despite the diversity in size and sequence of autotransporters, their domain architecture is fairly conserved. The passenger domain is present in the N terminus and varies in function and size. The C-terminal domain, which is crucial for the transport process, has a conserved structure consisting of a β-barrel of 12 or 14 strands and is typically $\sim$30

kDa in size for the 12 stranded barrel [149]. The translocator domain is believed to tether the protein to the outer membrane and mediate the translocation of the passenger domain through the outer membrane. Another conserved feature in the translocator domain is that the N-terminus of the β-barrel structure leads to a short α-helical linker peptide. Non-conservative mutations in these linker peptides hinder the proper folding of the respective translocator domains and either completely eliminate or reduce the efficiency of the transport process [44, 151]. Deletion of the linker peptide affects the targeting of the translocator domain to the outer membrane [38]. The loss of autotransporter function caused by deletion of linkers has been demonstrated to be restored by the use of recombinant linkers [152].

The NalP autotransporter from *Neisseria meningitidis* facilitates the processing of other autotransporter proteins through its 70 kDa passenger domain (NalP_{1-783}), which functions as a serine protease. Additionally, the functional domain catalyzes the release of its own passenger domain at the outer membrane of the cell [153]. A crystal structure has been determined for the translocator domain of NalP ($\text{NalP}_{784-1083}$), showing a 12 stranded β-barrel ($\text{NalP}_{817-1083}$) that is preceded by the linker peptide ($\text{NalP}_{784-816}$). In the reported structure, the NalP linker peptide is folded as an α-helix [38]. Interestingly, this helix is located in the central pore of the β-barrel. Structures are also known for the translocator domain of autotransporters EspP and Hbp (*Escherichia coli*) and for the full length autotransporter EstA (*Pseudomonas aeruginosa*) [40, 43, 39, 43]. The linker peptide is folded as an α-helix in the pore of the barrel in these structures as well. The location of the linker helix inside the barrel, the ubiquitous presence of such a linker sequence in known sequences of autotransporters and its importance in autotransporter fold and function is an indication that the linker peptide may play an important role in the folding and assembly of the β-barrel of autotransporters.

The autotransporter moniker is misleading in the sense that the assembly of the proteins

in the outer membrane is not completely independent, rather it is modulated by chaperone proteins of the Omp85 super family. Models for the function of Omp85 chaperones have been proposed based on crystal structures determined for the membrane chaperones BamA and TamA from *E. coli* [82, 61]. Omp85 chaperones have been suggest to mediate the folding and membrane insertion of outer membrane proteins including autotransporters by multiple mechanisms. Proposed mechanisms include creating a localized loss of order in the membrane and providing a template for strand formation for the nascent OMPs by a lateral gating mechanism.

Here, the linker peptide from NalP has been expressed recombinantly and structurally characterized in aqueous and hydrophobic environments. Based on the data, the relation between the structural properties of the linker in these different environments and the role of the linker peptide in the folding and processing of the translocator domains is discussed.

2.2 Experimental Procedures

2.2.1 Cloning and Purification of NalP Linker Peptide

NalP linker peptide between residues 784-816 of the full length protein (LAATVYAD-STAAHADMQGRRLKAVSDGLDHNGT) was expressed as a fusion protein construct with Smt3, a Small Ubiquitin-like Modifier Protein (SUMO) protein from *Saccharomyces cerevisiae*, cloned upstream to the peptide sequence [154]. Smt3 protein gene template was generously provided by Dr. Pingwei Li, Texas A & M University. The gene was amplified using polymerase chain reaction (PCR)and cloned into pET28b vector (EMD Millipore Biosciences, Billerica, MA, USA) using restriction enzymes NdeI and SacI (New England Biosciences, Ipswich, MA, USA), leaving a 6x His tag in the N-terminus of the SUMO tag to facilitate purification using immobilized metal ion affinity chromatography (IMAC). The genomic DNA of *N. meningitidis* (American Type Culture Collection, Manassas, VA 20110 USA) was used as the gene template for NalP protein. The DNA sequence for the

NalP linker region was amplified using PCR and was cloned between restriction enzyme sites for SacI and HindIII. The plasmid was transformed into BL21(DE3) and a single colony inoculated in 20 mL Luria Bertani (LB) medium with 50 mg/L kanamycin and grown overnight to be used as a starter culture at 37 °C shaken at 200 rpm. The starter culture was used to inoculate 4 L of LB with kanamycin. The cells were harvested at an optical density of 0.7 in sterile centrifuge bottles and suspended in 1 L of expression medium. The cells were then incubated at 16 °C and shaken at 200 rpm. The cells were cultured for 1 h and then induced by adding IPTG to a final concentration of 1 mM and cultured for 16 h. The expression medium used was LB broth or Terrific broth for unlabeled protein expression or a modified M9 minimal medium with $^{15}NH_4Cl$ and $^{13}C_6$-glucose for expression of isotopically labeled peptides.

The peptide is vulnerable to proteolysis, therefore all purifications were performed at 4 °C. The cultured cells were harvested by centrifugation at 4500 rpm for 20 minutes and resuspended in buffer A_1 described below. Cell lysis was achieved by sonication in six cycles of 2 min each interspersed by cooling periods of 5 min. Cell lysate was kept at a temperature of 4 °C at all times. The fusion protein was purified from the cell lysate by IMAC using HisTrap HP column (GE Lifesciences) using buffer A_1 (20 mM sodium phosphate, 500 mM sodium chloride, 20 mM imidazole pH 7.3) and buffer B_1 (20 mM sodium phosphate, 500 mM sodium chloride, 500 mM imidazole pH 7.3). The cell lysate was loaded on the column and washed with 40 mL buffer A_1. Elution was done using a step gradient of 15 mL each of 10%, 20%, 30% and 40% buffer B_1. The fractions containing the fusion protein were identified by polyacrylamide gel electrophoresis and pooled. 2-mercaptoethanol was added to a final concentration of 5 mM. Ulp1 protease, expressed and purified previously [154], was added to a final concentration of 0.05 mg/mL to cleave the SUMO tag. The reaction was simultaneously dialyzed against 20 mM tris, 5 mM 2-mercaptoethanol, pH 8.5 for 12 h. The SUMO tag of the fusion construct and

the Ulp1 protease are removed by passing the dialyzed solution through the HisTrap HP column. The SUMO tag and the protease bind to the column whereas $NalP_{777-816}$ peptide does not. The peptide was further purified by cation exchange chromatography using a HiTrap Q XL column (GE Lifesciences, Piscataway, NJ, USA) and buffer A_2 (20 mM tris, pH 8.5) and buffer B_2 (20 mM tris, 5 mM sodium chloride, pH 8.5). Step gradient for elution was set up similar to the IMAC protocol. The fractions containing the peptide were pooled and dialyzed against distilled water for 12 h and lyophilized to a dry powder. The lyophilized peptide was dissolved in H_2O with 0.1% trifluoroacetic acid to a final volume of 300 µL and the peptide solution was purified using reversed phase HPLC using a Vydac C4 Column (Grace, Deerfield, IL, USA). Peptide was eluted across a 0% to 100% gradient between solvent A_3 (H_2O with 0.1% trifluoroacetic acid) and solvent B_3 (acetonitrile with 0.08% trifluoroacetic acid) using a 90 mL solvent volume using a flow rate of 1 mg/min. The peptide fraction was lyophilized to remove solvents. The cleavage using the Ulp1 protease leaves an additional glutamic acid amino acid residue on the N-terminus of the peptide, making the leucine residue indicated in the sequence above the second residue in the peptide used.

2.2.2 Circular Dichroism (CD) Spectroscopy

Far UV wavelength scan CD spectra were measured on a Model 62DS CD Spectrometer (AVIV Biomedical Inc., Lakewood, NJ, USA). Samples were made by dissolving 7 µM peptide in 20 mM sodium phosphate buffer (pH 6.8). Samples containing detergent micelles additionally contained 100 mM sodium dodecyl sulfate (SDS). Samples in trifluoroethanol (TFE) were prepared by dissolving 7 µM peptide in TFE (Alfa Aesar, Ward Hill, MA). All samples were degassed by performing three cycles of freezing and thawing under vacuum. Wavelength scans were measured at 288 K between 190 nm and 320 nm with a step size of 1 nm and a signal averaging time of 10 s.

2.2.3 NMR Spectroscopy of NalP Linker Peptide and Structure Determination

NMR samples were prepared by dissolving nominally 1 mM NalP linker peptide in 20 mM sodium phosphate, 3 mM NaN_3, 1 mM, 4,4-dimethyl-4-silapentane-1-sulfonic acid, 5% v/v ^2H_2O (pH 6.8). Samples in SDS micelles additionally contained 100 mM SDS. Samples in TFE were dissolved in 2,2,2-TFE-1-$^2H_2$ (Cambridge Isotope Laboratories, Andover, MA) with 1 mM tetramethylsilane. All spectra were measured at a magnetic field of 11.7 T on an Avance III spectrometer using a TCI triple resonance cryoprobe (Bruker, Billerica, MA, USA). All experiments for the peptide in the aqueous buffer were measured at 283 K, for the detergent micelles at 310 K and for TFE at 298 K.

Sequential backbone and sidechain carbon chemical shifts were assigned using HNCA, HNCACB, CBCACONH, HN(CA)CO, HNCO, HCC(CO)NH (DIPSI2 mixing sequence, 13 ms mixing time at 10 kHz) experiments. Backbone and sidechain proton chemical shifts were assigned using ^{15}N-resolved TOCSY (MLEV-17 mixing sequence, 100 ms mixing time at 10.7 kHz) and HNHA experiments. Aromatic proton resonances were assigned in (HB)CB(CGCD)HD, (HB)CB(CGCD)HE experiments. For the sample in SDS detergent micelles, H(CCCO)NH (DIPSI2 mixing sequence, 13 ms mixing time at 8.6 kHz) experiment was used instead of the ^{15}N resolved TOCSY experiment to assign the proton side chain chemcial shifts.

Nuclear Overhauser effect (NOE) crosspeaks were obtained ^{15}N-resolved NOESY (150 ms mixing time) and ^{13}C-resolved NOESY (150 ms mixing time) spectra. $^3J_{H^N H^\alpha}$ coupling constants were measured using HNHA spectra [155]. Peaks from the NOESY spectra were picked manually and were automatically assigned using the CANDID module in CYANA software [156]. The structure calculation was done in 7 cycles of simulated annealing, starting from 100 randomized conformers. The 20 conformers with lowest target function values were selected in each cycle [157]. Peptide structures were visualized

and relevant interatomic distances and angles were measured using PyMol [158].

2.2.4 Cloning, Folding of Purification of NalP Translocator and NalP β-barrel Domains.

N. meningitidis genomic DNA was used as the gene templates for NalP translocator domain and NalP β-barrel and the gene sequences were amplified using PCR and cloned into pET28b expression vector using restriction enzymes NcoI and HindIII (New England Biolabs). The plasmid was transformed into BL21(DE3) for expression. Overnight starter cultures were grown from a single colony of transformed bacteria in 10 mL of LB with kanamycin. Cells were then transferred into 1 L expression medium of choice. Protein was expressed in LB for production of unlabeled protein or in a minimal medium containing $^{15}NH_4Cl$ prepared in $^{2}H_2O$ for isotopically enriched protein samples. For each liter of cell culture, the cells were resuspended in 40 mL of 20 mM tris, 5 mM ethylenediamine tetra acetic acid (EDTA), pH 8.0 and lysed by six cycles of sonication for two minutes with 5 minutes of cooling in between each cycle. Inclusion bodies were harvested by centrifugation at 4300 rpm for 1 h. The inclusion bodies were resuspended and washed with 40 mL of 20 mM tris 5 mM EDTA, 0.1% Triton-X-100, pH 8.0, at 37 °C for 30 min. The insoluble protein was pelleted by centrifugation at 4300 rpm for 30 min. The pellet was resuspended in 40 mL of 20 mM tris 5 mM, pH 8.0, and incubated at 37 °C for 30 min. The resuspended protein was pelleted by centrifugation at 4300 rpm for 30 min. The pelleted inclusion body protein was unfolded and dissolved in 5 mL of 20 mM tris, 8 M urea, 100 mM glycine, pH 8.0. Insoluble cell debris was separated by centrifuging at 15,000 rpm for 30 min and filtration through a 0.2 µm pore size filter. The final concentration of the protein was estimated by UV absorbance at 280 nm and adjusted to 10 mg/mL.

Folding of protein was done by rapid 1:10 dilution of the protein into folding buffers listed in Table 2.1 and incubated in 37 °C for 48 h. Samples for measurement of CD and

Table 2.1: Buffers used for folding, CD spectroscopy and NMR spectroscopy of NalP translocator domain with linker and NalP β-barrel domain.

Buffer	Composition
Folding buffers	20 mM tris 1 M sodium chloride, 1.5% SB-12, pH 8.0
	20 mM tris, 1 M sodium chloride, 1.5% DPC, pH 8.0
	20 mM tris, 1 M sodium chloride, 1.5% LDAO, pH 8.0
	20 mM tris, 1 M sodium chloride, 2.0% DHPC, pH 8.0
	20 mM tris, 1 M sodium chloride, 2.0% β-OG, pH 8.0
NMR buffers	20 mM sodium phosphate, 150 mM SB-12, pH 6.8
	20 mM sodium phosphate, 150 mM DPC, pH 6.8
	20 mM sodium phosphate, 150 mM LDAO, pH 6.8
	20 mM sodium phosphate, 250 mM DHPC, pH 6.8
CD buffers	20 mM sodium phosphate, 80 mM SB-12, pH 6.8
	20 mM sodium phosphate, 80 mM DPC, pH 6.8
	20 mM sodium phosphate, 80 mM LDAO, pH 6.8
	20 mM sodium phosphate, 160 mM DHPC, pH 6.8
Abbreviations:	1 1,2-dihexanoyl-sn-glycero-3-phosphocholine (DHPC)
	n-dodecylphosphocholine (DPC)
	N,N-Dimethyldodecylamine N-oxide (LDAO)
	n-Dodecyl-N,N-dimethyl-3-ammonio-1-propanesulfonate (SB-12)
	β-octyl glucoside (β-OG)

NMR spectra were exchanged into the respective buffers by three cycles of concentrating the purified protein to a volume of 1 mL and diluting it ten fold into the corresponding buffers listed in Table 2.1. CD samples were adjusted to a final concentration of 0.1 mg/mL. For NMR samples, the last cycle of buffer exchange was done in buffer prepared in 10% $^{2}H_2O$ and the protein concentration was adjusted to 1 mM as quantified by absorbance at 280 nm. [^{1}H-^{15}N]-TROSY measurements were done at a temperature of 318 K.

2.3 Results

2.3.1 Assessment of Sample Purification of NalP Linker Peptide and Preliminary Investigation

After an overnight reaction, Ulp1 protease cleaves nearly all the fusion construct to give the SUMO tag and the linker peptide (Figure 2.1 a). The peptide released by cleavage has apparent molecular size of $<$5 kDa as determined by SDS PAGE, which is correct for the expected molecular size of $\sim$3.5 kDa. The HPLC purification protocol used provides a clean product with single peak with a good peak shape and no overlap with any detectable contaminants (Figure 2.1 b). The identity of the peptide purified by HPLC was verified by measuring the mass of the component using a Matrix Assisted Laser Desorption Ionization-Mass Spectroscopy (MALDI-MS) (Figure 2.1 d). The MALDI gives a mass of 3541 Da, which is close to the expected mass of 3542 kDa for the peptide. 1-D ^{1}H spectra for the sample measured in all three conditions no observable contaminants were observed (Figure 2.1 c).

2.3.2 Secondary Structure of NalP Linker Peptide in Different Environments.

Far UV wavelength scan CD spectra of the NalP linker peptide were measured in a buffered aqueous medium, SDS detergent micelles and in TFE (Figure 2.2). The signature of the CD spectrum in aqueous medium resembles that of a random coiled peptide, with

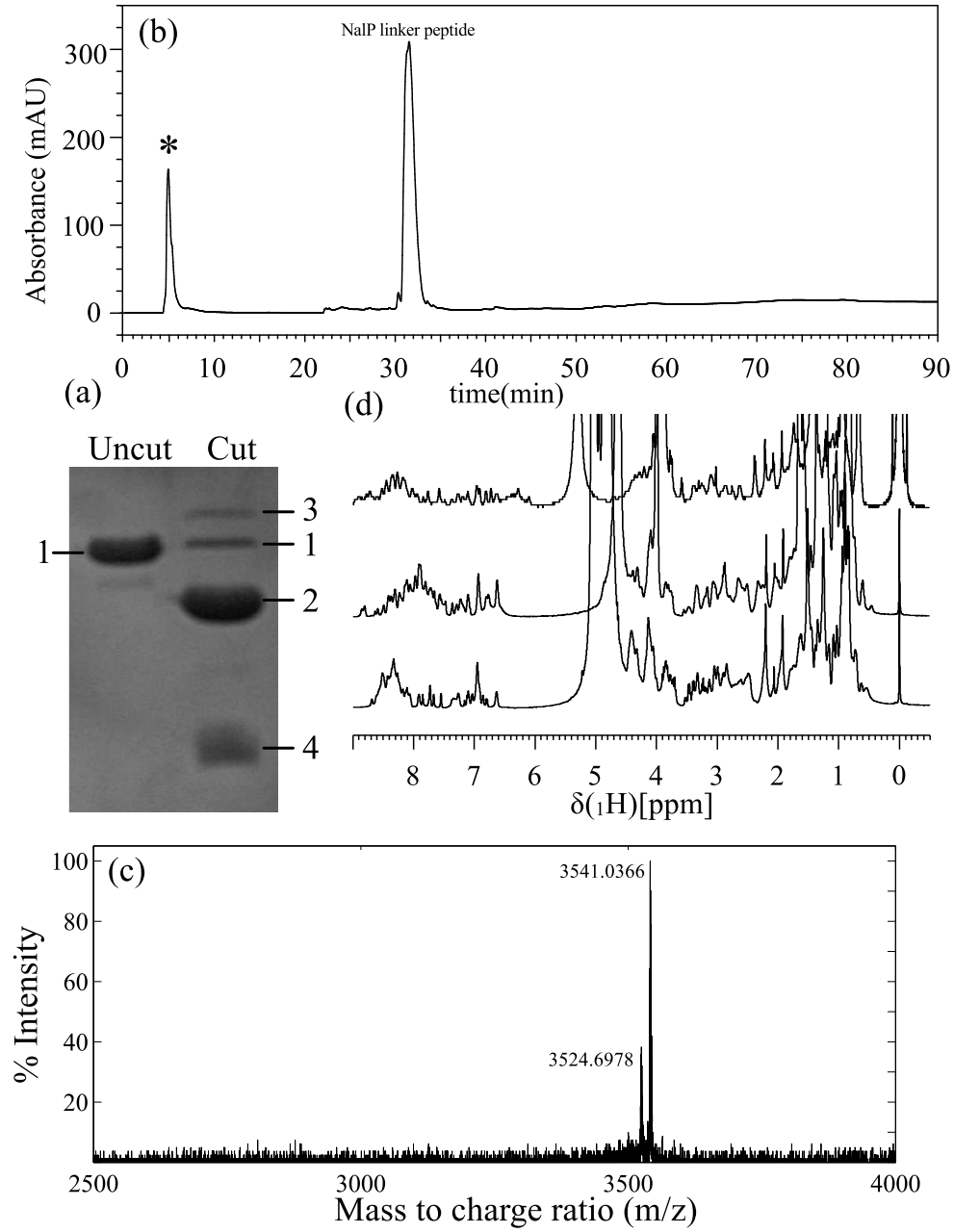

Figure 2.1: (a) SDS-PAGE showing the cleavage of SUMO fusion construct of NalP linker peptide. Components indicated are 1-Uncut SUMO-NalP linker fusion construct, 2-Cleaved SUMO tag, 3-Ulp1 protease, 4-NalP linker peptide. (b) Purification of NalP linker peptide using HPLC, the peak on the chromatogram indicated with a (*) is a pressure spike from the injection of the sample. (c) MALDI-MS of NalP linker peptide. (d) ^{1}H NMR spectra of NalP linker peptide in water, SDS detergent micelles and in TFE (top to bottom).

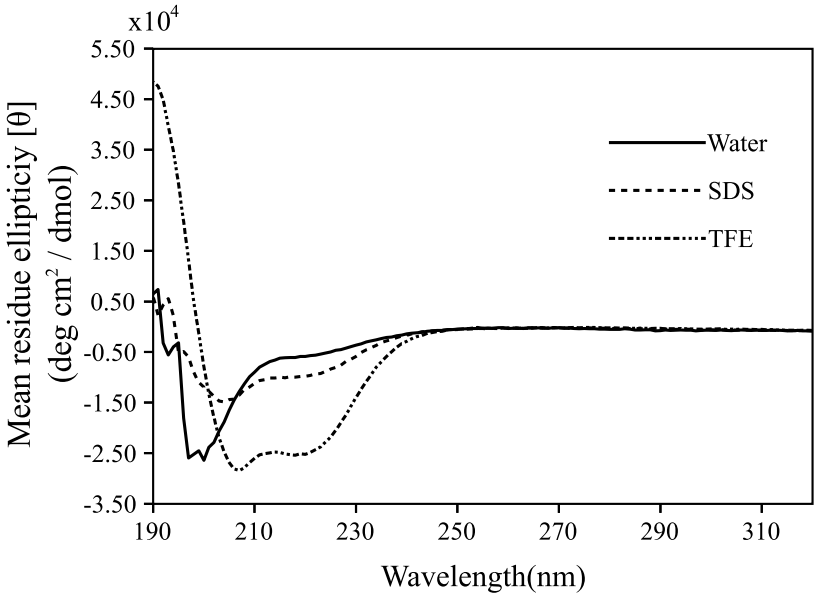

Figure 2.2: Circular dichroism spectra of NalP linker peptide in water, TFE and SDS detergent micelles measured at a temperature of 288 K.

a minimum mean residue ellipticity at 200 nm. The spectrum indicates low content of ordered secondary structure in the aqueous medium. In TFE, the CD spectrum of the peptide has two local minima at 208 nm and at 222 nm, which is typically observed for α-helical secondary structures. In SDS also, a minimum at 208 nm and a shoulder at 222 nm can be identified. The absolute value of the ellipticity is much smaller compared to the values measured in TFE, which suggests that the percentage helicity (p_h) of the peptide in SDS micelles is lower than in TFE. The percentage helicity of the peptide was calculated from the mean residue ellipticities (θ) of the peptide at 222 nm using equation 2.1 [159].

$$p_h = \left(\frac{\theta_{222\text{nm}(obs)} - \theta_{222\text{nm}(coil)}}{\theta_{222\text{nm}(helix)} - \theta_{222\text{nm}(coil)}} \right) \tag{2.1}$$

$\theta_{222\text{nm}(obs)}$ is the observed mean residue ellipticity at 222 nm. $\theta_{222\text{nm}(helix)}$ and $\theta_{222\text{nm}(coil)}$ are the theoretically expected values of mean residue ellipticity in deg cm^2 dmol^{-1}, for

a completely helical peptide and a completely coiled peptide respectively, calculated by equation 2.2 and equation 2.3 [159, 160].

$$\theta_{222\text{nm}(helix)} = -40000\left(1 - \frac{x}{N}\right) + 100T \tag{2.2}$$

$$\theta_{222\text{nm}(coil)} = 640 - 45T \tag{2.3}$$

N is the number of residues in the peptide, x is the correction factor for the number of backbone carbonyl atoms in the peptide that cannot form a hydrogen bond as a helix and thus will not contribute to the mean residue ellipticity, and T is the temperature in °C. The percentage helicity in buffered aqueous medium was found to be 15.9%, in SDS detergent micelles it was found to be 26.6% and in TFE it was found to be 69.5%. The peptide exhibits lowest percentage helicity in the aqueous medium, and has increasing percentage helicity in SDS detergent micelles and in TFE.

2.3.3 Structural Investigations of NalP Linker Peptide by NMR Spectroscopy

The [^{1}H-^{15}N]-HSQC spectra of the peptide in the three conditions are shown (Figure 2.3, 2.4, 2.5) and the the amide crosspeaks peaks are well resolved in all three conditions. . Line widths are larger in the sample with SDS micelles, which could be due to association of the peptide with the detergent micelle. The peptide in SDS micelles was hence measured at a higher temperature of 318 K. The peptide sample in water was measured at a lower temperature of 288 K because at higher temperatures the peptide degraded sooner than the duration of the experiments. The chemical shifts were assigned using NMR experiments for obtaining sequential connectivity and sidechain and sidechain chemical shifts, strips from the HNCACB spectrum of the peptide in TFE is shown (Figure 2.6).

Chemical shifts were assigned for ^{13}C, ^{15}N and ^{1}H spins (Table 2.2). Based on these assignments, secondary shift values were calculated for H^{α}, C^{α} and C^{β} resonances (Figure

Table 2.2: Statistics from chemical shift assignment and structure calculation of NalP linker peptide.

Parameter	**Water**	**SDS**	**TFE**
Chemical Shift Assignment (%)			
All shifts	80.52	82.34	82.51
Backbone shifts	95.95	97.69	98.27
Sidechain shifts	67.93	69.81	69.81
Distance constraints			
Intra-residual	34	97	98
Sequential	55	134	109
Medium Range	10	119	94
Long Range	0	1	10
J-coupling constraints			
$^{3}J_{H^{N}H^{\alpha}}$ coupling constants	32	33	33
Target function	0.011±0.008	0.20±0.063	0.27±0.075
Root mean square deviation from mean structure (Å)			
Backbone atoms from residues L2-G33	6.22 ± 0.82	3.22 ± 0.76	4.15 ± 0.86
Heavy atoms from residues L2-G33	6.86 ± 0.75	3.98 ± 0.76	4.96 ± 0.94
Backbone atoms from residues L2-K23	3.68 ± 0.78	2.52 ± 0.67	1.44 ± 0.64
Heavy atoms from residues L2-K23	4.75 ± 0.74	3.53 ± 0.76	2.30 ± 0.71
Ramachandran plot statistics			
Residues in allowed regions (%)	100	100	100
Residues in disallowed regions (%)	0	0	0

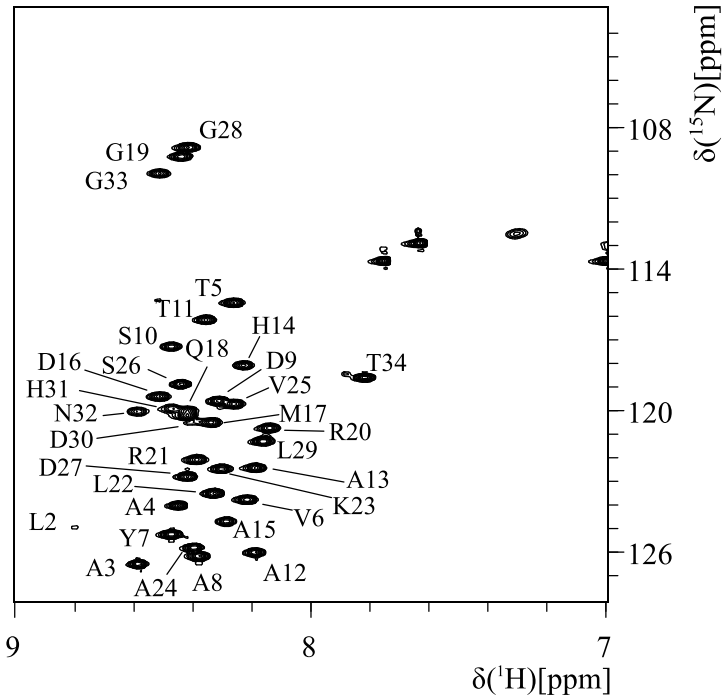

Figure 2.3: [^{1}H-^{15}N]-HSQC of NalP linker peptide in aqueous medium at 283 K measured at a field strength of 11.7 T

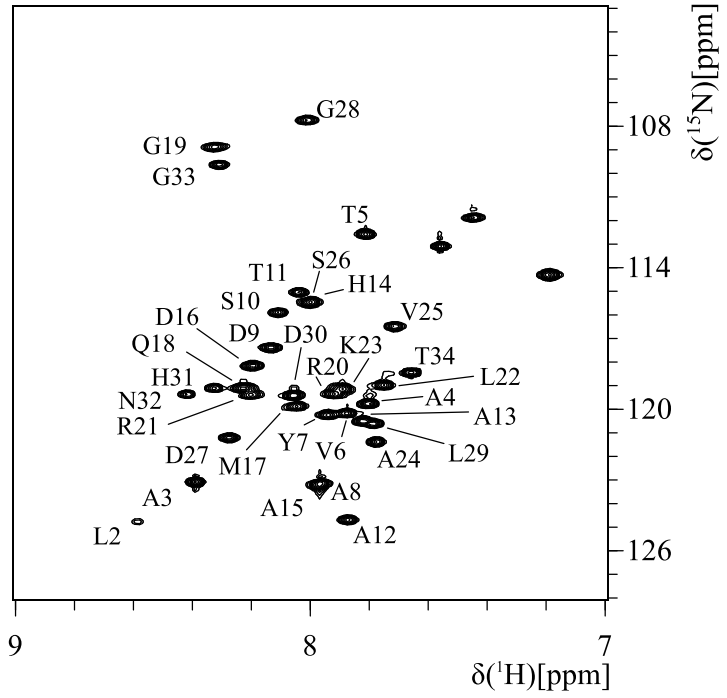

Figure 2.4: [^{1}H-^{15}N]-HSQC of NalP linker peptide in SDS detergent micelles at 310 K measured at a field strength of 11.7 T

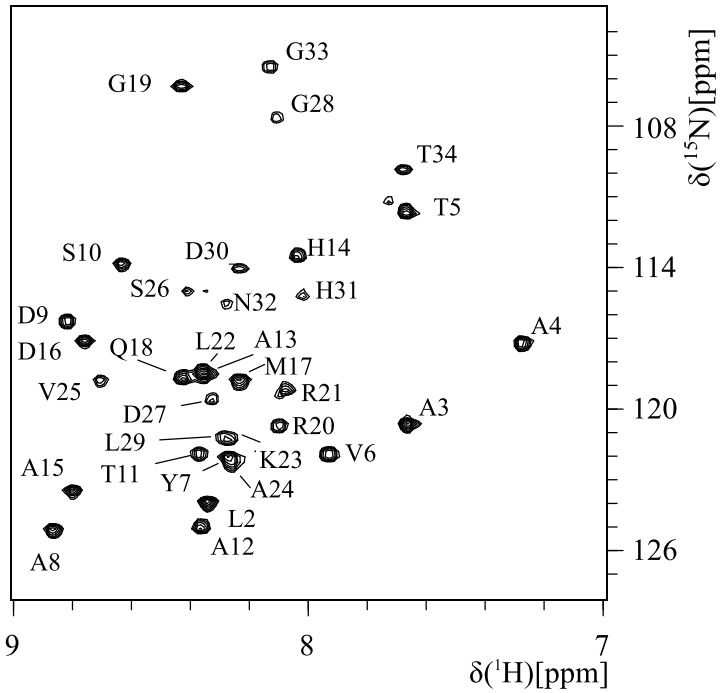

Figure 2.5: [^{1}H-^{15}N]-HSQC of NalP linker peptide in TFE at 298 K measured at a field strength of 11.7 T

2.7). For the sample in water secondary shift values were all close to zero, indicating that the measured chemical shift values were very similar to expected values for a random coiled peptide (Figure 2.7 a, d, g). In the presence of SDS detergent micelles, greater secondary shift values were observed in comparison to water (Figure 2.7 b, e, h). In particular, regions between L2-T11 and G19-D27 have negative H^{α} and C^{β} secondary shifts, and positive C^{α} secondary shifts. Among the three conditions largest secondary shift values were measured in TFE. A continuous stretch of positive secondary shifts are observed for C^{α} and negative secondary shifts for H^{α} and C^{β} are found between residues L2 and S26 (Figure 2.7 c, f, i). Negative secondary shift values for H^{α} and C^{β}, and positive secondary shifts for C^{α} are characteristic of α-helical secondary structure in proteins [161, 162, 163]. Although, it should be noted that the solvent used in the reference data set for

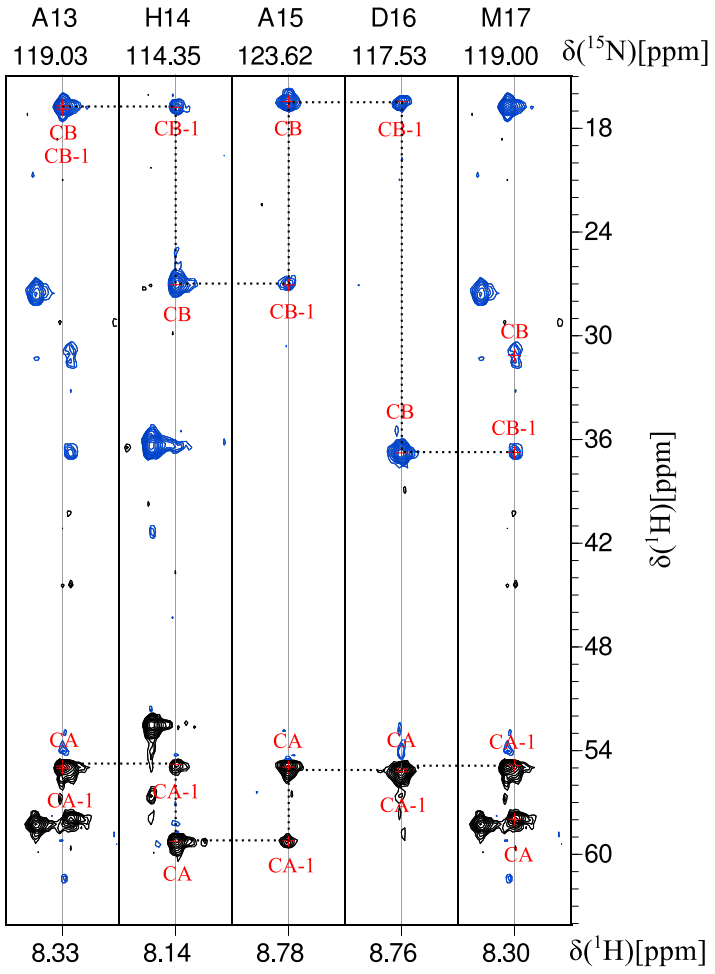

Figure 2.6: [$\delta(^{13}C)$,$\delta(^{1}H)$] strips of residues Ala-13 to Met-17 from HNCACB spectra of NalP linker peptide in TFE. Strips are centered around the amide ^{1}H and amide ^{15}N chemical shifts of the respective residues.

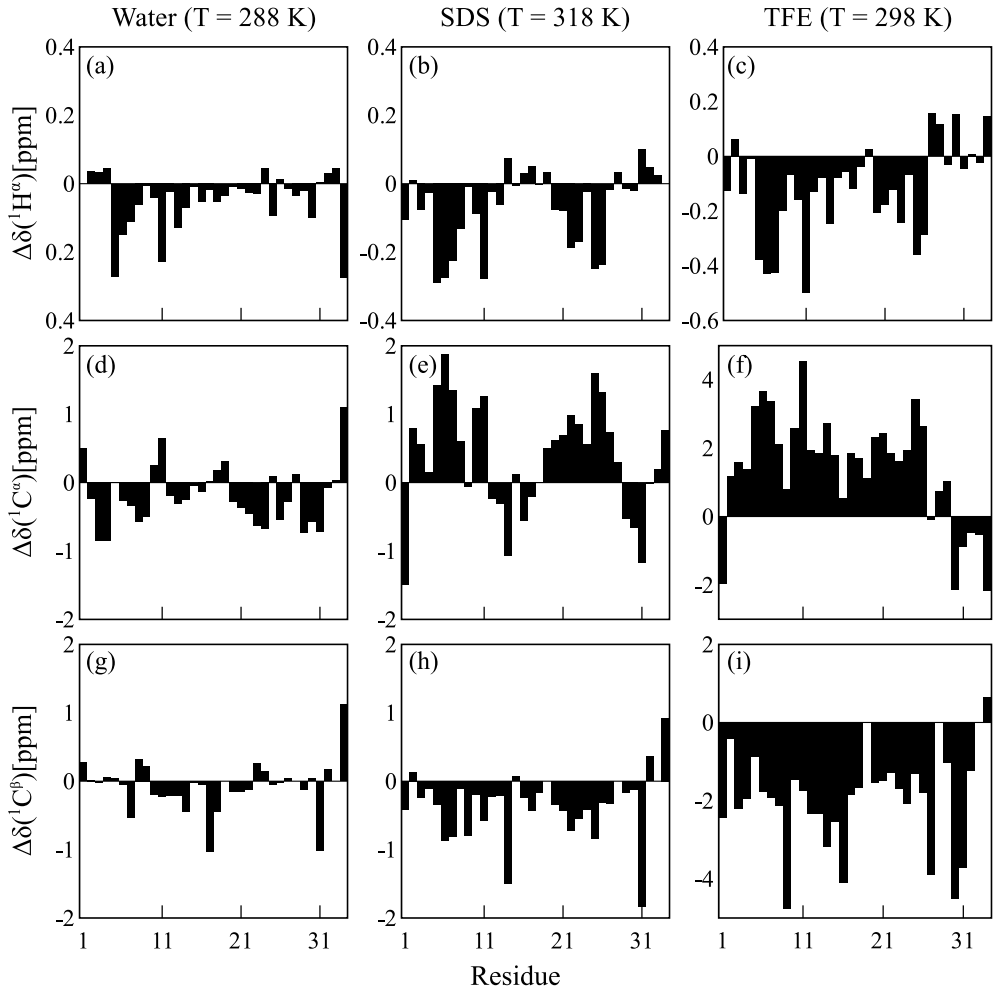

Figure 2.7: Chemical shift differences from random coil values for H^{α} (a), (b), (c), C^{α} (d), (e), (f) and C^{β} (g), (h), (i) for NalP linker peptide in water, SDS detergent micelles and TFE respectively.

calculating the chemical shift differences is water, which is chemically different from TFE.

Many residues with ${}^{3}J_{H^{N}H^{\alpha}}$ coupling constant values >5 Hz were observed for both the sample in water and the sample in SDS micelles (Figure 2.8). These values are typical for peptides that exhibit high conformational flexibility. However, in TFE the coupling constant values for residues are smaller, especially between residues L2-V25 (Figure 2.8), coupling constant values <5 Hz are observed for many residues. This is consistent with

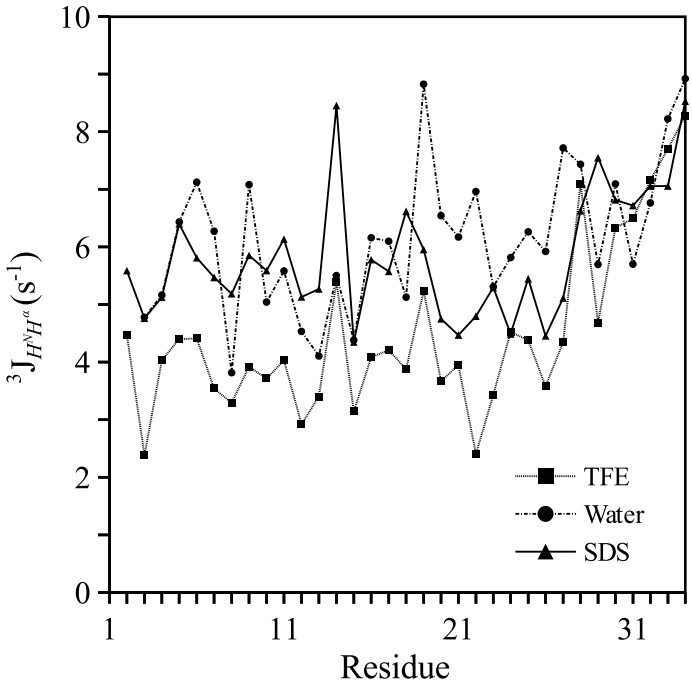

Figure 2.8: $^3J_{H^NH^\alpha}$ coupling constants, of NalP linker peptide in water, SDS detergent micelles and TFE.

dihedral angles for α-helical secondary structures, which give rise to coupling constant values below this cutoff value [164, 155, 165].

While empirical relations of secondary structure to chemical shift and J-coupling values are good indicators, NOEs provide a more direct observation of the structure itself. In α-helices, diagnostic NOE crosspeaks are typically observed for H^α(i) and H^N(i+3), H^α(i) and H^β(i+3), and H^α(i) and H^N(i+4) correlations. The number of intra-residual, diagnostic NOEs observed for each sample from the CANDID NOE assignment routine are shown in (Table 2.2). Diagnostic NOE crosspeaks were not observed for the sample in water. Considering this observation, along with the results of the CD experiment, and the secondary shift and J-coupling values observed in the NMR experiments, it can be concluded that the linker peptide in the aqueous medium is random coiled and lacks observable secondary structure. While the polypeptides of autotransporters interact with

periplasmic chaperones, they are considered to be in an unfolded configuration in the periplasm [54]. The linker peptide in an aqueous medium can be considered to be similar to such a conformation. In SDS micelles, the regions between L2-T11 and G19-D27 contain sparse connectivity of NOE crospeaks from H^{α}(i) and H^{N}(i+3), and H^{α}(i) and H^{β}(i+3) correlations. This is also the same region that has deviation from random coil chemical shifts in the secondary shift plots (Figure 2.7 b, e, h). However, only few NOE crosspeaks arising from H^{α}(i) and H^{N}(i+4) residues are observed. Instead, some NOEs from H^{α}(i) with H^{N}(i+2) (Figure 2.9 a) are observed. Considering all data, it appears that the linker peptide in the SDS micelles is not fully unstructured, and that a partial helical secondary structure may exist in this condition. The linker peptide in TFE yielded NOEs diagnostic of an α-helix between L2 and K23. Sequential NOEs between H^{α}(i) and H^{N}(i+3), H^{α}(i) and H^{β}(i+3),and H^{α}(i) and H^{N}(i+4) can be found (Figure 2.9 b). The presence of these sequential NOEs indicates strongly that residues L2-K23 in the linker peptide adopt an α-helical conformation in TFE. The helical secondary structure observed in the CD spectra together with the observed NMR parameters, *i.e.* the secondary shift and J-coupling values further support the helix formation by the linker peptide in TFE.

Calculations of peptide structure using the distance and dihedral angle restraints measured in water and in SDS detergent micelles did not yield conformers with well defined secondary structure. However, the presence of local non-random structure was still investigated in the conformers obtained from these calculations. Atom pairs from the backbone that are situated in configurations that permit them them to act as putative hydrogen bond donors and acceptors were identified. Donors and acceptors located at a distance smaller than a cutoff value of 3.4 Å (Figure 2.10) and a donor-hydrogen-acceptor angle greater than 55° were identified. In SDS micelles, some residues consistently converge with the donors and acceptors having inter atomic distances that would be conducive to the formation of hydrogen bonds. In the twenty lowest energy conformers, the amide group of A13

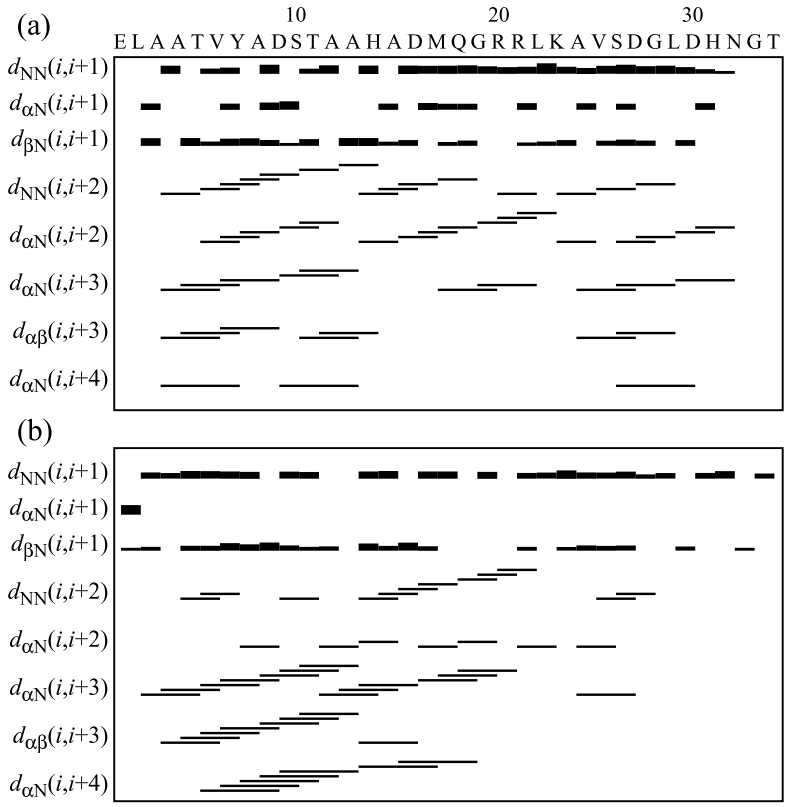

Figure 2.9: Short and medium range sequential NOEs crosspeaks observed in NalP linker peptide samples in SDS micelles (a) and TFE (b) from ^{13}C and ^{15}N resolved NOESY spectra.

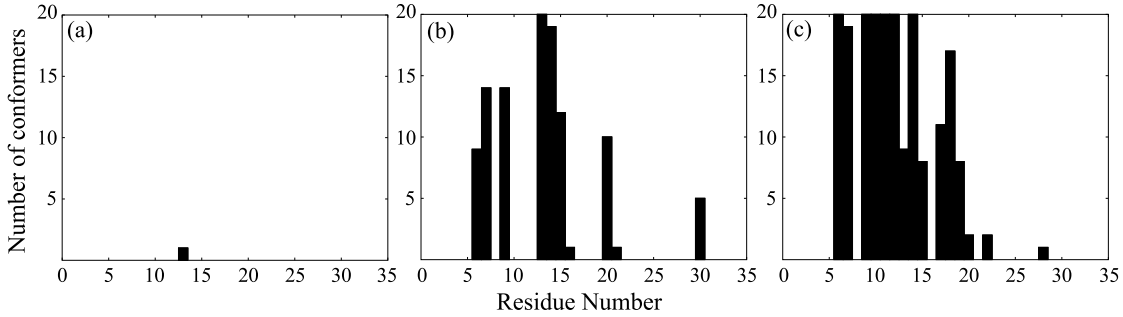

Figure 2.10: Number of conformers obtained from structure calculation in water (a), SDS micelles (b), and TFE (c) with carbonyl group in residue position i located $\leq$ 3.4 Å away from the amide group at residue i+4.

and the carbonyl group of D9 are located in spatial proximity such that the amide of A13 can act as a donor and the carbonyl of D9 can act as an acceptor. A (i+4)→(i) hydrogen bond of this kind is found in α-helices (Figure 2.10 b). However, in the water sample, of all the donor-acceptor pairs, none consistently converge in such spatial proximity in the different conformers (Figure 2.10 a). This method of determining putative hydrogen bond donors and acceptors may help identify small stretches or single turns of helix that are found in a large peptide. These features cannot be readily identified by aligning conformers and using RMSD values alone. In TFE, the structure converges into a well defined α-helix between residues L2-K23, however the residues between A24-T34 located in the C-terminus are unstructured (Figure 2.11). The calculated structures agree with the indications that the peptide in TFE has an α-helical secondary structure in the N-terminus, based on the chemical shift difference and $^{3}J_{H^{N}H^{\alpha}}$ coupling constant values. The overall RMSD for the entire peptide except the two terminal residues (L2-G33) is still very large, a lower RMSD value of 1.44 $\pm$ 0.64 Å for the backbone residues and 2.30 $\pm$ 0.71 Å for all heavy atoms was calculated for the region between residues L2-K23 (Table 2.2). Alignment of the different conformers obtained also shows that the α-helices in all conformers have similar backbone conformations (Figure 2.11).

2.3.4 Folding of NalP Translocator Domain and NalP β-barrel Constructs From Inclusion Bodies

Two constructs of NalP, the translocator domain with the linker and the β-barrel without linker, were made to investigate the effect of deletion of the linker on the in vitro folding of the translocator domain. Deletion of the linker peptide from NalP translocator domain affected the in vitro folding properties of the protein from urea unfolded inclusion bodies. In our attempts, the NalP translocator domain construct with the linker consistently yielded folded protein in detergent solutions commonly used for solubilizing the β-barrels,

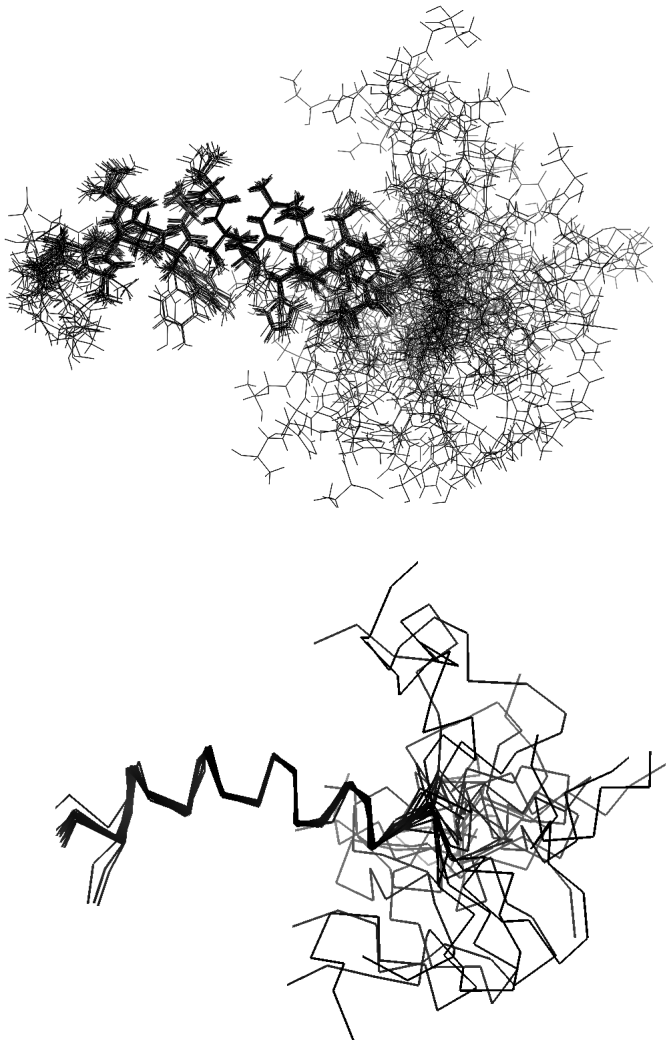

Figure 2.11: 20 least energy conformers obtained from structure calculation for the NalP linker peptide in TFE

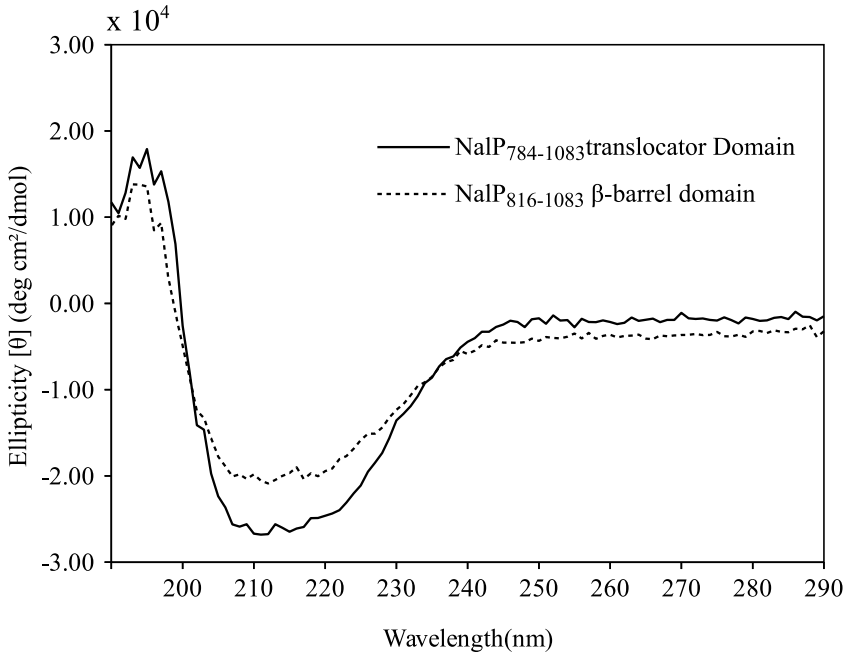

Figure 2.12: Far UV CD spectra of NalP translocator domain with linker and NalP β-barrel without linker in SB-12 detergent micelles.

namely 1,2-dihexanoyl-sn-glycero-3-phosphocholine (DHPC), n-dodecylphosphocholine (DPC), N,N-Dimethyldodecylamine N-oxide (LDAO), n-Dodecyl-N,N-dimethyl-3-ammonio-1-propanesulfonate (SB-12), β-octyl glucoside (β-OG). The CD spectrum of the translocator domain exhibited a minimum at 215 nm and a maximum at 195 nm in the CD spectrum, indicating the presence of β-sheet secondary structure (Figure 2.12). The presence of a small shoulder at 222 nm indicates small amount of α-helical secondary structure. The folded protein was obtainable at a high concentrations without excessive precipitation. The [^{1}H,^{15}N]-TROSY spectra of the construct shows well dispersed peaks characteristic of folded protein in SB-12 (Figure 2.13). A similar observation was also made in DPC, DHPC and LDAO (data not shown).

In contrast, with the NalP β-barrel construct, protein solutions that were prepared in all the different folding conditions precipitated over a duration of 48 hours. The CD spectra of

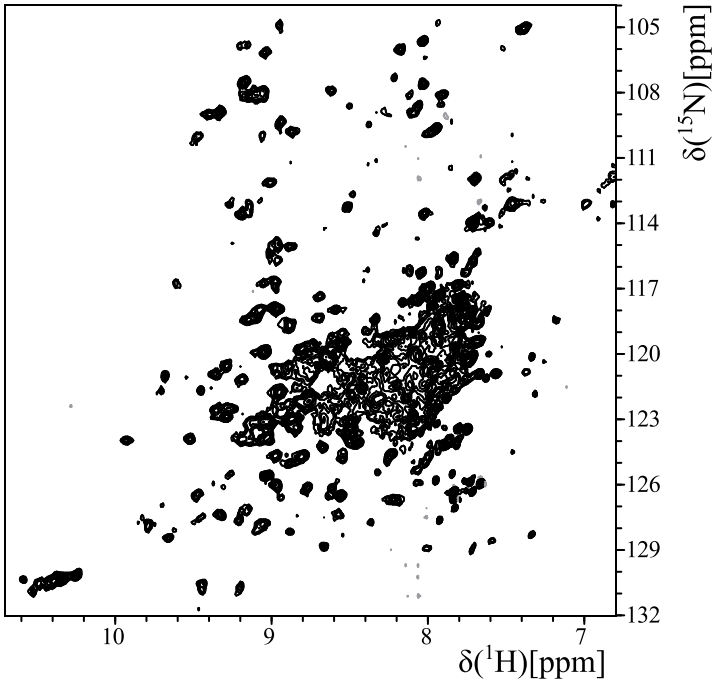

Figure 2.13: [^{1}H-^{15}N]-TROSY spectrum of NalP translocator domain in SB-12 detergent micelles at 318 K measured at 14.1 T.

freshly prepared samples of the protein in SB-12 indicate the presence of β sheet secondary structure (Figure 2.12). However, well dispersed peaks were not observed in the TROSY spectra of this construct despite the indication of secondary structure formation in the CD spectroscopy experiments. The deletion of the linker therefore seems to negatively affect the folding of the protein into detergent micelle solutions from urea unfolded inclusion bodies. The difference in the folding characteristics of the two constructs could be either due to improper folding of the barrel or due to low stability of the folded barrel in the absence of the helix formed by the linker peptide.

2.4 Discussion

Outer membrane proteins including autotransporters are believed to traverse the inner membrane in an non-native conformation and undergo interactions with periplasmic

chaperones in this stage [166, 76]. From this conformation they integrate into the outer membrane to attain their final fold. The NalP linker peptide investigated here folds into an α-helix that is located in the interior of the barrel [38]. The presence of such a helical linker in the pore of the barrel has also been established in the crystal structures of EspP (*E. coli*) and Hbp (*E. coli*) autotransporters in the pre-cleavage state and in the full length autotransporter EstA (*P. aeruginosa*) [40, 43, 39, 42]. After cleavage in EspP, a single turn of helix which is perpendicular to the axis of the barrel is retained in the pore of the β-barrel.

From the structure of these folded translocator domains alone, it is difficult to hypothesize a role for the linker in the assembly of the autotransporter or in the transport process. While the sequence of the linker peptide is varied across autotransporters from different organisms, it is conserved within families of similar autotransporters such as Serine Protease Autotransporters of Enterobacteriaceae (SPATEs). The linker seems to have a role in the transport and assembly of autotransporters because deletion of the linker or non-conservative mutations in the linker peptides either reduce or completely eliminate membrane localization and transport processes [152, 44, 151, 167].

In vivo, using a signal sequence from PhoE, [38] were able to target the NalP translocator domain both with and without the linker peptide to the outer membrane, but the mutant without the linker peptide had significantly lower levels of expression on the membrane. Additionally, the protein preparation protocols to obtain post cleavage constructs of both EspP and Hbp involve starting with larger constructs that include a small stretch of protein sequence upstream to the translocator domain, the final constructs were obtained after intra-barrel cleavage of the linker [40, 43]. Taking all the above factors and the results obtained in our translocator domain folding studies into consideration, the role of the linker peptide in the assembly of autotransporters appears to be non-trivial.

The structural studies with the linker peptide presented here indicate that the linker

peptide has increasing levels of helicity moving from water to SDS micelles and to TFE. The structure of an α-helix is stabilized by the formation of intramolecular hydrogen bonds between the amide groups and the carbonyl groups located on the backbone of the peptide. The hydrogen bond formed enthalpically compensates for the loss of entropy caused by the formation of the ordered structure [168]. Alternatively, the backbone residues can also form hydrogen bonds with the solvent water molecules, but these hydrogen bonds do not contribute to the stability of the helical structure. Organic co-solvents such as TFE stabilize helices by coating the peptide and causing the elimination of intermolecular hydrogen bonds between the peptide and the water molecules [169]. The low helicty of the NalP linker peptide in SDS and the random coiled structure in water can be explained by lack of intramolecular hydrogen bonds in those conditions, with intermolecular hydrogen bonds with water being present instead. On the biological membrane as well, the elimination of intermolecular hydrogen bonding with water would be required for the formation of a helix by the linker peptide. One way to achieve this would be by the burial of the peptide into the hydrophobic interior of the lipid bilayer. Subsequent assembly of the β-barrel around this nascent helix could lead to the formation of an α-helix, which is stabilized by interactions with the interior of the β-barrel. In EspP and related SPATEs, hydrophobic residues in the linker peptide have been shown to be conserved and are critical in the translocation process [167]. It has been suggested therein that these residues may either form a hydrophobic core or be involved in hydrophobic interactions that are critical for the function of the autotransporter. One possible hydrophobic interaction would be the interaction of the linker with the biological membrane. Many viral fusion peptides (some of which are located in the interior of the protein) serve to anchor larger fusion protein domains to the surface of the biological membrane. They function by forming a helix, upon interaction with the biological membrane [137]. The linker peptide may function in a mechanism analogous to that.

The assembly of outer membrane proteins including autotransporters is mediated by membrane chaperones belonging to the Omp85 family. The structures of outer membrane chaperones TamA and BamA were solved recently and they have enabled the development of more detailed models for OMP assembly in the outer membrane. In [82], simulations show that there may be localized destabilization of the membrane near strands 1 and 16 of the chaperone. This location has been proposed as an entry point for OMP integration into the membrane. Both [82] and [61] suggest a lateral gating mechanism at the interface of strands 1 and 16, where the β-barrel of the chaperone opens to form a hybrid barrel with the folding OMP. In [61], the structure of TamA, which is the chaperone specific to autotransporters, is reported. The folding of autotransporters and subsequently the position of the linker has been speculated therein. In one scenario, it has been suggested that the linker could diffuse through the lipid bilayer at a location adjacent to the β-barrel as folding occurs. This is consistent with the model discussed here, where the linker is buried into the lipid bilayer and folds into an α-helix. The assembly of the β-barrel could then occur around the linker to finally attain the folded structure of the autotransporter. In an alternative scenario, the secretion has been proposed to occur through a large hybrid barrel formed by β-strands from the chaperone and the autotransporter, enabling the linker to be located directly inside the barrel. In this case, there seem to be no obvious interactions between the linker and the biological membrane and the location of the linker in the β-barrel may be an outcome of the topology of the β-barrel. Since the linker seems to have no natural tendency to form a helix, the formation of the linker would then have to be mediated by interactions with residues either in the periplasmic domains of the chaperone or the interior of the pore. In either case, based on the results obtained here, it appears likely that the formation of the helix in the linker peptide occurs due to intermolecular interactions, presumably in a hydrophobic environment.

3. DETERMINATION OF THE STABILITY OF THE LINKER REGION OF THE NalP AUTOTRANSPORTER USING THERMAL DENATURATION EXPERIMENTS

3.1 Introduction

Thermal unfolding of peptides is commonly determined by measuring the circular dichroism of the peptide with increasing temperature. The unfolding reaction is modeled using helix coil transition models such as the Zimm-Bragg model [170] or the Lifson-Roig model [171] to obtain the thermodynamic parameters such as ΔH and the equilibrium constants for the formation of the helix and the helix nucleation parameter. These methods provide a macroscopic thermodynamic description of the peptide denaturation without much insight into the specific interactions that contribute to the helix coil transition of peptides. In these models, each helix forming unit on the peptide is considered to be equivalent and all neighboring residues are considered equivalent when describing the cooperativity in folding. However, in reality the specific sequence of different peptides affect their propensities to form helices and the stability of the helices thus formed. Thus residue specific interactions may play an important role in the secondary structure stability and helix coil transition of helical peptides. Investigation of such interactions requires site specific resolution as provided by NMR spectroscopy.

NMR spectroscopy is a very popular method for determining the structures of peptides. Apart from getting the structure by direct estimation of inter-proton distances, additional indicators can also be observed to gain insight into the structure of the peptide. The chemical shift of the different residues are statistically correlated to the secondary structure [163]. Values of J-coupling constants are related to the backbone dihedral angles by the Karplus relation [155]. Exchange rates and temperature coefficients of amide protons are

indicators of the presence of hydrogen bonds [172]. These parameters can be monitored over increasing temperatures to determine residue specific differences in the thermal unfolding of peptides.

Distance restraints for NMR structure calculation are obtained from NOEs. The presence of NOE crosspeaks between two spins indicates that they are in close spatial proximity. All other things equal, the intensity of an NOE crosspeak is proportional to the inverse sixth power to the distance between the spins. However, NOEs are not commonly used to determine thermal unfolding because the relation of NOE crosspeak intensity to temperature is not trivial. NOE crosspeak intensity depends on the global correlation time of the molecule, which depends on the temperature not only directly but also on factors such as viscosity of the solvent, which in turn depend on the temperature. Also exchange of labile protons with the solvent also may change the observed NOE intensity. Considering all these factors, it may be difficult to theoretically predict actual NOE intensity values as a function of temperature. Despite this, the relative change in NOE intensity over temperature been proposed to be a reliable indicator of unfolding in peptides [173].

In this study, the thermally induced unfolding of a peptide is studied using CD and NMR spectroscopy. The peptide used is the linker peptide of the autotransporter protein NalP from *N. meningitidis*. In the crystal structure of the translocator domain of the autotransporter, this linker peptide adopts an α-helical conformation. Previously, the structure of the peptide in water, SDS detergent micelles and in trifluoroethanol (TFE) was determined using NMR spectroscopy. In TFE, the linker peptide has an α-helical secondary structure in the N-terminus and the C-terminus exists in a random coiled conformation. In water, the peptide is unstructured and in SDS it has a relatively low content of α-helical secondary structure. The thermally induced unfolding of the peptide was characterized by measuring changes in chemical shifts and relative intensities of NOE crosspeaks with increasing temperatures.

3.2 Experimental Procedures

3.2.1 Sample Preparation

The NalP linker peptide used is expressed as a fusion construct with a SUMO tag. The tag is released by proteolytic cleavage and the peptide is subsequently purified as described in section 2.2.1. Samples were prepared for CD spectroscopy by dissolving the lyophilized peptide powder prepared from an unlabeled culture to a concentration of 7 μM peptide in TFE (Alfa Aesar, Ward Hill, MA). Peptide for the NMR samples were prepared from cultures grown in minimal media with $^{15}NH_4Cl$ and $^{13}C_6$-glucose acting as the nitrogen and carbon sources respectively. NMR samples were prepared by dissolving 1 mM peptide in 2,2,2-TFE-1-$^2H_2$ (Cambridge Isotope Laboratories, Andover, MA) with 1 mM tetramethylsilane. It is to be noted that the NMR sample is the same sample used in section 2.2.3 and the experiments described here require only ^{15}N isotopic enrichment.

3.2.2 Circular Dichroism Spectroscopy

All circular dichroism (CD) experiments were recorded on a Model 62DS CD Spectrometer (AVIV Biomedical Inc., Lakewood, NJ, USA). Initial wavelength scans were performed at temperatures of 288 K and 348 K. Wavelength scans were done between 320 nm and 190 nm, using a bandwidth of 1 nm and increments of 1 nm with a signal averaging time of 10 s at each wavelength point. Thermal denaturation experiments were measured at 222 nm by heating the sample from 288 K to 356 K with temperature increments being done at intervals of 1 K. An equilibration of 5 min was allowed for each temperature point with a signal averaging time of 30 s.

3.2.3 NMR Spectroscopy

NMR spectra were measured on a 11.7 T Avance III spectrometer fitted with a TCI triple resonance cryoprobe (Bruker, Billerica, MA, USA). The backbone and side chain

experiments were used to assign the backbone and sidechain chemical shifts at 298 K as described in section 2.2.3. [^{1}H-^{15}N] HSQC, ^{15}N resolved NOESY (150 ms) and ^{15}N resolved TOCSY (MLEV-17 mixing sequence, 100 ms at 10.7 kHz) experiments were measured at temperatures between 288 K and 248 K at intervals of 10 K. Using the initial assignments at 298 K as a reference, the HSQC and TOCSY experiments were used to assign the ^{1}H resonances at each temperature. The Sequential connectivity in the ^{15}N resolved NOESY experiment was used to verify the assignments of the mapped resonances. The ^{15}N resolved TOCSY experiment was not sufficiently sensitive at 288 K so a HCCCONH (DIPSI2 mixing sequence, 13 ms at 8.6 kHz) was used to obtain the ^{1}H sidechain assignments at that temperature.

3.2.4 Data Processing

Assignment of chemical shifts were done using the CARA software [174]. Initial assignments for the crosspeaks picked on the ^{15}N resolved NOESY spectrum were obtained at 298 K using the CANDID routine in the software CYANA [156]. The NOE assignments provided by CYANA were converted to spin links in CARA using a Lua script. The assignments were verified and corrected manually, and any other additional assignments were added manually. The list of spin links was restricted to a list of diagnostic peaks containing only H^{N}(i)$\rightarrow H^{N}$(i+2), H^{N}(i)$\rightarrow H^{N}$(i-2), H^{N}(i)$\rightarrow H^{A}$(i-3) and H^{N}(i)$\rightarrow H^{\alpha}$(i-4), H^{N}(i)$\rightarrow H^{\alpha}$(i-3) and H^{N}(i)$\rightarrow H^{\alpha}$(i-4) NOEs. The chemical shift change and normalized NOE intensity of the diagnostic peaks were plotted against temperature and fitted to their respective functions using MATLAB. A linear function was used to fit the chemical shift change over temperature and a cubic spline function was used to fit the NOE plots.

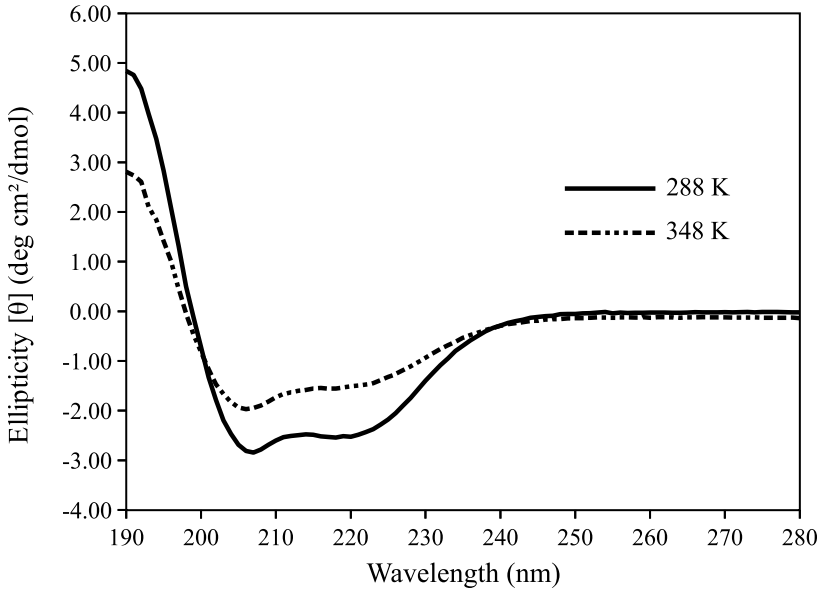

Figure 3.1: Far UV CD spectra of NalP linker peptide measured at temperatures of 288 K and 348 K.

3.3 Results

3.3.1 Thermal Denaturation of NalP Linker Peptide Using CD spectroscopy

The Far UV CD spectrum of the NalP linker peptide measured at 288 K has spectral features that are characteristic of α-helical secondary structure (Figure 3.1). The spectrum has a two minima at 208 nm and at 222 nm and a maximum at 190 nm. At 348 K, these features are still present in the spectrum, but the absolute values of the ellipticities are smaller than at 288 K. The fractional helicity (p_h) of the peptide was calculated from the mean residue ellipticities (θ) at 222 nm, using equation 2.1. The fractional helicity of the peptide, as measured using CD spectroscopy, reduces from an value of 68% at 288 K to 35% at 348 K.

The loss of helicity with increasing temperature was observed by measuring the circular dichroism at 222 nm with increasing temperature and calculating the value of the

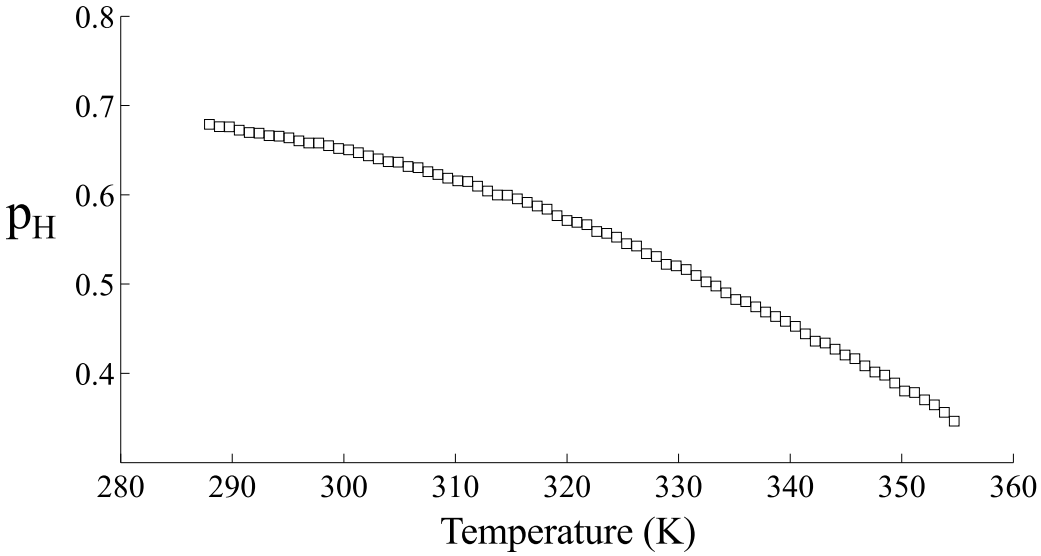

Figure 3.2: Fraction of helicity (θ_H) NalP linker peptide as measured using CD spectroscopy between temperatures of 288 K and 348 K.

fractional helicity (p_h) as described above (Figure 3.2). Helix-coil transitions of this type are usually modeled using the Zimm-Bragg model. It is however, not possible to fit this data using the Zimm-Bragg model for helix coil transitions because the fraction helicity even at the lowest temperature measured is 0.68, and the value does not seem to approach a value of 1 even for temperatures lower than those measured. In the NMR structure of the NalP linker peptide in TFE, solved at 298 K, a stretch of residues in the C-terminus of the peptide is unstructured and the peptide may not transition to a complete helix under the experimental conditions. For the Zimm-Bragg model for helix coil transition to be applicable, the peptide should be able to transition completely to both the helix and the coil state. However, the data shows that the fractional helicity reduces to half the initial value and that the peptide begins to unfold in these temperatures. The concave shape of the curve indicates that the initial temperatures in the experiment are below the melting temperature of the peptide.

3.3.2 Thermal Denaturation of NalP Linker Peptide Determined by NMR spectroscopy

Since the NMR experiments require measurement of spectra for extended periods of time at elevated temperatures, it was required to initially verify the quality of the sample at each temperature. [^{1}H-^{15}N]-HSQC spectra were measured at each temperature (Figure 3.3) and the number of amide crosspeaks was counted to check for the appearance of any new peaks from products of peptide degradation. In the HSQC spectra, at the higher temperatures of 328 K, 338 K, and 348 K, the appearance of small additional peaks were observed (Figure 3.3). It is likely that these peaks new peaks belong to products of degradation of the peptide because these additional peaks persist when HSQCs were measured again in the lower temperature after the completion of experiments at the higher temperatures (data not shown). Unambiguous assignments of side chain proton chemical shifts was still possible at the higher temperature from the ^{15}N resolved TOCSY spectra. Representative strips from the ^{15}N resolved TOCSY spectra are shown for residues Ala-8 and Asp-9 (Figure 3.4). In the strips, the peaks from the peptide are still well resolved and the appearance of these new peaks does not seem to interfere with the assignment of chemical shifts.

An overlay of the HSQC measured at different temperatures (Figure 3.5) shows that both the amide proton and amide nitrogen chemical shifts change with temperature and that the temperature dependence of these chemical shifts are different for each residue of the peptide. The amide chemical shifts are plotted against the temperature for each residue. The change in amide chemical shift is linear with temperature for all values except at the highest temperature. A straight line was fitted to the initial six points of the data, the slope of the line gives the amide proton temperature coefficients ($\Delta\delta(H^N)/\Delta T$) of the different residues. Amide proton temperature coefficients are affected by the exchange of the amide proton with the solvent, which in turn is affected by hydrogen bonding. Amide

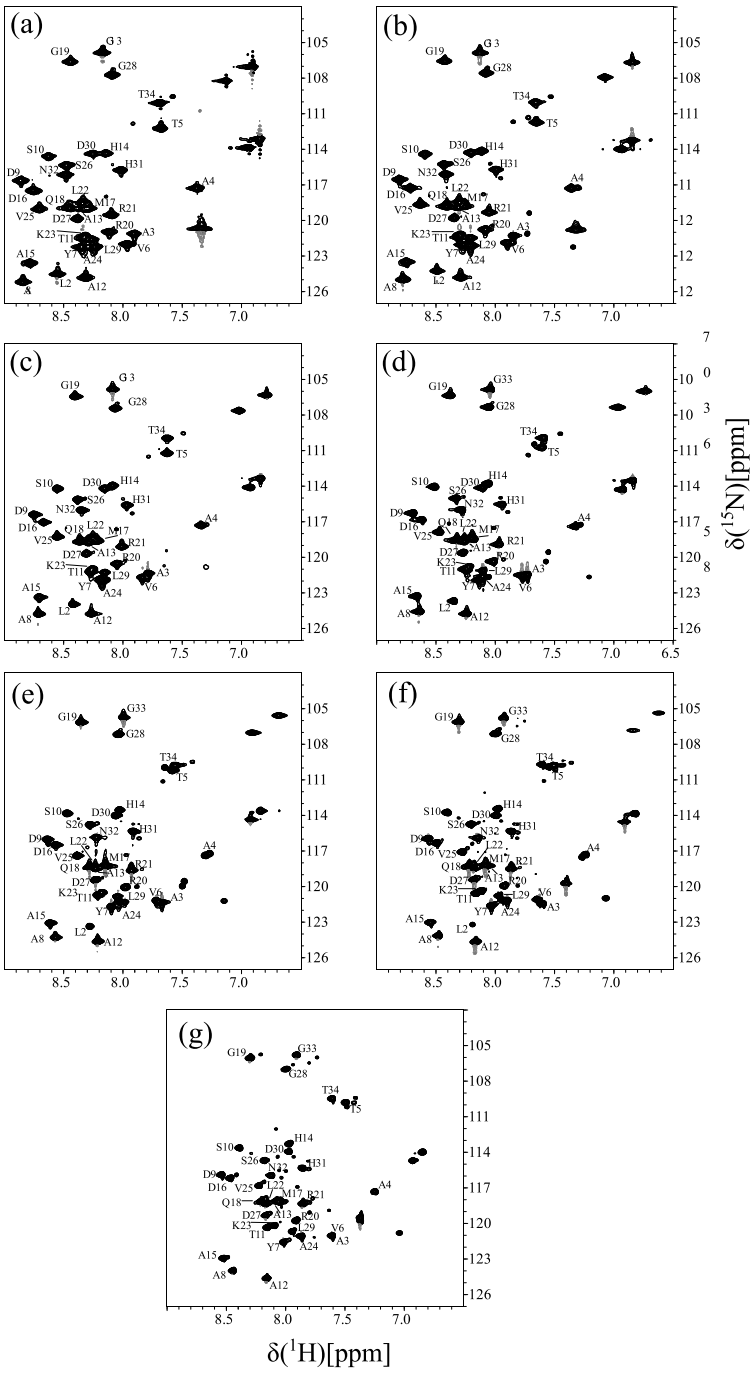

Figure 3.3: [^{1}H-^{15}N]-HSQC spectra of NalP linker peptide in TFE at (a) 288 K, (b) 298 K, (c) 308 K, (d) 318 K, (e) 328 K, (f) 338 K, and (g) 348 K.

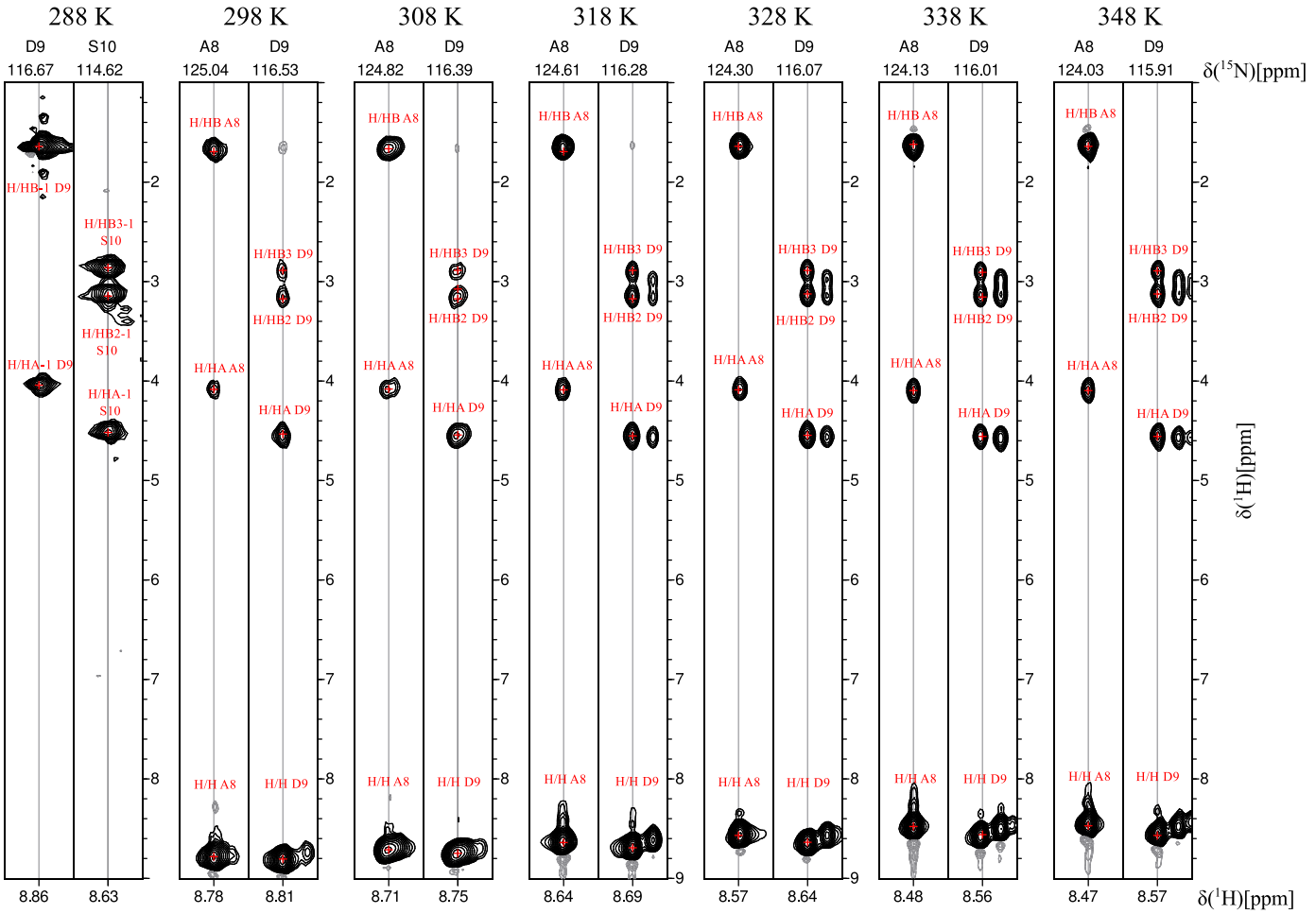

Figure 3.4: [δ(^{1}H),δ(^{1}H)] strips of residues Ala-8 and Asp-9 from ^{15}N resolved TOCSY spectra of NalP linker peptide measured at different temperatures as indicated. Strips are centered around the amide ^{1}H and amide ^{15}N chemical shifts of the respective residues at each temperature.

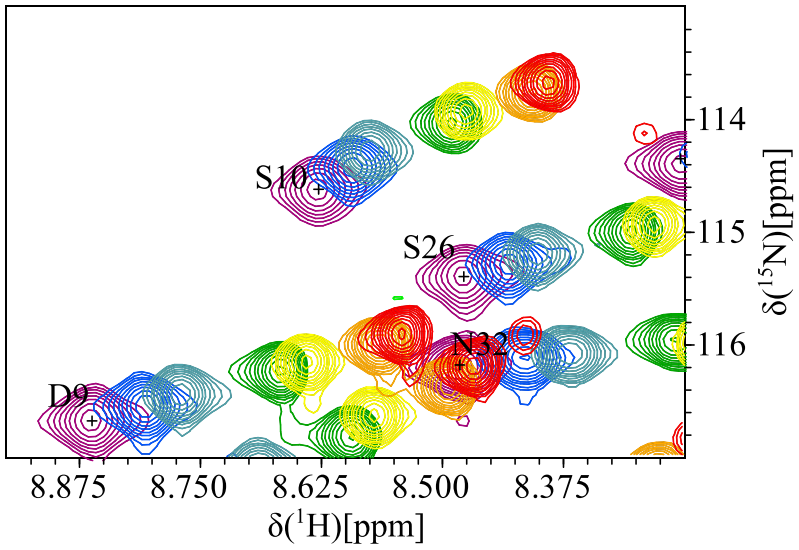

Figure 3.5: Overlay of [^{1}H-^{15}N] HSQC spectra of NalP linker peptide in TFE at 288 K (purple), 298 K (blue), 308 K (teal), 318 K (green), 328 K (yellow), 338 K (orange), and 348 K (red).

protons that do not form intramolecular hydrogen bonded will exchange more readily with the solvent and their chemical shifts will change strongly with increasing temperature compared to residues that are hydrogen bonded. In α-helices there is an N(i+4)$\rightarrow$CO hydrogen bond. The amide protons that are involved in intramolecular hydrogen bond will have exchange rates higher than -4.6 ppb/K. However, for hydrogen bonds present in α-helices, lower temperature coefficient values have been observed and it has been suggested that a lower cut off of -5.6 ppb/K may be applied [175, 172, 176]. The amide proton temperature coefficients of different residues of NalP linker peptide have been plotted (Figure 3.6). A continuous stretch of residues having temperature coefficients higher than -4.6 ppb/K exist between Ser-10 and Ala-24. In the NMR structure, these residues adopt an α-helical conformation. Residue number seven shows the lowest value of amide proton temperature coefficient, however this residue is a tyrosine. Aromatic residues sometime have abnormally low amide proton temperature coefficients because their chemical shifts

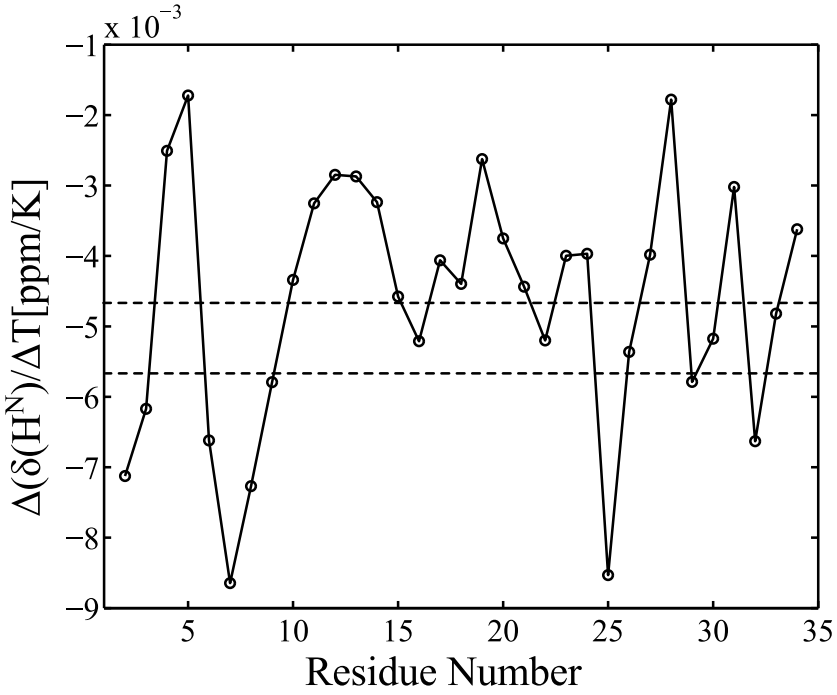

Figure 3.6: Temperature coefficients of the amide proton chemical shifts of NalP linker peptide ($\Delta\delta(H^N)/\Delta T$) plotted against the residue number. Dashed lines have been plotted at a temperature coefficient values of -4.6 ppb/K and -5.6 ppb/K.

are affected by ring current shift from the aromatic side chain. This effect may also extend to neighboring residues [176].

A weighted average chemical shift change parameter is often used as a qualitative index of structural changes in proteins [177, 178, 179]. The change in chemical shift for each type of spin is weighted by a factor that compensates for the variance in values observed for that type of spin. Here, a similar parameter is defined as in equation 3.1, where α_N is the scaling factor applied to amide nitrogen chemical shifts. $\Delta\delta(H^N)$ and $\Delta\delta(N)$ are the changes in amide proton and nitrogen chemical shifts from the initial value at 305K and a scaling factor of 0.154 was used [177].

$$\Delta_W\delta(H^N, N) = \sqrt{\Delta\delta(H^N)^2 + (\Delta\delta(N) \times \alpha_N)^2} \tag{3.1}$$

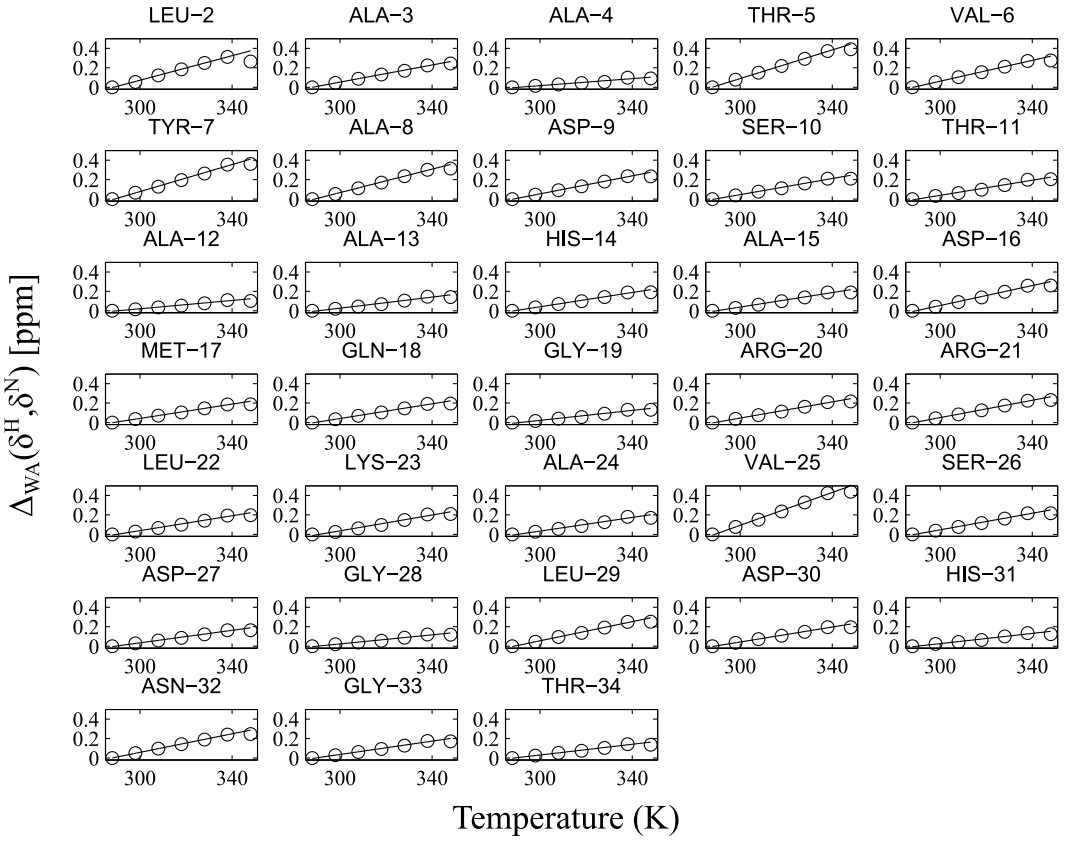

Figure 3.7: Change in weighted average chemical shift ($\Delta_W\delta(H^N, N)$) of different residues of NalP linker peptide plotted against temperature.

The weighted average chemical shift change ($\Delta_W\delta(H^N, N)$) was plotted against temperature (Figure 3.7). Like in the case of the amide proton chemical shift, the weighted average chemical shift is also linear for all values except the highest temperature. The temperature coefficient for the weighted average chemical shift change was obtained by fitting a straight line to data points for the initial six temperatures ($\Delta_W\delta(H^N, N)/\Delta T$). The $\Delta_W\delta(H^N, N)/\Delta T$ values obtained for each residue is indicated on the NMR structure of the NalP linker peptide (Figure 3.8).

Many residues in the stretch between position 2 and 8 have relatively higher values of $\Delta_W\delta(H^N, N)/\Delta T$. This may be due to the presence of the aromatic residue Tyr-7. How-

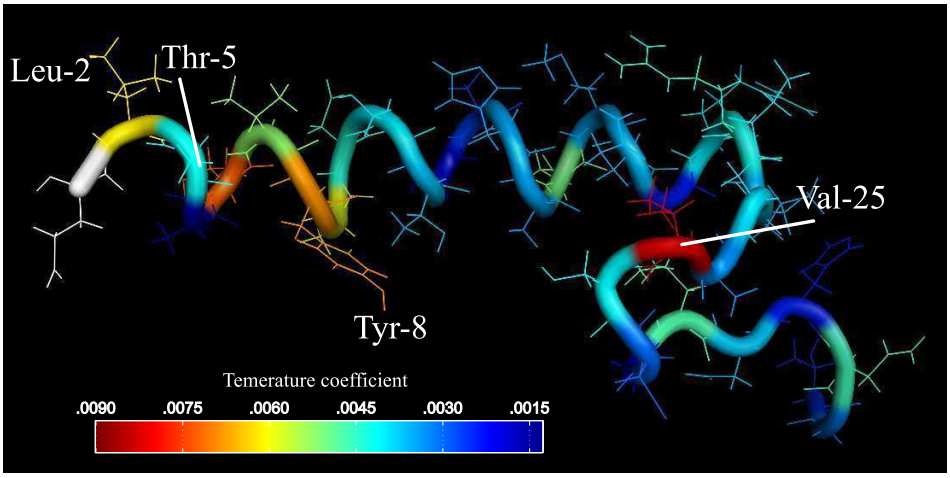

Figure 3.8: The NMR structure of NalP linker peptide in TFE. Individual residues are colored based on the values of the temperature coefficients of the weighted average chemical shifts ($\Delta_W\delta(H^N, N)/\Delta T$). The N-terminus is colored white since amide proton and nitrogen chemical shifts were not determined for this residue.

ever, even residues Lys-2 and Thr-5 that are not neighbors of Tyr-7 have higher values of $\Delta_W\delta(H^N, N)/\Delta T$. It is possible that the N-terminus of the peptide is less stable and may be frayed readily when the unfolding of the peptide occurs. The C-terminus of the peptide seems to be already unstructured in the lower temperature. The $\Delta_W\delta(H^N, N)/\Delta T$ are also lower for this region of the peptide. With the exception of Val-25, all residues have low $\Delta_W\delta(H^N, N)/\Delta T$ values.

H^N(i)$\rightarrow$ H^N(i+2), H^N(i)$\rightarrow$ H^N(i-2), H^N(i)$\rightarrow$ H^α(i-3), and H^N(i)$\rightarrow$ H^α(i-4)NOE crosspeaks are characteristic of α-helices. A restricted set of these NOE crosspeaks were picked from the NOESY spectra measured at each of the temperatures. Representative strips from the ^{15}N resolved NOESY spectra at the different temperatures are shown in (Figure 3.9). As expected, it can be seen that the intensity of the crosspeak decreases with increasing temperature. The intensity values for each NOE cross peak were normalized and plotted against temperature and fitted with a cubic spline function (Figure 3.10). The temperature at which the NOE intensity is half that of the initial value is calculated and

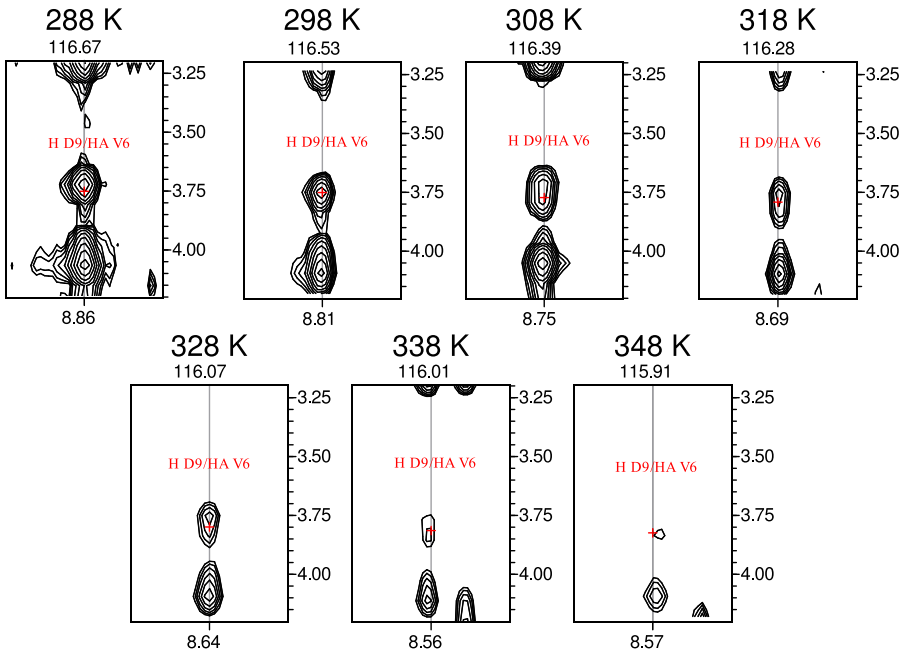

Figure 3.9: [$\delta(^1\mathrm{H})$,$\delta(^1\mathrm{H})$] strips of Asp-9 from ^{15}N resolved NOESY spectra of NalP linker peptide measured at different temperatures as indicated. Strips are centered around the amide ^{1}H and amide ^{15}N chemical shift of Asp-9 at each temperature. The peak H^N(i)$\rightarrow\mathrm{H}^\alpha$(i-3) NOE crosspeak with Val-6 is indicated in each strip.

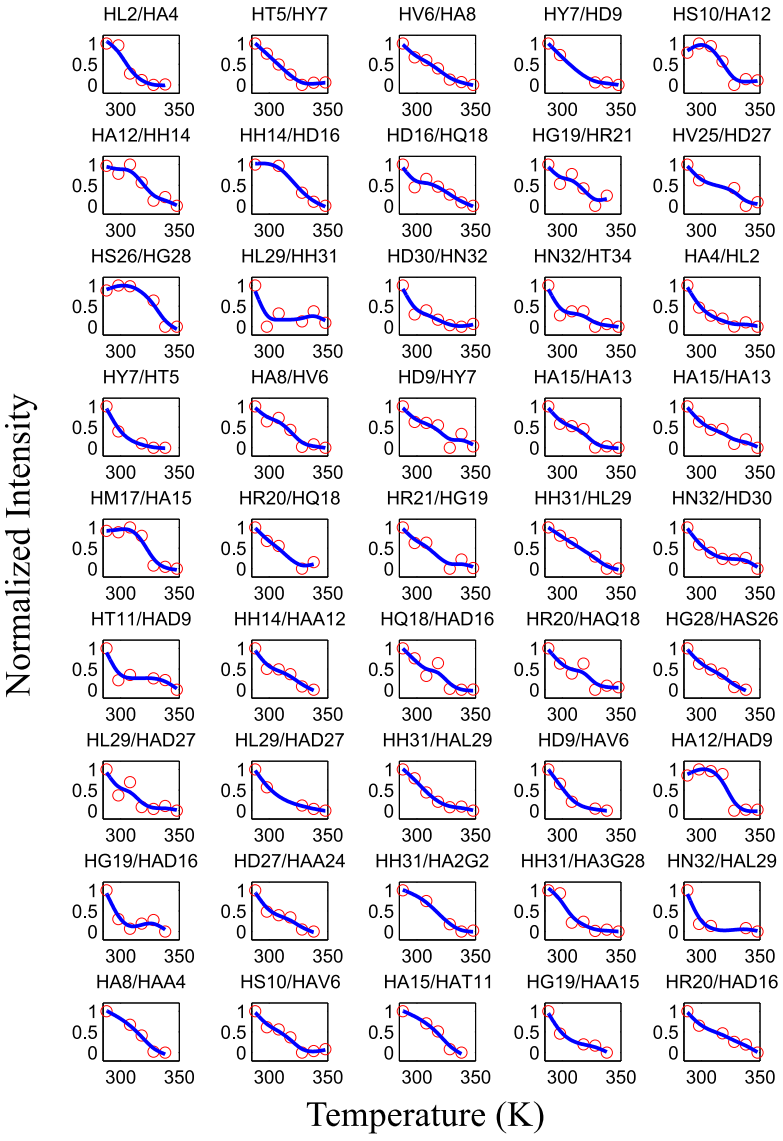

Figure 3.10: Relative intensity of NOE crospeaks from NalP linker peptide plotted as a function of temperature.

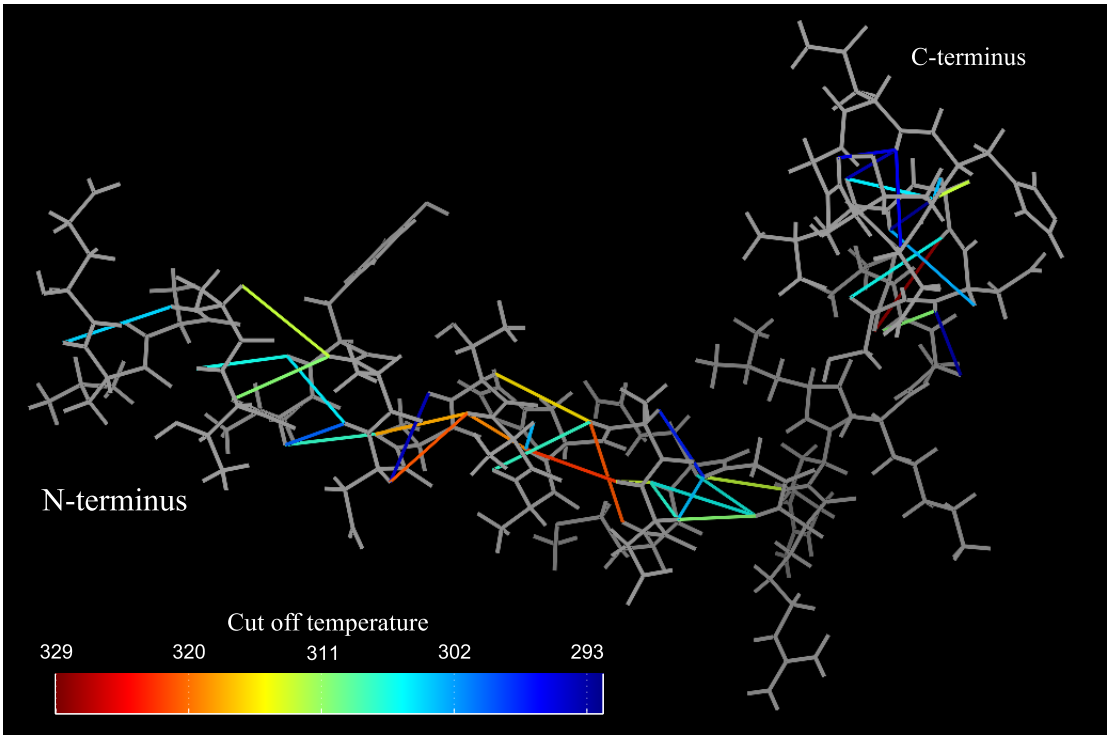

Figure 3.11: Structure of NalP linker peptide in TFE. NOE crosspeaks observed between different spins are indicated using a line. Lines are colored according to the cutoff temperatures calculated from (Figure 3.10).

used as a cutoff temperature. This cutoff temperature is indicated on the structure of the NalP linker peptide (Figure 3.11). All the NOE crosspeaks having relatively high cutoff temperatures arise from spins belonging to residues between Ala-8 and Gln-18 on the sequence. The NOEs from the C-terminus of the peptide all exhibit lower cut-off temperatures, in the NMR structure this region of the peptide is random coiled. All the NOE crosspeaks having relatively high cutoff temperatures arise from spins belonging to residues between Ala-8 and Gln-18 on the sequence. The cutoff temperatures for the NOEs from regions flanking this stretch are lower. This possibly indicates that the unfolding on the peptide may be initiated from the ends of the α-helix.

3.4 Discussion

The NalP linker peptide undergoes partial unfolding under the temperatures measured. From the CD experiments it can be seen that even in the highest temperature measured, there is some residual helicity in the peptide. The region between Ala-8 and Gln-18 on the peptide has the highest temperature cut-off values from the NOE experiment. This region also contains a continuous of stretch residues having amide proton temperature coefficients that are greater than the -4.6 ppb/K cut-off for hydrogen bonded protons. This region seems to be relatively higher stability than the other regions of the peptide and perhaps retains more of its structure in higher temperatures contributing to the residual helicity in those temperatures. The NOE cut off temperatures of residues adjacent to this stretch are lower in comparison. Upon increase of temperatures, it is likely that these regions will lose structure sooner than the region between Ala-8 and Gln-18, thus initiating the unfolding reaction in the termini of the helix.

In the NMR structure of the NalP linker peptide in TFE, we observed that the C-terminus is random coiled. However, in the crystal structure of the translocator domain of the NalP autotransporter [38], this region is an α-helix. It is possible that additional favorable interactions occur when the linker is positioned in the pore of the barrel adding to its stability. It has been hypothesized from the crystal structure that the presence of 7 seven salt bridges, 16 hydrogen bonds and other van der Waal's contacts act to stabilize the structure of the helix. Interestingly, the stable region identified in TFE also has some H^N(i)$\rightarrow$ H^α(i-3), and H^N(i)$\rightarrow$ H^α(i-4) NOEs in the sample of the NalP linker peptide in SDS detergent micelles. In SDS putative hydrogen bond donors identified also are from this region. This makes those set of residues a good candidate as the nucleation site for helix formation. Also functionally, since the C-terminus of the peptide is attached to the translocator domain, it may be required to be more mobile until the linker attains its final

folded conformation. Thus it can be speculated that the initiation of the helix formation happens in the stretch of stable residues and is propagated from there and the C-terminus is finally stabilized in the β-barrel after other tertiary contacts are formed.

4. THERMALLY INDUCED HELIX-COIL TRANSITIONS IN MEMBRANE ASSOCIATING PEPTIDES

4.1 Introduction

Two important categories of membrane associating peptides are cationic antimicrobial peptides and viral fusion peptides. While both categories differ in their designated functions, their mode of action is primarily based on an interaction of the peptide with the biological membrane [138]. The amino acid composition and sequences of the two families of peptides are very different. Cationic antimicrobial peptides are amphipathic in nature. They are usually soluble in water, while at the same time have the ability to interact with the cell membrane. They are composed of up to $\sim$50% hydrophobic residues and have multiple cationic residues, giving them a net positive charge at neutral pH [128]. The cationic residues are usually spaced out on the sequence of the protein such that upon formation of a helix, the residues are located on one face of the helix, with hydrophobic residues populating the other face. This arrangement enables them to adopt configurations where the hydrophobic face of the peptide is buried into the lipid bilayer and the charged surface is positioned near the polar head groups of the lipid [125, 126, 180]. On the other hand, the sequences of viral fusion peptides contain a very high fraction of glycine and alanine residues. It is believed that this composition enables them to have a higher conformational mobility when interacting with the membrane [136]. While antimicrobial peptides have a net positive charge between +2 and +9, fusion peptides are usually neutral or sometimes even anionic [138].

Cationic antimicrobial peptides are minimal in their design. They do not possess any special binding pockets or motifs that recognize the target organism. Despite this, they are able to interact with the membranes of the pathogen and cause toxicity while creating

no such effect in the host organism [123]. It has been suggested that the selective toxicity of these peptides towards bacterial hosts stems from the negative charge of the bacterial cell membrane compared to that of eucaryotes [131, 128]. The ability to interact with the membrane and the selectivity of this interaction is derived from the sequence of the peptides. The effect of physical properties of the peptide such as hydrophobicity and charge, on its toxicity and specificity of the peptide have been studied. It has been observed that both the net positive charge and the presence of positive charges on the hydrophilic face of the peptide are determinant factors for biological activity. In the antimicrobial peptide L-V13K studied, the reduction of net charge below a threshold of +4 eliminated antimicrobial effect of the peptide [181, 182].

Many viral fusion peptides have negatively charged residues [183, 15]. The fusion activity of these peptides are also often triggered by a change in pH. In the host organism, this is realized by endocytosis of the virus [139, 137]. The pH inside the endosome is acidic when compared to the extracellular milieu. The change in pH has been shown in some cases to cause the protonation of the negatively charged residues to mediate a conformational change that enables the fusion process [13]. In viral fusion peptides also, charge, or lack thereof, is a determining factor of biological activity. Thus, it is of interest to biophysically characterize electrostatic interactions between membrane associating peptides and the biological membrane.

Two membrane associating peptides, the cationic antimicrobial peptide Magainin2 and a G1V mutant of the hemagglutinin viral fusion peptide from the influenza virus have been selected as model molecules. Magainin2 is a 23 residue cationic peptide (sequence - GIGKFLHSAKKFGKAFVGEIMNS) that was first discovered in the skin of *Xenopus laevis* [184]. It has four lysine residues in positions 4,10,11 and 14 respectively and glutamate at position 19, giving it a net charge of +3 at neutral pH. Magainin2 is unstructured in water. However, it adopts an α-helical structure in SDS and DPC detergent micelles and

in the helix stabilizing organic solvent TFE [144, 185]. The three phenylalanine residues that are present in the peptide are positioned on the same face of the peptide. That face is rich in hydrophobic residues and additionally has two isoleucine, one valine and one alanine residues. The HA G1V peptide (sequence - VLFGAIAGFIENGWEGMIDG) is a fusion incompetent variant of the hemagglutinin fusion peptide [15]. In DPC detergent micelles, the NMR structure of the peptide has been solved, and it adopts a helical structure between residues Phe-3 and Glu-15 (PDB ID: 2MAG). The sequence of the peptide has two glutamate and one aspartate residues, giving a net charge of -3 at neutral pH.

In this work, the role played by charge in the interaction of the two membrane associating peptides with membrane mimetics is determined by a combination of CD and NMR spectroscopy. The membrane mimetics used are detergent micelles. The charge of the detergent micelles was changed by using detergent micelles of an anionic detergent (sodium dodecyl sulfate), a cationic detergent (dodecyl trimethyl ammonium chloride) and a zwitterionic detergent (dodecylphoshpocholine). Thermally induced denaturation of the peptides was observed in three different detergent micelles of differing charge using CD spectroscopy. Furthermore, residue specific effects caused by altering the net charge of the detergent micelle were investigated using NMR spectroscopy by observing changes of chemical shift and peak intensity of NOEs in the Magainin2 peptide in SDS and DPC micelles.

4.2 Experimental Procedures

4.2.1 Sample Preparation

Peptide samples for Magainin2 and HA G1V, prepared by solid phase peptide synthesis, were obtained commercially (Anaspec Fremont, CA, USA). The peptide powder provided by the manufacturer was dissolved in 10 mL 30% (v/v) acetonitrile with 0.1% (v/v) trifluoroacetic acid for each 1 mg of peptide powder. Peptides were portioned out for

each sample to be prepared by aliquoting a measured volume of the peptide solution and lyophilizing the peptide to remove the solvent. Samples were prepared by subsequently dissolving the aliquoted peptide powder in the buffer of choice. Samples for CD spectroscopy were prepared by dissolving 0.05 mg/mL of either peptide in 20 mM sodium phosphate with 100 mM of the respective detergents adjusted to pH 6.8. Samples were prepared in the cationic detergent dodecyl trimethyl ammonium chloride (DTAC), the anionic detergent sodium dodecyl sulfate (SDS) and the zwitterionic detergent dodecyl phosphatidylcholine (DPC). Samples for NMR spectroscopy were prepared by dissolving 1 mM Magainin2 peptide in 20 mM sodium phosphate 1 mM 4,4-dimethyl-4-silapentane-1-sulfonic acid (DSS), 5% v/v ^2H_2O along with 150 mM or either SDS or DPC detergent respectively. Samples were degassed by four cycles of freezing and thawing under vacuum, and sealed under nitrogen gas for the NMR measurements at higher temperatures.

4.2.2 CD Spectroscopy

Circular dichroism experiment were done on a Model 62DS CD Spectrometer (AVIV Biomedical Inc., Lakewood, NJ, USA). Initial wavelength scan measurements of the peptides were done at a temperature of 288 K between 300 nm and 190 nm in increments of 1 nm, and a bandwidth of 1 nm with a signal averaging time of 10 s. Thermal denaturation experiments were done at a measurement wavelength of 222 nm which shows a characteristic minimum for α-helical secondary structure. The temperature scan was started at a temperature of 288 K with increments of 1 K upto 368 K providing 5 min equilibration time between each temperature point and 30 s of signal averaging.

4.2.3 NMR spectroscopy

All experiments were done on an 11.7 T Avance III spectrometer with a TCI triple resonance cryoprobe (Bruker, Billerica, MA, USA). Temperatures were increased starting at 305 K to 345 K at intervals of 10 K. At each temperature, NOESY (150 ms mixing time)

and TOCSY (MLEV-17 mixing sequence, 100 ms mixing time at 10.7 kHz) experiments were measured.

4.2.4 Chemical Shift Assignment and NOE Intensity Integration

Spectra were processed with TOPSPIN software (Bruker) and calibrated using the DSS internal standard. The NOESY and TOCSY spectra measured at a temperature of 315 K were used to obtain initial chemical shift assignments for Magainin2 peptide in both SDS and DPC detergent micelles. The assignments obtained were compared to the assignments reported in [144]. The assignments at 315 K were used as a reference to map the assignments at higher temperatures. Chemical shift differences from the initial values were plotted against temperature and the best fit straight line was calculated. The slope of the graphs give the temperature coefficients of the chemical shifts [176]. NOE crosspeaks were picked out in NOESY spectra at 315 K and assigned using the CANDID module in CYANA software [156]. The assigned NOEs were verified, and an identical set of NOE crosspeaks were picked at all the temperatures. Peaks were integrated at the different temperatures using CARA and normalized between the lowest and highest integral values for each peak. The normalized intensities of H^N(i)$\rightarrow$ H^α(i-3), H^N(i)$\rightarrow$ H^α(i-4) and H^α(i)$\rightarrow$ H^β(i+3) NOE crosspeaks were plotted against temperature. A cubic spline function was used to fit the data points and the temperature at which the normalized intensity is half the initial value was taken as an empirical cutoff temperature [173].

4.3 Results

4.3.1 Monitoring Thermal Denaturation of Magainin2 and HA G1V Peptides by CD Spectroscopy

Far UV CD scans were measured for Magainin2 (Figure 4.1) and HA G1V (Figure 4.2) in all three different detergent micelles at 288 K. In all three detergents, both the peptides have an α-helical secondary structure, which is indicated by the presence of two minima

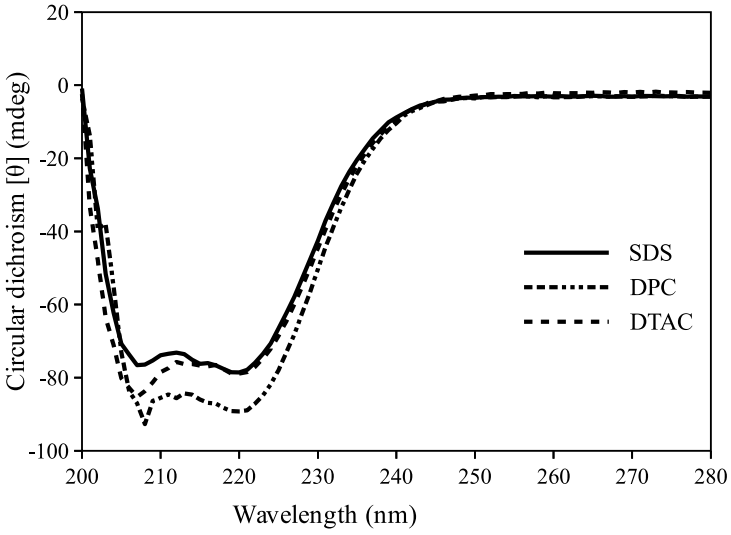

Figure 4.1: Far UV CD spectrum of Magainin2 peptide in SDS, DPC and DTAC detergent micelles.

at 222 nm and 208 nm. In the case of HA G1V, since the peptide sequence contains one tryptophan residue, quantification of the sample was done by measuring the absorbance of the sample at 280 nm. The peptide concentrations obtained for each sample were within a range of $\pm$ 2.5% from the mean concentration value. Accurate determination of sample concentration was not possible in Magainin2, due to low final sample concentrations and absence of any tyrosine and tryptophan residues in Magainin2. However, based on the consistently similar sample concentrations measured for the HA G1V samples, the preparations of Magainin2 by an identical method have been considered to have similar concentrations among themselves. For each peptide, similar circular dichroism values were observed in all three different detergents indicating that the choice of the detergent micelle had an insignificant effect on the net secondary structure content of the two peptides.

Thermally induced unfolding of the two peptides was monitored by measuring the CD signal at 222 nm (θ_{222nm}). The CD signal was plotted against temperature for HA G1V peptide (Figure 4.3 a). Since the sample concentrations and also the initial fraction

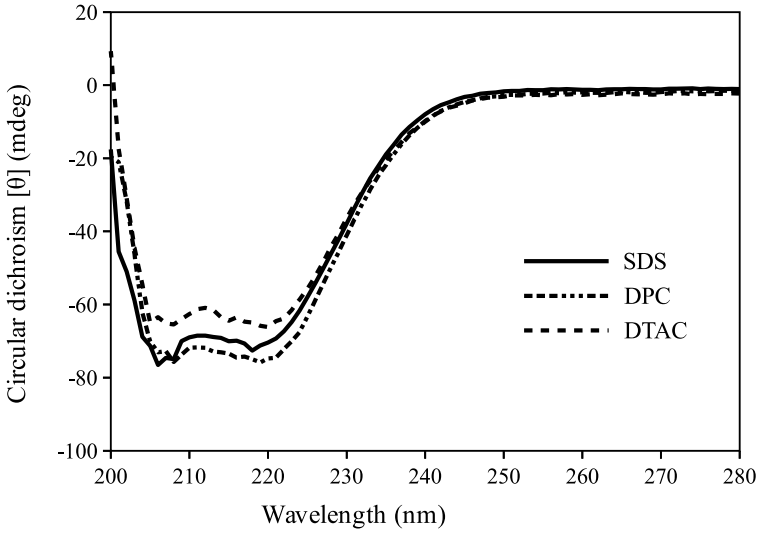

Figure 4.2: Far UV CD spectrum of HA G1V peptide in SDS, DPC and DTAC detergent micelles.

of helicity of the peptide may be different for each peptide, the relative change in the observed circular dichroism from initial value at 288 K ($\Delta\theta/\theta_{288K}$) against temperature (Figure 4.3 b). In the HA G1V sample, a clear difference is seen in the curvature of the plots obtained for the three detergents. In SDS micelle, the response of $\Delta\theta/\theta_{288K}$ to increasing temperatures follows a curve that is concave. On the other hand, in DTAC detergent micelle the plot is convex. For the peptide measured in DPC micelles, the plot has a curvature that lies between that of either detergent. A clear difference can be seen in the first derivative of $\Delta\theta/\theta_{288K}$ with respect to temperature for the three detergents.

Since accurate determination of sample concentrations was possible in HA G1V, the mean residue ellipticity value at 222 nm was used to calculate the fractional helicity (p_H) using equation 2.1. The theoretical mean residue ellipticity values at 222 nm for both the α-helix and the random coil depend on the temperature according to equations 2.2. and 2.3. respectively. The calculated fractional helicity (p_H) was plotted as a function of temperature (Figure 4.3 c). The calculated percentage helicity plots for HA G1V are all

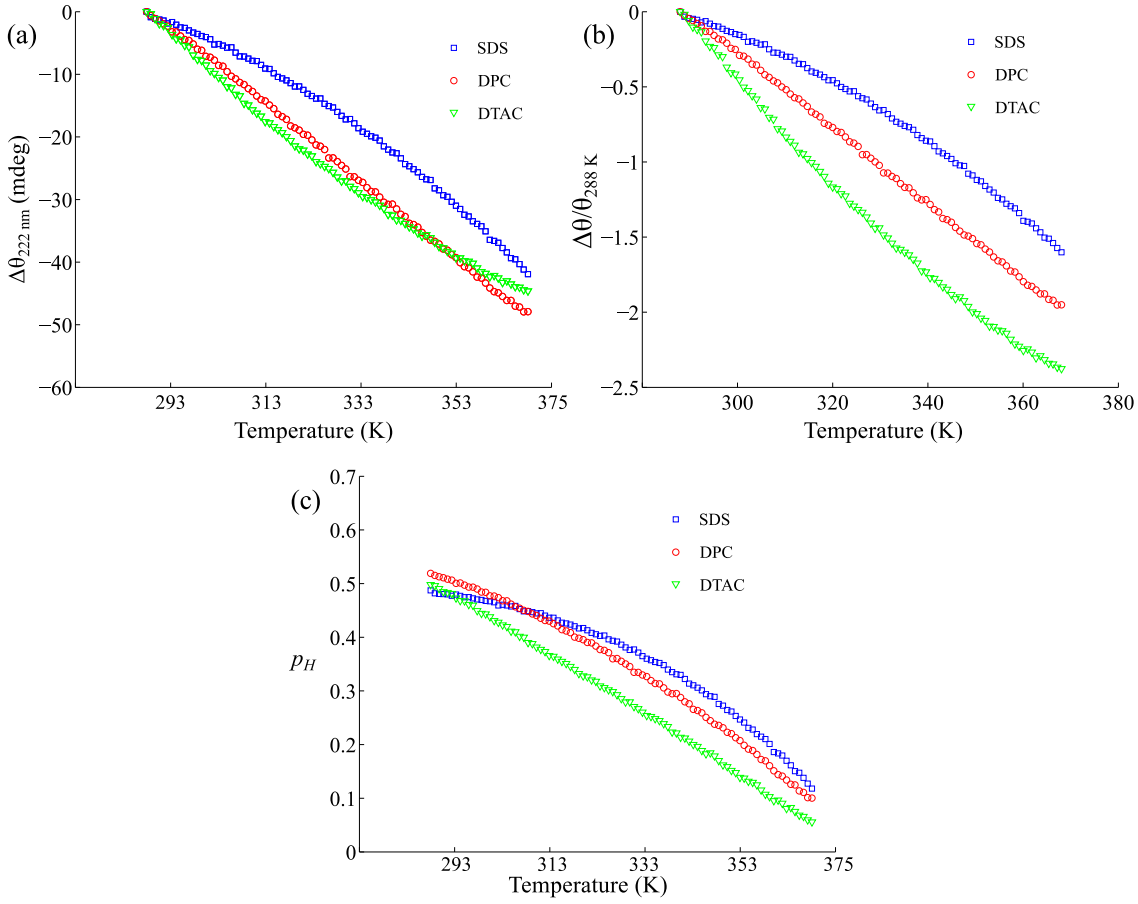

Figure 4.3: Thermal denaturation curves for HA G1V peptide. θ_{222nm} (a), $\Delta\theta/\theta_{288K}$ at 222 nm (b) and p_H (c) of HA G1V peptide are plotted as a function of temperature in SDS, DPC and DTAC detergent micelles. The sample concentration is 0.05 mg/mL.

concave downwards but their curvatures are different, with the samples in DTAC, DPC and SDS detergent micelles having increasing levels of curvature. The curvature observed in this plot is different from those observed in the plots of θ_{222nm} and $\Delta\theta/\theta_{288K}$ against temperature because the theoretical values of mean residue ellipticities for random coil and helix used to calculate the fraction helicity depend on the temperature.

θ_{222nm} and $\Delta\theta/\theta_{288K}$ values for Magainin2 are plotted against temperature (Figure 4.4 a, b) In the case of Magainin2, difference in the curvatures of thermal denaturation plots of the three different micelles is not as not as high as that of HA G1V. In Magainin2, the peptide in SDS detergent micelle the values of $\Delta\theta/\theta_{288K}$ follow a curve that is convex at higher temperatures. For the peptide in DPC and DTAC detergent micelles such a feature is not observed and it is difficult to discern and differences between the two micelles. However, when the sample concentration of Magainin2 was doubled, to 1 mg/mL, a larger difference in the shapes of the curves can be observed (Figure 4.4 c, d). The DTAC detergent micelle shows the greatest curvature, while SDS shows the least curvature. In the case of Magainin2, since accurate determination of the sample concentration was not possible, fractional helicities are not reported. In both Magainin2 and in HA G1V, the DTAC sample shows the greatest decrease in $\Delta\theta/\theta_{288K}$, while SDS shows the least decrease in $\Delta\theta/\theta_{288K}$ with increasing temperatures. However, the curvatures of the thermal denaturation plots are opposite. In HA G1V, the sample in DTAC detergent micelle shows the least curvature and the sample in SDS shows the highest curvature. Whereas in Magainin2, the sample in SDS shows the least curvature while the sample in DTAC shows the highest curvature.

The curvature of the helix coil transition can be explained using the Zimm-Bragg theory for helix coil transition [170], which provides a thermodynamic description of the helix coil transition. In the model the helix initiation and propagation steps are considered separately and the helix coil transition is defined in terms of the nucleation factor(σ) and the propagation parameter (s). The equilibrium constant for the nucleation of helix formation

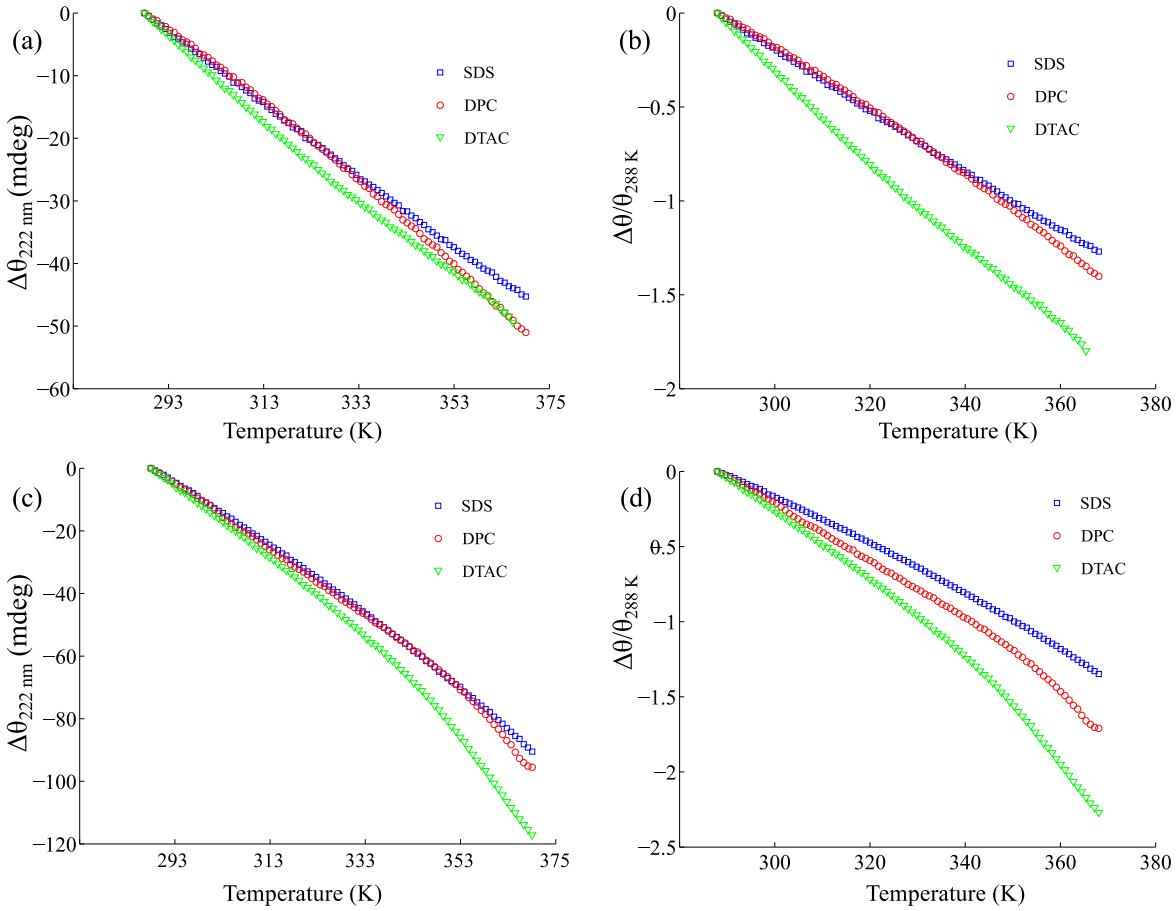

Figure 4.4: Thermal denaturation curves for Magainin2 peptide. θ_{222nm} (a, c) and $\Delta\theta/\theta_{288K}$ at 222 nm(b,d) of Magainin2 peptide are plotted as a function of temperature in SDS, DPC and DTAC detergent micelles. The sample concentrations are 0.05 mg/mL (a, b) and 0.1 mg/mL (c, d).

is defined to be σs and the equilibrium constant for adding every additional unit of helix is s. Values for σ range between 0 and 1. When σ=1, the plot of p_H against temperature will have no curvature and it represents a case when there is no cooperativity in the coil to helix transition. In the Zimm-Bragg model, higher cooperativity refers to a greater tendency of the peptide to form contiguous stretches of helix once the initial entropic barrier for the nucleation of the helix is crossed. In the data obtained here, in the presence of a like charge the peptides show a greater curvature in the thermal denaturation plot and hence a greater cooperativity in the transition from coil to helix. When considering the transition from coil to helix, the presence of a like charges should likely make the helix more unstable thus disfavoring the formation of the helix. It seems counter-intuitive how the presence of such a destabilizing effect would contribute to greater cooperativity in the folding of the helix but a closer examination of the mechanism of helix coil transitions provides a possible explanation. The addition of a single helical unit in a helix coil transition involves the formation of a (i+4)$\rightarrow$(i) hydrogen bond. In the case of nucleation, this would involve loss of conformational entropy due to loss of mobility at six rotational angles and this loss of conformational entropy is partially compensated by the formation of a hydrogen bond [168]. However, addition of further helical units require only the conformational restriction of two additional rotational angles making it favorable to add additional helical units to the initial nucleation site to compensate for the initial loss of conformational entropy. In the case of peptides on detergent micelles, additional factors possibly contribute to the energetics of the system than just the formation of the hydrogen bond itself. It is possible that when a new helical unit is added, some residues are buried into the hydrophobic interior of the lipid and others are exposed at the surface of the micelle in proximity to the lipid head group. In amphipathic helices, it is likely that the charged and polar residues are positioned hear the head group of the lipid. When like charges are present on the peptide and on the the head group of the detergent, the electrostatic interactions between the head

group of the detergent and the charged residues of the peptide are unfavorable and may reduce the extent to which the addition of a helical unit compensates for the loss of conformational entropy. Thus more helical units have to be added to an initial nucleation site until the loss of conformational entropy from the nucleation event is compensated, and this results in greater cooperativity in the folding process. In the presence of opposite charges, the addition of fewer helical units may already compensate for the loss of conformational entropy from the initial nucleation event by gaining favorable electrostatic interactions and hence in this case the cooperativity will be lower.

Unfolding of short α-helical peptides in solution is typically reversible, but the same is not true in all cases for proteins. This is possibly due to the fact that these peptides do not have any long range contacts and interactions, but the folding and stability of proteins depends on these additional interactions. In detergent micelles, apart from intramolecular interactions, peptides also have additional interactions with the detergent micelle. Therefore, it was also verified if the folding and unfolding reactions are equivalent. Full wavelength scan CD spectra were measured in increasing temperatures between 288 K and 368 K and backwards (Figure 4.5 a and b). In the measured spectra, an isodichroic point could not be identified because of the high absorbance at wavelengths smaller than 205 nm, due to absorbance from components of the buffer and the detergent micelle. Thus, it could not be unequivocally verified that only two states were involved in the helix coil transition. The ellipticity value at 222 nm were plotted for both the heating and cooling process (Figure 4.5 c). The ellipticity values obtained from the heating and cooling processes at each temperature were different. A much higher value of ellipticity was obtained during the cooling process. This implies that the peptide is not able to completely refold after thermal denaturation under the conditions tested. In DPC detergent micelles, this difference between the heating and cooling process is larger than that observed for SDS micelles (Figure 4.5 d).

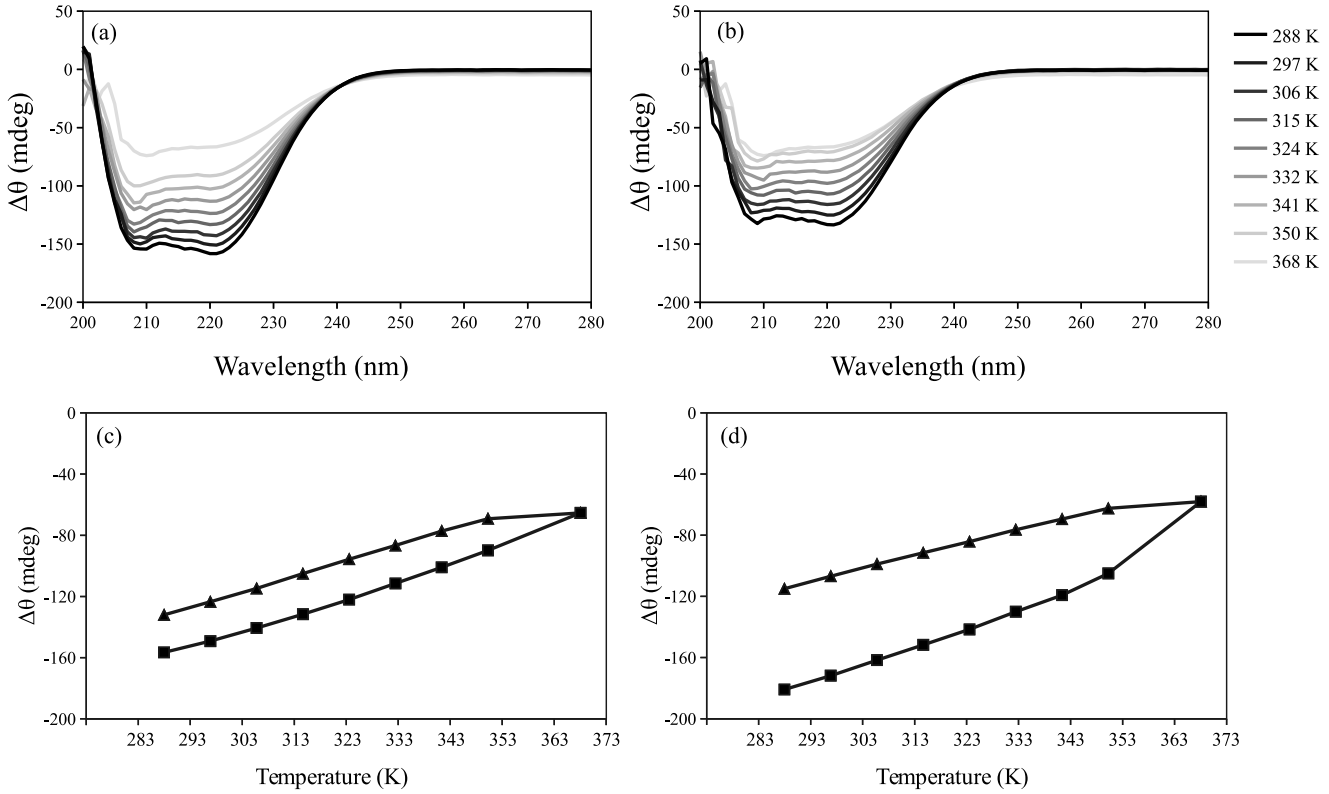

Figure 4.5: Far UV CD spectrum of 0.1 mg/mL Magainin2 recorded in increasing (a) and decreasing (b) temperatures. Ellipticity of mg/mL Magainin2 in (c) SDS detergent micelles and (d) DPC detergent micelles. Squares represent dichroism values from the heating experiment and the triangles represent circular dichroism values from the cooling experiment.

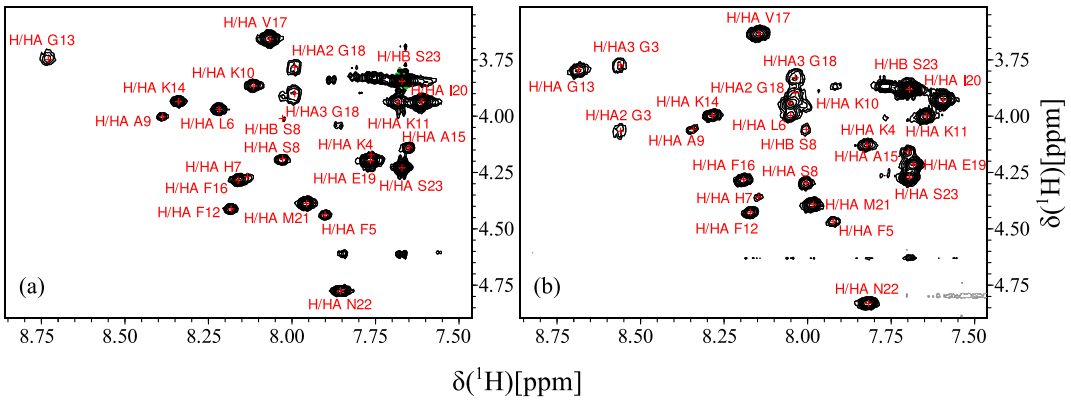

Figure 4.6: The finger print region from the TOCSY spectra of Magainin2 peptide in (a) DPC detergent micelle (b) SDS detergent micelle at 315 K.

4.3.2 Thermal Denaturation of Magainin2 Monitored by NMR Spectroscopy

Chemical shift assignment of Magainin2 peptide was completed in SDS and DPC detergent micelles at increasing temperatures between 305 K and 345 K. The chemical shifts were assigned from TOCSY and NOESY experiments at 315 K. The chemical shifts reported by [144] were used as a reference to assign the chemical shifts of the different peptide resonances in the two detergent micelles. In all temperatures, the spectra are well resolved, the fingerprint region of the TOCSY spectra at 315 K are shown as an example (Figure 4.6). An overlay of the TOCSY spectra shows that the H^{α} and H^{N} chemical shifts change with temperature in either detergent micelles (Figure 4.7). The change in chemical shift of the H^{α} and H^{N} from the initial value at 305 K was plotted against temperature (Figure 4.8 and 4.9). Different residues of the peptide show varied dependence on temperature in the plot. In either detergent micelles, the value of H^{α} chemical shifts increased with temperature, whereas the value of H^{N} chemical shift decreased with increasing temperature.

The the temperature coefficients H^{N} and H^{α} $(\Delta\delta(H)/\Delta T)$for each residue was obtained from the slope of the linear portion of the plots in (Figure 4.8 and 4.9) and plotted

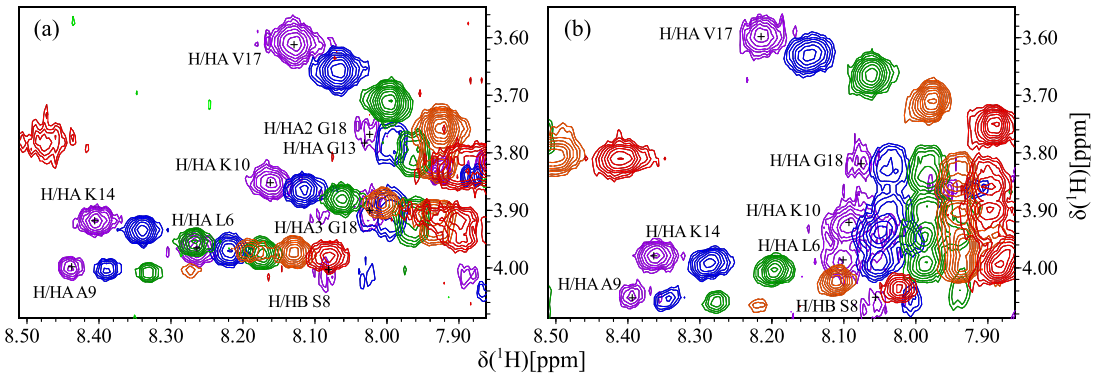

Figure 4.7: Overlay of TOCSY spectra of Magainin2 measured at increasing temperatures. Spectra were measured at 305 K (violet), 315 K (blue circles), 325 K (green), 335 K (orange) and 345 K (red triangles) respectively.

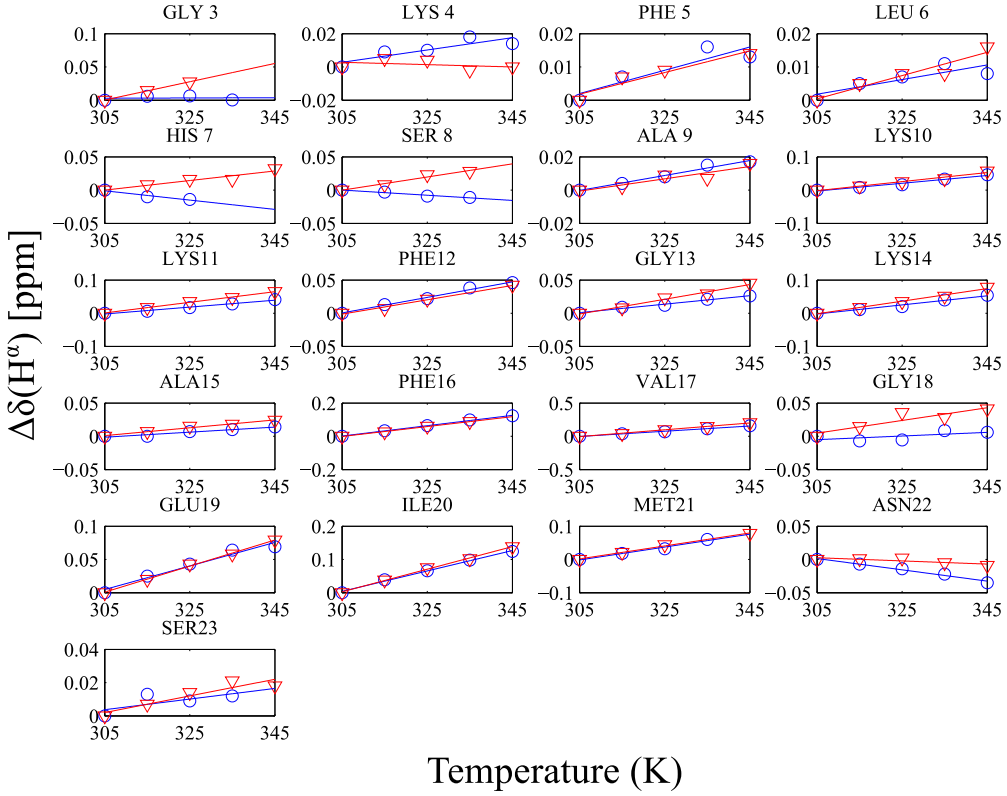

Figure 4.8: The change in H^{α} chemical shift from initial value at 305 K plotted as a function of temperature for Magainin2 in SDS (blue circles) and in DPC (red triangles)

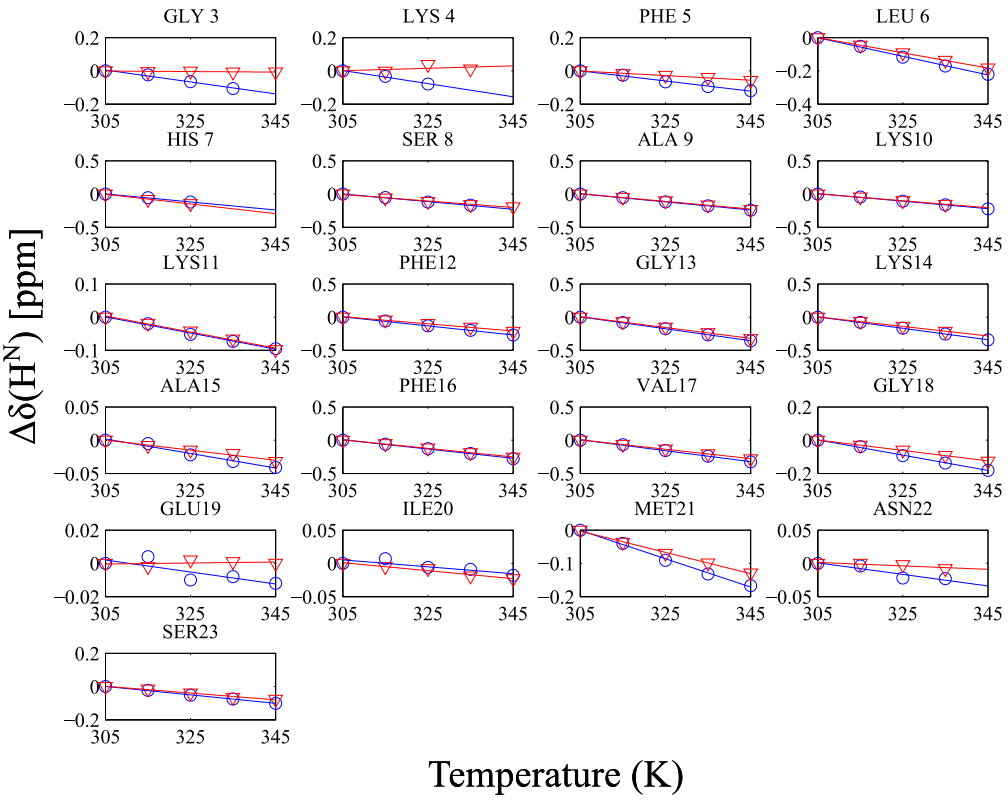

Figure 4.9: The change in H^N chemical shift from initial value at 305 K plotted as a function of temperature for Magainin2 in SDS (blue circles) and in DPC (red triangles)

against the residue number on the sequence of the peptide. The greater change in chemical shift can be used as a qualitative indicator of a greater change in the chemical environment with increasing temperature. The change in chemical shift in the case of amide proton is significantly affected by exchange with the solvent. The presence of intramolecular hydrogen bonds in a protein greatly increases the temperature coefficient to a greater positive value [176]. In soluble proteins, this has been used an indicator of the presence of intramolecular hydrogen bonds. In Magainin2, the sample in DPC has temperature coefficients that are comparable to or greater than those in SDS detergent micelles. For soluble proteins, a cut off of $>$-4.6 ppb/K has been considered as an indicator for the presence of hydrogen bonds in soluble proteins [172, 175]. For hydrogen bonds present in α-helices the cut off can be relaxed to $>$-5.6 ppb/K [172]. The $\Delta\delta(H^{\alpha})/\Delta T$ values for each residue of Magainin2 in DPC detergent micelles are either comparable to or greater than the values for that of SDS (Figure 4.10 a). However, the absolute value of $\Delta\delta(H^{N})/\Delta T$ for all residues in DPC are lower than those in SDS. The differences in these values are small making it difficult to interpret the data unequivocally. .

The intensities of NOE crosspeaks depend on inter-proton distances and are a good indicator of structure. An α-helical secondary structure is characterized by the presence of H^{N}(i)$\rightarrow$ H^{α}(i-3), H^{N}(i)$\rightarrow$ H^{α}(i-4) and H^{α}(i)$\rightarrow$ H^{β}(i+3) NOEs. However, it must be considered that the actual intensity of the NOE depends on factors other than inter-proton distances such as the local order parameter and correlation time. These parameters are affected by temperature both directly and also indirectly by changing of solvent properties such as viscosity. Despite this, NOEs can still be used as an indicator of changes in intermolecular distances with increasing temperature [173, 186].

NOE intensity values from H^{N}(i)$\rightarrow$ H^{α}(i-3), H^{N}(i)$\rightarrow$ H^{α}(i-4) and H^{α}(i)$\rightarrow$ H^{β}(i+3) NOE crosspeaks were normalized with respect to the initial observed value and plotted against temperature and fit with a cubic spline function for DPC(Figure 4.11) and SDS

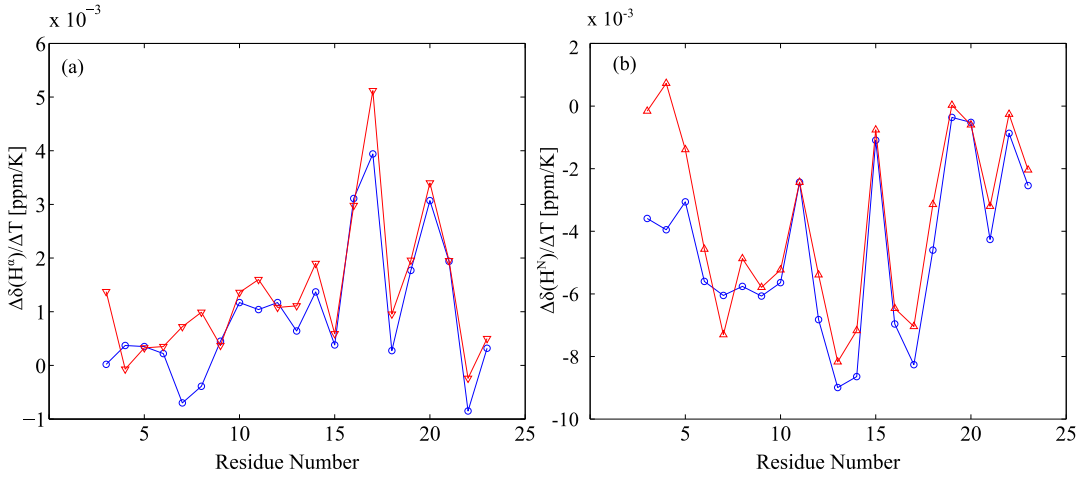

Figure 4.10: Temperature coefficients of H^{α} ($\Delta\delta(H^{\alpha})/\Delta T$) (a) and H^{N} ($\Delta\delta(H^{N})/\Delta T$) (b) for Magainin2 plotted against residue number in SDS (blue circles) and in DPC (red triangle)

(Figure 4.12) detergent samples. The temperature corresponding to a normalized intensity of 0.5 was obtained from the spline function and used as a cut-off temperature. A similar empirical cut-off value has been previously reported as a reliable indicator to study the thermal denaturation of TrypZip peptide [173]. The cut-off values obtained from (Figure 4.11 and 4.12) have been plotted on the structure of Magainin2 peptide (PDB ID: 2MAG) (Figure 4.13).

The sample of Magainin2 in DPC detergent micelles gave more H^{N}(i)$\rightarrow$ H^{α}(i-3), H^{N}(i)$\rightarrow$ H^{α}(i-4) and H^{α}(i)$\rightarrow$ H^{β}(i+3) NOE crosspeaks at the initial temperatures than in SDS micelles. A similar observation can also made in the data presented in [144]. Overall, the cut off temperature values obtained in DPC are much larger than those obtained in the SDS detergent micelle. However, it may be misleading to directly compare the cut-off values of the NOE crosspeaks between the two detergent samples because the size of the detergent molecule and aggregation number of the detergent micelles are different. The expected size of the detergent micelles for DPC and SDS are $\sim$18 kDa and $\sim$24 kDa re-

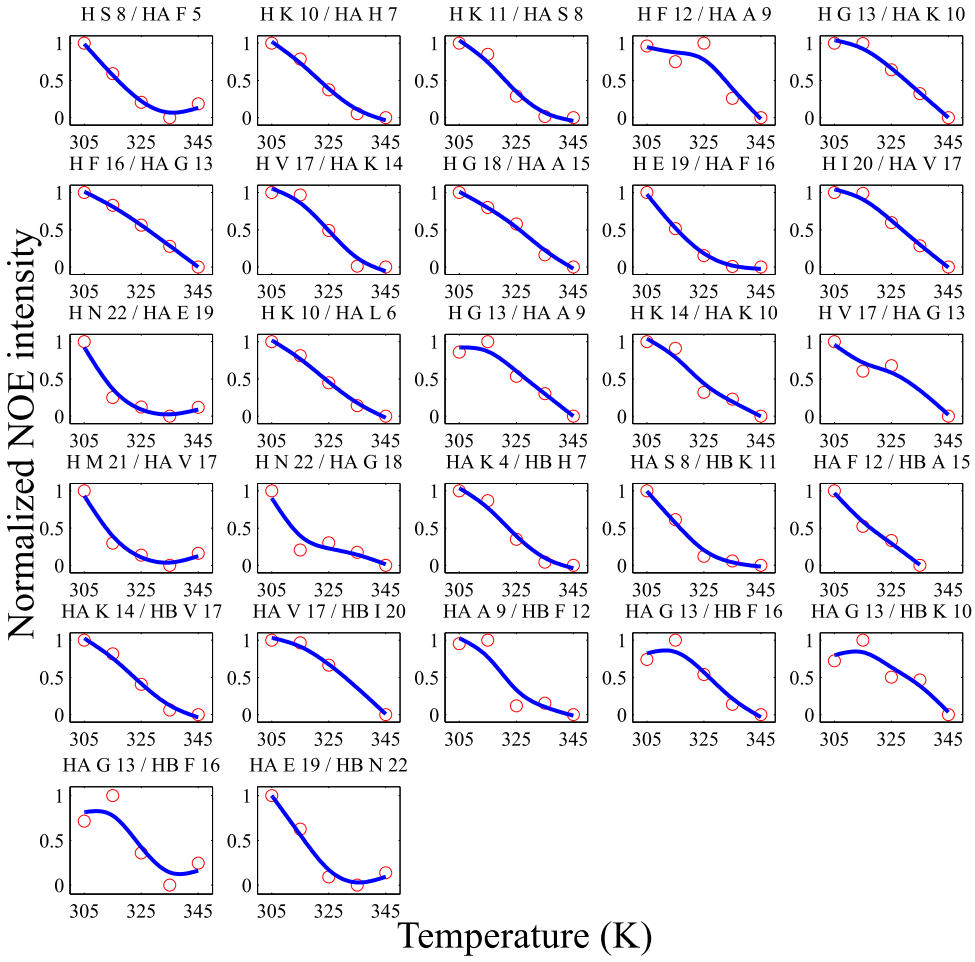

Figure 4.11: Normalized intensity values for NOE cross peaks for Magainin2 peptide in DPC detergent micelles plotted against temperature.

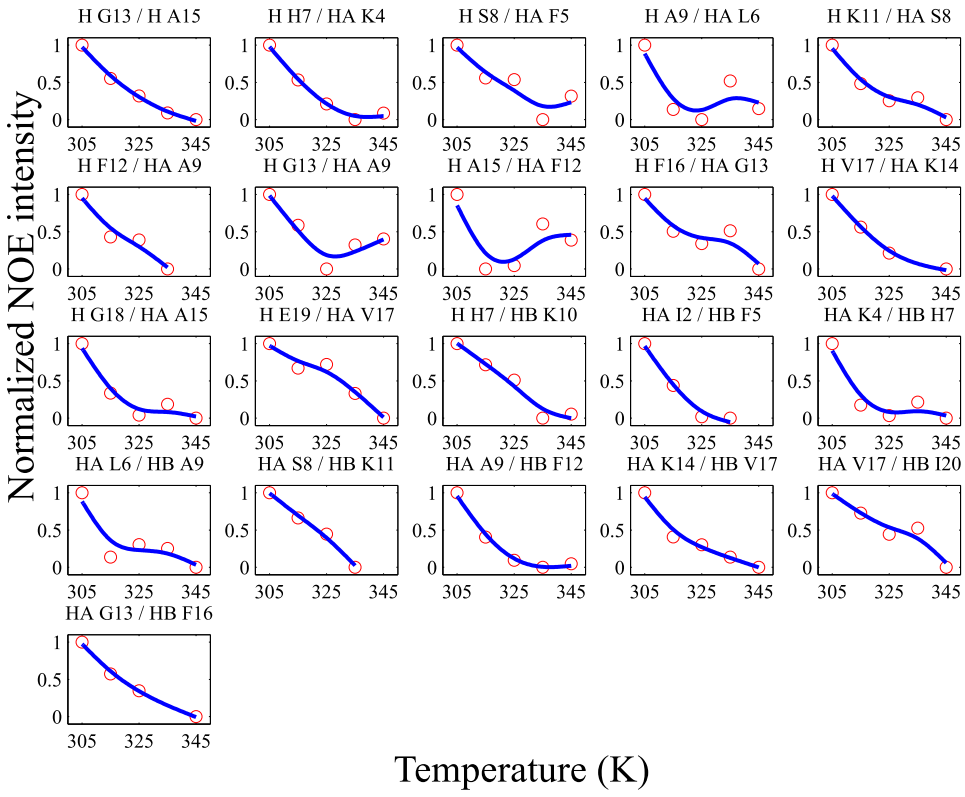

Figure 4.12: Normalized intensity values for NOE crosspeaks for Magainin2 peptide in SDS detergent micelles plotted against temperature.

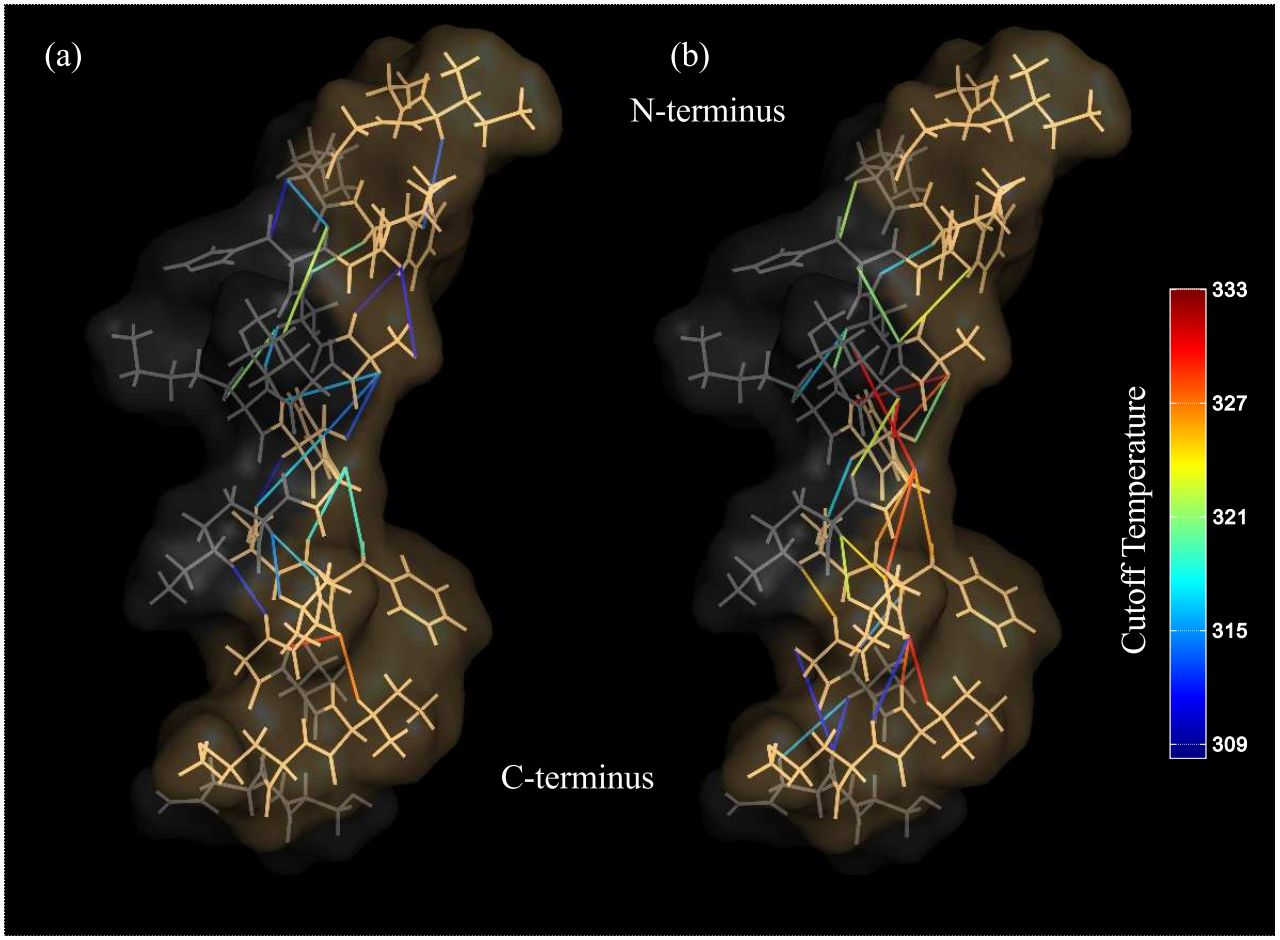

Figure 4.13: NOE crosspeaks observed between different spins in SDS (a) and DPC (b) are indicated on the structure of Maga-inin2 (PDBID:2MAG) as lines. Lines are colored according to the cutoff temperatures calculated from (Figure 4.11 and 4.12). On the peptide, the hydrophobic residues are colored beige and the other residues are colored grey.

spectively. While the effect of temperature on the correlation time for global motion can be expected to be similar for all resonances in the same micelle, the same is not reasonable to assume for the two detergent micelles of different sizes. In the DPC detergent micelle, cut-off value range between 312 K and 333 K. Most of the NOEs with higher cut-off values are located in the middle of the peptide between residues Ser-8 and Phe-16. In DPC, the C-terminus of the peptide has many NOEs with higher cut-off values with the exception of the H^N(V17)$\rightarrow$ H^α(G13) and H^α(V17)$\rightarrow$ H^β(I20) crosspeaks. In SDS detergent micelles, as in the case of DPC higher crosspeaks with higher cut off temperatures are localized in the middle of the peptide. Unlike in the case of DPC detergent micelles, no NOE crosspeaks with noticeable low cutoff temperatures are detected in the C-terminus of the peptide. However, only two representative NOEs were observed in this region of the peptide. In the N-terminus of the peptide however, more NOEs are found in the sample in SDS detergent micelles, however these NOE crosspeaks have relatively lower cut-off temperature values. The peptide in (Figure 4.13) has been rendered such that the hydrophobic face residues of the peptide is towards the right side, hydrophobic residues have been colored in beige whereas polar and hydrophilic residues are colored grey. In the NMR structure of Magainin2 in DPC, the helix is curved in shape. The hydrophobic face of the peptide is concave, while the hydrophilic face is convex. In SDS, the NOEs from either face of the peptide have comparable values of cutoff temperatures. In DPC, the NOEs from the hydrophobic face of the peptide have significantly higher cutoff temperatures than that of the hydrophilic face. The NOEs with the higher cut-off temperature populate the concave face of the peptide.

4.4 Discussion

From the circular dichroism data, it can be clearly seen that the presence of like charges on the peptide and the detergent micelle causes a higher cooperativity in the unfolding of

the peptide. Since the trend was verified using peptides of opposite charge, it can be justified that the observation was not merely the outcome of any experimental artifacts caused by dependence of micelle properties such as aggregation number or critical micelle concentration to temperature. When opposite charges are present on the micelle and on the peptide, it may possibly have a stabilizing effect on the α-helix, and the helix to coil transition may not happen readily. On the other hand, the presence of like charges on the peptide and on the micelle might have a destabilizing effect on the α-helix causing the unfolding reaction to proceed more readily. In the zwitterionic micelle, it shows an intermediate effect to that of the cationic and anionic micelle in each case. If the mere presence of a charge, or absence thereof determined the curvature of the helix coil transitions, the thermal denaturation curve of the zwitterionic detergent would resemble one of the two other detergent micelles. However, thermal denaturation plots for the zwitterionic detergent is not comparable to either the cationic or anionic detergent.

On the residue specific level, the only observable difference was that in DPC there was a greater difference between temperature cutoff values from the hydrophobic face of the peptide and that of the hydrophilic face of the peptide. In SDS detergent micelles, the temperature cutoff values from either face of the peptide were comparable. This suggests that the presence of negative charges exclusively on the SDS micelles adds to the stability of the hydrophilic face of the peptide. In the case of DPC, the zwitterionic character of the peptide due to the presence of both positive and negative charges does not stabilize the hydrophilic face as effectively. It has to be considered that the difficulty in discerning the differences between the two systems might arise from the intrinsic nature of the system. It is certainly plausible that the specific details of interaction of the membrane mimetic to the peptide such as angle of insertion into the micelle, depth of insertion into the micelle and the bend in the structure peptide are different between the two systems. The peptide should orient itself in the micelle with a structure and a configuration that is energetically the most

favorable. It is therefore possible that microscopic adjustments in structure and orientation renders the differences between the peptide in the two different micelles unobservable.

For Magainin2, the highest cooperativity was observed in a cationic detergent micelle, however the bacterial membrane is negatively charged. Hence, mere cooperativity in folding may not be a determining factor in the antimicrobial activity of the peptides. The stability and orientation of the peptide on the membrane may play a more important role. Hydrophobic interactions of the membrane with the residues of the peptide, solvation of charged residues, favorable or unfavorable interactions with the charge on the head group of the lipid may all play a role in the stability and orientation of the peptide. It is likely that a loss in a favorable interaction with an opposite charge on the surface of the micelle is compensated by burying the hydrophobic portion of the peptide to a depth that is optimally favorable. This becomes more complicated when residues of opposite charge are present on the peptide, which is true in the case of Magainin2. In Magainin2, the cationic lysine residues are present in positions 4, 10, 11 and 14 of the peptide and a glutamate residue at position 19. In the SDS micelle, while the negative charge can have favorable interactions with the positively charged lysine residues, the unfavorable interactions with the glutamate residue are also present. The combination of these effect might influence the depth and angle of insertion of the peptide.

Most experiments in this study examine the helix to coil transition of peptides, which is an unfolding process. However, the function of both cationic antimicrobial peptides as well as viral fusion peptides are determined by a coil to helix transition, which is an folding process. From the cooling experiments performed using CD spectroscopy, there are indications that the two processes may not be equivalent. Helix coil transitions in solvents are readily reversible, but the same may not necessarily hold true for peptides in detergent micelles. One explanation is that thermal unfolding of the peptide populates states from which recovery back to the helical configuration may not be straightforward.

It is possible that hydrophobically collapsed intermediate states with interactions with the lipid cause energy minima from which recovery to a helical conformation is not kinetically favorable. Thus, it would be relevant to further investigate the coil to helix transitions of these peptides. Between the SDS and DPC detergent micelles in the cooling experiment shown in (Figure 4.5), the sample in SDS is able to recover to a greater extent to its initial helical fold than the sample in DPC detergent micelles. The observed difference in recovery may depend on the extent to which the peptide unfolds at the highest temperature in each micelle.

From a functional point of view, this study represents a very simplistic approach to determine the effect of charge in the helix to coil transition and stability of the α-helices of membrane associating peptides. The biological membrane is more complicated than a detergent micelle and is constituted of a combination of different lipids. Each of these lipids alter the charge, rigidity and chemical nature of the membrane. Additionally, the micelle is spherical, whereas the the membrane is flatter and parameters such as membrane curvature have been shown to affect the activity of these peptides [128]. It will be more challenging to model the exact variables that contribute to the physiological activity of these peptides. But measuring microscopic parameters such as depth and angles of insertion of peptides, and correlating these values to the toxicity and selectivity of the peptide may enable rational design of more effective antimicrobial peptides.

5. CONCLUSIONS

Many biologically active peptides including antimicrobial peptides, viral fusion peptides and transmembrane segments of α-helical membrane proteins interact with the biological membrane. The function of these peptides often involves a change in the structure of the peptide upon interaction with the membrane. CD and NMR spectroscopy methods are often used to investigate the interaction these peptide with detergent micelles, to provide insight about the interaction of the peptide with the biological membrane.

In this work, the linker peptide from the autotransporter NalP, the antimicrobial peptide Magainin2 and the mutant viral fusion peptide HA G1V have been studied. The linker peptide from the autotransporter NalP exhibits a random coil secondary structure in an aqueous medium. In the presence of a detergent micelle, the peptide has been shown to exist in a partially helical conformation. In the organic solvent TFE, the NMR structure of the peptide has been determined and the peptide folds into an α-helix. The different secondary structures of the linker peptide in water, SDS detergent micelles and in TFE suggest that the linker peptide may also be involved in interactions with the biological membrane during the protein secretion function of the autotransporter.

Apart from the determination of the structure of the linker peptide in TFE, the thermal denaturation of the α-helix formed by the linker peptide was also investigated using CD and NMR spectroscopy. Upon heating, the peptide undergoes denaturation, however a significant residual helicity can be observed. A helicity of 35% was determined at 345 K compared to the initial value of 68% at 288 K. Residue specific effects of heating on the folding of the peptide were determined by observing changes in chemical shifts and relative intensities of NOE crosspeaks. Residues located in the middle of the α-helix display higher values of an empirically defined cutoff temperature and we suggest that this

region of the peptide has a greater thermal stability compared to those located towards the termini. This observation suggests that the ends of the α-helix may get frayed readily and that the unfolding of the helix may initiate at the termini of the helix. It would be of significance to investigate whether lower thermal stability of termini is a common feature for all α-helices.

Thermal denaturation of peptides in detergent micelles having different charge has been investigated by using a combination of NMR and CD spectroscopy. The peptides used in this study, Magainin2 and HA G1V, have opposite charge and were observed in cationic, anionic and zwitterionic detergent micelles. When like charges are present on the peptide and on the detergent micelle the measured thermal denaturation curve has a greater curvature. The increased curvature of the thermal denaturation plot suggests an increase in the cooperative effect in the helix coil transition of the peptide in the presence of like charges. While clear differences exist in the overall behavior of the peptide in the different detergent micelles, no unambiguous differences were observed for the peptides at the residue specific level.

In the above studies, we observe peptides in aqueous media as well as in detergent micelles and organic solvents. Detergent micelles are a relatively simple and robust medium for observation of peptides. The structures and stability of peptides in these media can often be used as an indicator for the interaction of the peptide in the lipid bilayer. On a detergent micelle the peptide experiences electrostatic and hydrophobic interactions. These interactions determine the stability and folding cooperativity of the peptide. But to gain a complete picture additional parameters such as depth, angle and azimuth of the insertion of the peptide in the detergent micelle are to be investigated as well. This can be performed by measuring additional NMR experiments such as resiual dipolar coupling, paramagnetic relaxation enhancement NMR and exchange rate of labile protons. Moreover, the NOE and chemical shift based method for determining thermal denaturation can be improved

upon by measuring additional experiments to determine NOE buid up rate and J-coupling constants as indicators of structure of the peptide.

While all the peptides studied here by thermal denaturation here are straight, some peptides fold to form kinked helices and helical hairpins. The investigation of the thermal stability of these peptides would be very interesting. Determination of residue effects of temperature on these peptides would indicate the effect of the kink or the hairpin structure on the folding and unfolding mechanisms of these peptides.

This work addresses only the interaction of the linker with the membrane. It is also additionally possible that the linker peptide is involved in interactions with the periplasmic domains or the laterally opened β strands of the membrane chaperone. However, determination of these interactions are likely to be challenging.The mechanism of membrane insertion and protein translocation by autotransporters is poorly characterized. It is believed that the folding of the translocator domain and the translocation processes are interrelated. Determination of the sequence of events and description of individual steps that occur in the folding and transport process will provide a more detailed functional model. One approach to determine these events would be to kinetically resolve the intermediates of autotransporter folding by using time-resolved tryptophan quenching experiments.

The determination of structures of peptides on membrane membrane mimetics and characterizing their interactions with the membrane mimetic provides insight into the physiological function of these peptides. Understanding the contributions of various interactions towards the structure and stability of the peptide enables design of custom peptides of desirable function. This can be applied for the design of cell penetrating and antimicrobial peptides.

REFERENCES

[1] A. Krogh, B. Larsson, G. von Heijne, and E. L. Sonnhammer. Predicting transmembrane protein topology with a hidden Markov model: application to complete genomes. *Journal of Molecular Biology*, 305(3):567–580, 2001.

[2] Fei P. Gao and Timothy A. Cross. Recent developments in membrane-protein structural genomics. *Genome Biology*, 6(13):244, 2006.

[3] Kenneth Lundstrom. Structural genomics on membrane proteins: the MePNet approach. *Current Opinion in Drug Discovery and Development*, 7(3):342–346, 2004.

[4] John P. Overington, Bissan Al-Lazikani, and Andrew L. Hopkins. How many drug targets are there? *Nature Reviews Drug Discovery*, 5(12):993–996, 2006.

[5] Helen M. Berman, John Westbrook, Zukang Feng, Gary Gilliland, T. N. Bhat, Helge Weissig, Ilya N. Shindyalov, and Philip E. Bourne. The Protein Data Bank. *Nucleic Acids Research*, 28(1):235–242, 2000.

[6] Ray D. Krueger-Koplin, Paul L. Sorgen, Suzanne T. Krueger-Koplin, Iván O. Rivera-Torres, Sean M. Cahill, David B. Hicks, Leo Grinius, Terry A. Krulwich, and Mark E. Girvin. An evaluation of detergents for NMR structural studies of membrane proteins. *Journal of Biomolecular NMR*, 28(1):4357, 2004.

[7] T. Surrey and F. Jähnig. Refolding and oriented insertion of a membrane protein

into a lipid bilayer. *Proceedings of the National Academy of Sciences of the United States of America*, 89(16):7457–7461, 1992.

[8] Matthew Waas, Subarna Bhattacharya, Sandra Chuppa, Xiaogang Wu, Davin R. Jensen, Ulrich Omasits, Bernd Wollscheid, Brian F. Volkman, Kathleen R. Noon, and Rebekah L. Gundry. Combine and conquer: Surfactants, solvents, and chaotropes for robust mass spectrometry based analyses of membrane proteins. *Analytical Chemistry*, 86(3):1551–1559, 2014.

[9] Arpana Dutta, Kalyan C. Tirupula, Ulrike Alexiev, and Judith Klein-Seetharaman. Characterization of membrane protein non-native states. 1. Extent of unfolding and aggregation of rhodopsin in the presence of chemical denaturants. *Biochemistry*, 49(30):6317–6328, 2010.

[10] Harinder S. Garewal and Aaron R. Wasserman. Triton X-100-4 M urea as an extraction medium for membrane proteins. I. Purification of chloroplast cytochrome b_{559}. *Biochemistry*, 13(20):4063–4071, 1974.

[11] Lech Czerski and Charles R. Sanders. Functionality of a membrane protein in bicelles. *Analytical Biochemistry*, 284(2):327–333, 2000.

[12] Leah S. Cohen, Katrina E. Fracchiolla, Jeff Becker, and Fred Naider. GPCR structural characterization: Using fragments as building blocks to determine a complete structure. *Peptide Science*, pages 223–243, 2014.

[13] Justin L. Lorieau, John M. Louis, Charles D. Schwieters, and Adriaan Bax. pH-

triggered, activated-state conformations of the influenza hemagglutinin fusion peptide revealed by NMR. *Proceedings of the National Academy of Sciences of the United States of America*, 109(49):19994–19999, 2012.

[14] Soyoun Hwang and Christian Hilty. Folding determinants of disulfide bond forming protein B explored by solution nuclear magnetic resonance spectroscopy. *Proteins: Structure, Function, and Bioinformatics*, 79(5):13651375, 2011.

[15] Tianpeng Du, Ling Jiang, and Maili Liu. NMR structures of fusion peptide from influenza hemagglutinin H3 subtype and its mutants. *Journal of Peptide Science*, 20(4):292–297, 2014.

[16] F. X. Zhou, M. J. Cocco, W. P. Russ, A. T. Brunger, and D. M. Engelman. Interhelical hydrogen bonding drives strong interactions in membrane proteins. *Nature Structural Biology*, 7(2):154–160, 2000.

[17] D. M. Engelman. An implication of the structure of bacteriorhodopsin. *Biophysical Journal*, 37(1):187–188, 1982.

[18] Stephen H. White. Biophysical dissection of membrane proteins. *Nature*, 459(7245):344–346, 2009.

[19] Susan K. Buchanan. β-barrel proteins from bacterial outer membranes: structure, function and refolding. *Current Opinion in Structural Biology*, 9(4):455–461, 1999.

[20] Georg E. Schulz. β-barrel membrane proteins. *Current Opinion in Structural Biol-*

ogy, 10(4):443–447, 2000.

[21] Thomas J. Silhavy, Daniel Kahne, and Suzanne Walker. The bacterial cell envelope. *Cold Spring Harbor Perspectives in Biology*, 2(5):a000414, 2010.

[22] Sebastian Hiller, Jeff Abramson, Carmen Mannella, Gerhard Wagner, and Kornelius Zeth. The 3D structures of VDAC represent a native conformation. *Trends in Biochemical Sciences*, 35(9):514–521, 2010.

[23] Harald Engelhardt, Thomas Meins, Melissa Poynor, Volker Adams, Stephan Nussberger, Wolfram Welte, and Kornelius Zeth. High-level expression, refolding and probing the natural fold of the human voltage-dependent anion channel isoforms I and II. *Journal of Membrane Biology*, 216(2-3):93–105, 2007.

[24] Thomas J. Malia and Gerhard Wagner. NMR structural investigation of the mitochondrial outer membrane protein VDAC and its interaction with antiapoptotic Bcl-x$_L$. *Biochemistry*, 46(2):514–525, 2007.

[25] William C. Wimley. Toward genomic identification of β-barrel membrane proteins: Composition and architecture of known structures. *Protein Science*, 11(2):301–312, 2002.

[26] Martin B. Ulmschneider and Mark S. P. Sansom. Amino acid distributions in integral membrane protein structures. *Biochimica et Biophysica Acta, Biomembranes*, 1512(1):1–14, 2001.

[27] Heedeok Hong, Sangho Park, Ricardo H Flores Jiménez, Dennis Rinehart, and Lukas K Tamm. Role of aromatic side chains in the folding and thermodynamic stability of integral membrane proteins. *Journal of the American Chemical Society*, 129(26):8320–8327, 2007.

[28] C. Fernández, C. Hilty, G. Wider, P. Güntert, and K. Wüthrich. NMR structure of the integral membrane protein OmpX. *Journal of Molecular Biology*, 336:1211–1221, 2004.

[29] Joachim Vogt and Georg E Schulz. The structure of the outer membrane protein OmpX from *Escherichia coli* reveals possible mechanisms of virulence. *Structure*, 7(10):1301–1309, 1999.

[30] H. Hong, D. R. Patel, L. K. Tamm, and B. van den Berg. The outer membrane protein OmpW forms an eight-stranded β-barrel with a hydrophobic channel. *Journal of Biological Chemistry*, 281:7568–77, 2006.

[31] Hiroshi Nikaido. Molecular basis of bacterial outer membrane permeability revisited. *Microbiology and Molecular Biology Reviews*, 67(4):593–656, 2003.

[32] Özkan Yildiz, Kutti R. Vinothkumar, Panchali Goswami, and Werner Kühlbrandt. Structure of the monomeric outer-membrane porin OmpG in the open and closed conformation. *EMBO Journal*, 25(15):3702–3713, 2006.

[33] Andrew D. Ferguson, Eckhard Hofmann, James W. Coulton, Kay Diederichs, and Wolfram Welte. Siderophore-mediated iron transport: Crystal structure of FhuA

with bound lipopolysaccharide. *Science*, 282(5397):2215–2220, 1998.

[34] M. R. Yen, C. R. Peabody, S. M. Partovi, Y. Zhai, Y. H. Tseng, and M. H. Saier. Protein-translocating outer membrane porins of Gram-negative bacteria. *Biochimica et Biophysica Acta*, 1562:6–31, 2002.

[35] Jack C. Leo, Iwan Grin, and Dirk Linke. Type V secretion: mechanism(s) of autotransport through the bacterial outer membrane. *Philosophical Transactions of the Royal Society of London. Series B, Biological Sciences*, 367(1592):1088–1101, 2012.

[36] I. R. Henderson, F. Navarro-Garcia, M. Desvaux, R. C. Fernandez, and D. Ala'Aldeen. Type V protein secretion pathway: the autotransporter story. *Microbiology and Molecular Biology Reviews*, 68:692–744, 2004.

[37] Denisse L. Leyton, Amanda E. Rossiter, and Ian R. Henderson. From self sufficiency to dependence: mechanisms and factors important for autotransporter biogenesis. *Nature Reviews. Microbiology*, 10(3):213–225, 2012.

[38] C. J. Oomen, P. van Ulsen, P. Van Gelder, M. Feijen, J. Tommassen, and P. Gros. Structure of the translocator domain of a bacterial autotransporter. *EMBO Journal*, 23:1257–1266, 2004.

[39] T. J. Barnard, N. Dautin, P. Lukacik, H. D. Bernstein, and S. K. Buchanan. Autotransporter structure reveals intra-barrel cleavage followed by conformational changes. *Nature Structural and Molecular Biology*, 14:1214–1220, 2007.

[40] Nami Tajima, Fumihiro Kawai, Sam-Yong Park, and Jeremy R. H. Tame. A novel intein-like autoproteolytic mechanism in autotransporter proteins. *Journal of Molecular Biology*, 402(4):645–656, 2010.

[41] G. Y. Meng, N. K. Surana, J. W. St Geme III, and G. Waksman. Structure of the outer membrane translocator domain of the *Haemophilus influenzae* Hia trimeric autotransporter. *EMBO Journal*, 25:2297–2304, 2006.

[42] B. van den Berg. Crystal structure of a full-length autotransporter. *Journal of Molecular Biology*, 396:627–633, 2010.

[43] Travis J. Barnard, James Gumbart, Janine H. Peterson, Nicholas Noinaj, Nicole C. Easley, Nathalie Dautin, Adam J. Kuszak, Emad Tajkhorshid, Harris D. Bernstein, and Susan K. Buchanan. Molecular basis for the activation of a catalytic asparagine residue in a self-cleaving bacterial autotransporter. *Journal of Molecular Biology*, 415(1):128–142, 2012.

[44] M. Kostakioti and C. Stathopoulos. Role of the α-helical linker of the C-terminal translocator in the biogenesis of the serine protease subfamily of autotransporters. *Infection and Immunity*, 74:4961–9, 2006.

[45] Shekeb Khan, Hira S. Mian, Linda E. Sandercock, Nickolay Y. Chirgadze, and Emil F. Pai. Crystal structure of the passenger domain of the *Escherichia coli* autotransporter EspP. *Journal of Molecular Biology*, 413(5):985–1000, 2011.

[46] Kaoru Nishimura, Nami Tajima, Young-Ho Yoon, Sam-Yong Park, and Jeremy

R. H. Tame. Autotransporter passenger proteins: virulence factors with common structural themes. *Journal of Molecular Medicine*, 88(5):451–458, 2010.

[47] J. Domingo Meza-Aguilar, Petra Fromme, Alfredo Torres-Larios, Guillermo Mendoza-Hernández, Ulises Hernandez-Chiñas, Roberto A. Arreguin-Espinosa de los Monteros, Carlos A. Eslava Campos, and Raimund Fromme. X-ray crystal structure of the passenger domain of plasmid encoded toxin (Pet), an autotransporter enterotoxin from enteroaggregative *Escherichia coli* (EAEC). *Biochemical and Biophysical Research Communications*, 445(2):439–444, 2014.

[48] Paul Emsley, Ian G. Charles, Neil F. Fairweather, and Neil W. Isaacs. Structure of *Bordetella pertussis* virulence factor P.69 pertactin. *Nature*, 381(6577):90–92, 1996.

[49] Kelly A. Gangwer, Darren J. Mushrush, Devin L. Stauff, Ben Spiller, Mark S. McClain, Timothy L. Cover, and D. Borden Lacy. Crystal structure of the *Helicobacter pylori* vacuolating toxin p55 domain. *Proceedings of the National Academy of Sciences of the United States of America*, 104(41):16293–16298, 2007.

[50] Guoyu Meng, Nicole Spahich, Roma Kenjale, Gabriel Waksman, and Joseph W. St Geme Iii. Crystal structure of the *Haemophilus influenzae* Hap adhesin reveals an intercellular oligomerization mechanism for bacterial aggregation. *EMBO Journal*, 30(18):3864–3874, 2011.

[51] Troy A. Johnson, Jiazhou Qiu, Andrew G. Plaut, and Todd Holyoak. Active-site gating regulates substrate selectivity in a chymotrypsin-like serine protease: The struc-

ture of *Haemophilus influenzae* immunoglobulin A1 protease. *Journal of Molecular Biology*, 389(3):559–574, 2009.

[52] Ben R. Otto, Robert Sijbrandi, Joen Luirink, Bauke Oudega, Jonathan G. Heddle, Kenji Mizutani, Sam-Yong Park, and Jeremy R. H. Tame. Crystal structure of hemoglobin protease, a heme binding autotransporter protein from pathogenic *Escherichia coli*. *Journal of Biological Chemistry*, 280(17):17339–17345, 2005.

[53] Ramanujan S. Hegde and Harris D. Bernstein. The surprising complexity of signal sequences. *Trends in Biochemical Sciences*, 31(10):563–571, 2006.

[54] F. Ruiz-Perez, I. R. Henderson, D. L. Leyton, A. E. Rossiter, Y. Zhang, and J. P. Nataro. Roles of periplasmic chaperone proteins in the biogenesis of serine protease autotransporters of *Enterobacteriaceae*. *Journal of Bacteriology*, 191(21):6571–6583, 2009.

[55] W. S. Jong, C. M. ten Hagen-Jongman, T. den Blaauwen, D. J. Slotboom, J. R. Tame, D. Wickström, J. W. de Gier, B. R. Otto, and J. Luirink. Limited tolerance towards folded elements during secretion of the autotransporter Hbp. *Molecular Microbiology*, 63:1524–1536, 2007.

[56] Esteban Veiga, Vctor De Lorenzo, and Luis Angel Fernández. Structural tolerance of bacterial autotransporters for folded passenger protein domains. *Molecular Microbiology*, 52(4):1069–1080, 2004.

[57] F. Jacob-Dubuisson, R. Fernandez, and L. Coutte. Protein secretion through auto-

transporter and two-partner pathways. *Biochimica et Biophysica Acta, Molecular Cell Research*, 1694:235–257, 2004.

[58] T. J. Wells, J. J. Tree, G. C. Ulett, and M. A. Schembri. Autotransporter proteins: novel targets at the bacterial cell surface. *FEMS Microbiology Letters*, 274:163–172, 2007.

[59] D. G. Thanassi, C. Stathopoulos, A. Karkal, and H. L. Li. Protein secretion in the absence of ATP: the autotransporter, two-partner secretion and chaperone/usher pathways of Gram-negative bacteria (Review). *Molecular Membrane Biology*, 22:63–72, 2005.

[60] A. Saurí, Z. Soprova, D. Wickström, J. W. de Gier, R. C. Van der Schors, A. B. Smit, W. S. Jong, and J. Luirink. The Bam (Omp85) complex is involved in secretion of the autotransporter haemoglobin protease. *Microbiology*, 155:3982–3991, 2009.

[61] Fabian Gruss, Franziska Zähringer, Roman P. Jakob, Björn M. Burmann, Sebastian Hiller, and Timm Maier. The structural basis of autotransporter translocation by TamA. *Nature Structural and Molecular Biology*, 20(11):1318–1320, 2013.

[62] Ana Saurí, Corinne M. ten Hagen-Jongman, Peter van Ulsen, and Joen Luirink. Estimating the size of the active translocation pore of an autotransporter. *Journal of Molecular Biology*, 416(3):335–345, 2012.

[63] Harris D. Bernstein. Are bacterial 'autotransporters' really transporters? *Trends in Microbiology*, 15(10):441–447, 2007.

[64] J. H. Peterson, P. Tian, R. Ieva, N. Dautin, and H. D. Bernstein. Secretion of a bacterial virulence factor is driven by the folding of a C-terminal segment. *Proceedings of the National Academy of Sciences of the United States of America*, 107:17739–17744, 2010.

[65] T. Klauser, J. Pohlner, and T. F. Meyer. Selective extracellular release of cholera toxin B subunit by escherichia coli: Dissection of *Neisseria* Iga_{β}-mediated outer membrane transport. *EMBO Journal*, 11:2327–2335, 1992.

[66] Mirco Junker, Richard N. Besingi, and Patricia L. Clark. Vectorial transport and folding of an autotransporter virulence protein during outer membrane secretion. *Molecular Microbiology*, 71(5):1323–1332, 2009.

[67] Wanyoike Kang'ethe and Harris D. Bernstein. Stepwise folding of an autotransporter passenger domain is not essential for its secretion. *Journal of Biological Chemistry*, 288(49):35028–35038, 2013.

[68] A. Pautsch, J. Vogt, K. Model, C. Siebold, and G. E. Schulz. Strategy for membrane protein crystallization exemplified with OmpA and OmpX. *Proteins: Structure, Function, and Bioinformatics*, 34(2):167–172, 1999.

[69] H. Tafer, S. Hiller, C. Hilty, C. Fernandez, and K. Wüthrich. Nonrandom structure in the urea-unfolded escherichia coli outer membrane protein X (OmpX). *Biochemistry*, 43:860–869, 2004.

[70] S. Hiller, G. Wider, L. L. Imbach, and K. Wüthrich. Interactions with hydropho-

bic clusters in the urea-unfolded membrane protein OmpX. *Angewandte Chemie. International Edition in English*, 47:977–81, 2008.

[71] L. K. Tamm, A. Arora, and J. H. Kleinschmidt. Structure and assembly of β-barrel membrane proteins. *Journal of Biological Chemistry*, 276:32399–32402, 2001.

[72] L. K. Tamm, H. Hong, and B. Liang. Folding and assembly of β-barrel membrane proteins. *Biochimica et Biophysica Acta*, 1666:250–63, 2004.

[73] J. H. Kleinschmidt and L. K. Tamm. Time-resolved distance determination by tryptophan fluorescence quenching: probing intermediates in membrane protein folding. *Biochemistry*, 38(16):4996–5005, 1999.

[74] J. H. Kleinschmidt, T. den Blaauwen, A. J. Driessen, and L. K. Tamm. Outer membrane protein A of *Escherichia coli* inserts and folds into lipid bilayers by a concerted mechanism. *Biochemistry*, 38(16):5006–5016, 1999.

[75] J. H. Kleinschmidt and L. K. Tamm. Folding intermediates of a β-barrel membrane protein. Kinetic evidence for a multi-step membrane insertion mechanism. *Biochemistry*, 35:12993–13000, 1996.

[76] J. G. Sklar, T. Wu, D. Kahne, and T. J. Silhavy. Defining the roles of the periplasmic chaperones SurA, Skp, and DegP in *Escherichia coli*. *Genes and Development*, 21(19):2473–2484, 2007.

[77] Elena B. Volokhina, Jan Grijpstra, Michiel Stork, Ingrid Schilders, Jan Tommassen,

and Martine P. Bos. Role of the periplasmic chaperones Skp, SurA, and DegQ in outer membrane protein biogenesis in *Neisseria meningitidis*. *Journal of Bacteriology*, 193(7):1612–1621, 2011.

[78] Joel Selkrig, Khedidja Mosbahi, Chaille T. Webb, Matthew J. Belousoff, Andrew J. Perry, Timothy J. Wells, Faye Morris, Denisse L. Leyton, Makrina Totsika, Minh-Duy Phan, Nermin Celik, Michelle Kelly, Clare Oates, Elizabeth L. Hartland, Roy M. Robins-Browne, Sri Harsha Ramarathinam, Anthony W. Purcell, Mark A. Schembri, Richard A. Strugnell, Ian R. Henderson, Daniel Walker, and Trevor Lithgow. Discovery of an archetypal protein transport system in bacterial outer membranes. *Nature Structural and Molecular Biology*, 19(5):506–510, 2012.

[79] Christine L. Hagan, Thomas J. Silhavy, and Daniel Kahne. β-barrel membrane protein assembly by the Bam complex. *Annual Review of Biochemistry*, 80(1):189–210, 2011.

[80] Raffaele Ieva, Pu Tian, Janine H. Peterson, and Harris D. Bernstein. Sequential and spatially restricted interactions of assembly factors with an autotransporter β domain. *Proceedings of the National Academy of Sciences of the United States of America*, 108(31):E383–E391, 2011.

[81] Christine L. Hagan, Seokhee Kim, and Daniel Kahne. Reconstitution of outer membrane protein assembly from purified components. *Science*, 328(5980):890–892, 2010.

[82] Nicholas Noinaj, Adam J. Kuszak, James C. Gumbart, Petra Lukacik, Hoshing

Chang, Nicole C. Easley, Trevor Lithgow, and Susan K. Buchanan. Structural insight into the biogenesis of β-barrel membrane proteins. *Nature*, 501(7467):385–390, 2013.

[83] Nathan W. Rigel, Dante P. Ricci, and Thomas J. Silhavy. Conformation-specific labeling of BamA and suppressor analysis suggest a cyclic mechanism for β-barrel assembly in *Escherichia coli*. *Proceedings of the National Academy of Sciences of the United States of America*, 110(13):5151–5156, 2013.

[84] A. Arora, F. Abildgaard, J. H. Bushweller, and L. K. Tamm. Structure of outer membrane protein a transmembrane domain by NMR spectroscopy. *Nature Structural Biology*, 8(4):334–338, 2001.

[85] Peter M. Hwang, Wing-Yiu Choy, Eileen I. Lo, Lu Chen, Julie D. Forman-Kay, Christian R. H. Raetz, Gilbert G. Privé, Russell E. Bishop, and Lewis E. Kay. Solution structure and dynamics of the outer membrane enzyme PagP by NMR. *Proceedings of the National Academy of Sciences of the United States of America*, 99(21):13560–13565, 2002.

[86] S. Hiller, R.G. Garces, T.J. Malia, V.Y. Orekhov, M. Colombini, and G. Wagner. Solution structure of the integral human membrane protein VDAC-1 in detergent micelles. *Science*, 321(5893):1206–1210, 2008.

[87] Yoshihito Niimura, Mahito Terabe, Takashi Gojobori, and Kin-ichiro Miura. Comparative analysis of the base biases at the gene terminal portions in seven eukaryote genomes. *Nucleic Acids Research*, 31(17):5195–5201, 2003.

[88] Jiangping Bai, Douglas J. Swartz, Irina I. Protasevich, Christie G. Brouillette, Patina M. Harrell, Ellen Hildebrandt, Brigitte Gasser, Diethard Mattanovich, Andrew Ward, Geoffrey Chang, and Ina L. Urbatsch. A gene optimization strategy that enhances production of fully functional P-glycoprotein in *Pichia pastoris*. *PLoS ONE*, 6(8):e22577, 2011.

[89] Sang Ho Park, Bibhuti B. Das, Fabio Casagrande, Ye Tian, Henry J. Nothnagel, Mignon Chu, Hans Kiefer, Klaus Maier, Anna A. De Angelis, Francesca M. Marassi, and Stanley J. Opella. Structure of the chemokine receptor CXCR1 in phospholipid bilayers. *Nature*, 491(7426):779–783, 2012.

[90] W.D. Van Horn, H.-J. Kim, C.D. Ellis, A. Hadziselimovic, E.S. Sulistijo, M.D. Karra, C. Tian, F.D. Sönnichsen, and C.R. Sanders. Solution nuclear magnetic resonance structure of membrane-integral diacylglycerol kinase. *Science*, 324(5935):1726–1729, 2009.

[91] A. Gautier, H.R. Mott, M.J. Bostock, J.P. Kirkpatrick, and D. Nietlispach. Structure determination of the seven-helix transmembrane receptor sensory rhodopsin II by solution NMR spectroscopy. *Nature Structural and Molecular Biology*, 17(6):768–774, 2010.

[92] T. P. Roosild. NMR structure of Mistic, a membrane-integrating protein for membrane protein expression. *Science*, 307(5713):1317–1321, 2005.

[93] Yunpeng Zhou, Tomasz Cierpicki, Ricardo H. Flores Jimenez, Stephen M. Lukasik, Jeffrey F. Ellena, David S. Cafiso, Hiroshi Kadokura, Jon Beckwith, and John H.

Bushweller. NMR solution structure of the integral membrane enzyme DsbB: functional insights into DsbB-catalyzed disulfide bond formation. *Molecular Cell*, 31(6):896–908, 2008.

[94] S. Reckel, D. Gottstein, J. Stehle, F. Löhr, M.-K. Verhoefen, M. Takeda, R. Silvers, M. Kainosho, C. Glaubitz, J. Wachtveitl, F. Bernhard, H. Schwalbe, P. Güntert, and V. Dötsch. Solution NMR structure of proteorhodopsin. *Angewandte Chemie. International Edition in English*, 50(50):11942–11946, 2011.

[95] Innokentiy Maslennikov, Christian Klammt, Eunha Hwang, Georgia Kefala, Mizuki Okamura, Luis Esquivies, Karsten Mörs, Clemens Glaubitz, Witek Kwiatkowski, Young Ho Jeon, Senyon Choe, and Robert M. Stroud. Membrane domain structures of three classes of histidine kinase receptors by cell-free expression and rapid NMR analysis. *Proceedings of the National Academy of Sciences of the United States of America*, 107(24):10902–10907, 2010.

[96] N.K. Goto, K.H. Gardner, G.A. Mueller, R.C. Willis, and L.E. Kay. A robust and cost-effective method for the production of Val, Leu, Ile (δ1) methyl-protonated ^{15}N, ^{13}C, ^{2}H labeled proteins. *Journal of Biomolecular NMR*, 13(4):369–374, 1999.

[97] Kevin H. Gardner and Lewis E. Kay. The use of ^{2}H, ^{13}C, ^{15}N multidimensional NMR to study the structure and dynamics of proteins. *Annual Review of Biophysics and Biomolecular Structure*, 27(1):357–406, 1998.

[98] Manfred Schwaiger, Mario Lebendiker, Hagit Yerushalmi, Murray Coles, Adriane Gröger, Christian Schwarz, Shimon Schuldiner, and Horst Kessler. NMR investi-

gation of the multidrug transporter EmrE, an integral membrane protein. *European Journal of Biochemistry*, 254(3):610–619, 1998.

[99] Vinit K. Rastogi and Mark E. Girvin. Structural changes linked to proton translocation by subunit c of the ATP synthase. *Nature*, 402(6759):263–268, 1999.

[100] Alexander M. Klibanov. Why are enzymes less active in organic solvents than in water? *Trends in Biotechnology*, 15(3):97–101, 1997.

[101] A. Dong, J. D. Meyer, B. S. Kendrick, M. C. Manning, and J. F. Carpenter. Effect of secondary structure on the activity of enzymes suspended in organic solvents. *Archives of Biochemistry and Biophysics*, 334(2):406–414, 1996.

[102] Lu Yang, Jonathan S. Dordick, and Shekhar Garde. Hydration of enzyme in non-aqueous media is consistent with solvent dependence of its activity. *Biophysical Journal*, 87(2):812–821, 2004.

[103] J. H. Kleinschmidt, M. C. Wiener, and L. K. Tamm. Outer membrane protein A of *E. coli* folds into detergent micelles, but not in the presence of monomeric detergent. *Protein Science*, 8(10):2065–2071, 1999.

[104] Yu Wang and Nico Tjandra. Structural insights of tBid, the caspase-8-activated bid, and its BH3 domain. *Journal of Biological Chemistry*, 288(50):35840–35851, 2013.

[105] Tanxing Cui, David Mowrey, Vasyl Bondarenko, Tommy Tillman, Dejian Ma, Eliz-

abeth Landrum, Jose Manuel Perez-Aguilar, Jing He, Wei Wang, Jeffery G. Saven, Roderic G. Eckenhoff, Pei Tang, and Yan Xu. NMR structure and dynamics of a designed water-soluble transmembrane domain of nicotinic acetylcholine receptor. *Biochimica et Biophysica Acta, Biomembranes*, 1818(3):617–626, 2012.

[106] Alexey Neumoin, Leah S. Cohen, Boris Arshava, Subramanyam Tantry, Jeffrey M. Becker, Oliver Zerbe, and Fred Naider. Structure of a double transmembrane fragment of a G-protein-coupled receptor in micelles. *Biophysical Journal*, 96(8):3187–3196, 2009.

[107] K. Pervushin, R. Riek, G. Wider, and K. Wüthrich. Attenuated T2 relaxation by mutual cancellation of dipole-dipole coupling and chemical shift anisotropy indicates an avenue to NMR structures of very large biological macromolecules in solution. *Proceedings of the National Academy of Sciences of the United States of America*, 94(23):12366–12371, 1997.

[108] Konstantin Pervushin, Roland Riek, Gerhard Wider, and Kurt Wüthrich. Transverse relaxation-optimized spectroscopy (TROSY) for NMR studies of aromatic spin systems in ^{13}C-labeled proteins. *Journal of the American Chemical Society*, 120(25):63946400, 1998.

[109] Kevin H. Gardner, Xiaochen Zhang, Kalle Gehring, and Lewis E. Kay. Solution NMR studies of a 42 KDa *Escherichia Coli* maltose binding protein/β-cyclodextrin complex: Chemical shift assignments and analysis. *Journal of the American Chemical Society*, 120(45):11738–11748, 1998.

[110] C. Hilty, C. Fernández, G. Wider, and K. Wüthrich. Side chain NMR assignments in the membrane protein OmpX reconstituted in DHPC micelles. *Journal of Biomolecular NMR*, 23:289–301, 2002.

[111] Daniel Gottstein, Sina Reckel, Volker Dötsch, and Peter Güntert. Requirements on paramagnetic relaxation enhancement data for membrane protein structure determination by NMR. *Structure*, 20(6):1019–1027, 2012.

[112] J. L. Battiste and G. Wagner. Utilization of site-directed spin labeling and high-resolution heteronuclear nuclear magnetic resonance for global fold determination of large proteins with limited nuclear Overhauser effect data. *Biochemistry*, 39(18):5355–5365, 2000.

[113] I. Solomon. Relaxation processes in a system of two spins. *Physical Review*, 99(2):559–565, 1955.

[114] Ad Bax and Nico Tjandra. High-resolution heteronuclear NMR of human ubiquitin in an aqueous liquid crystalline medium. *Journal of Biomolecular NMR*, 10(3):289–292, 1997.

[115] Tomasz Cierpicki and John H. Bushweller. Charged gels as orienting media for measurement of residual dipolar couplings in soluble and integral membrane proteins. *Journal of the American Chemical Society*, 126(49):16259–16266, 2004.

[116] G. Marius Clore, Mary R. Starich, and Angela M. Gronenborn. Measurement of residual dipolar couplings of macromolecules aligned in the nematic phase of a col-

loidal suspension of rod-shaped viruses. *Journal of the American Chemical Society*, 120(40):10571–10572, 1998.

[117] Donghan Lee, Korvin F. A. Walter, Ann-Kathrin Brückner, Christian Hilty, Stefan Becker, and Christian Griesinger. Bilayer in small bicelles revealed by lipid-protein interactions using NMR spectroscopy. *Journal of the American Chemical Society*, 130(42):13822–13823, 2008.

[118] C. Fernández, C. Hilty, G. Wider, and K. Wüthrich. Lipid-protein interactions in DHPC micelles containing the integral membrane protein OmpX investigated by NMR spectroscopy. *Proceedings of the National Academy of Sciences of the United States of America*, 99:13533–13537, 2002.

[119] W. Braun, G. Wider, K. H. Lee, and K. Wüthrich. Conformation of glucagon in a lipid-water interphase by ^{1}H nuclear magnetic resonance. *Journal of Molecular Biology*, 169(4):921–948, 1983.

[120] Christian Hilty, Gerhard Wider, César Fernández, and Kurt Wüthrich. Membrane protein-lipid interactions in mixed micelles studied by NMR spectroscopy with the use of paramagnetic reagents. *ChemBioChem*, 5(4):467–473, 2004.

[121] Anirban Bhunia, Prerna N. Domadia, and Surajit Bhattacharjya. Structural and thermodynamic analyses of the interaction between melittin and lipopolysaccharide. *Biochimica et Biophysica Acta, Biomembranes*, 1768(12):3282–3291, 2007.

[122] Anirban Bhunia, Ayyalusamy Ramamoorthy, and Surajit Bhattacharjya. Helical

hairpin structure of a potent antimicrobial peptide MSI-594 in lipopolysaccharide micelles by NMR spectroscopy. *Chemistry–A European Journal*, 15(9):2036–2040, 2009.

[123] Min-Duk Seo, Hyung-Sik Won, Ji-Hun Kim, Tsogbadrakh Mishig-Ochir, and Bong-Jin Lee. Antimicrobial peptides for therapeutic applications: a review. *Molecules*, 17(10):12276–12286, 2012.

[124] Mohammad Rahnamaeian. Antimicrobial peptides. *Plant Signaling and Behavior*, 6(9):1325–1332, 2011.

[125] Yechiel Shai. Mechanism of the binding, insertion and destabilization of phospholipid bilayer membranes by α-helical antimicrobial and cell non-selective membrane-lytic peptides. *Biochimica et Biophysica Acta, Biomembranes*, 1462(12):55–70, 1999.

[126] Katsumi Matsuzaki. Why and how are peptide-lipid interactions utilized for self-defense? Magainins and tachyplesins as archetypes. *Biochimica et Biophysica Acta, Biomembranes*, 1462(12):1–10, 1999.

[127] Gerald Ehrenstein and Harold Lecar. Electrically gated ionic channels in lipid bilayers. *Quarterly Reviews of Biophysics*, 10(01):1–34, 1977.

[128] Vitor Teixeira, Maria J. Feio, and Margarida Bastos. Role of lipids in the interaction of antimicrobial peptides with membranes. *Progress in Lipid Research*, 51(2):149–177, 2012.

[129] Y. Pouny, D. Rapaport, A. Mor, P. Nicolas, and Y. Shai. Interaction of antimicrobial dermaseptin and its fluorescently labeled analogues with phospholipid membranes. *Biochemistry*, 31(49):12416–12423, 1992.

[130] Paulo F. Almeida. Membrane-active peptides: Binding, translocation, and flux in lipid vesicles. *Biochimica et Biophysica Acta, Biomembranes*, 1838(9):2216–2227, September 2014.

[131] Evgenia Glukhov, Margareta Stark, Lori L. Burrows, and Charles M. Deber. Basis for selectivity of cationic antimicrobial peptides for bacterial versus mammalian membranes. *Journal of Biological Chemistry*, 280(40):33960–33967, 2005.

[132] Roberto Bessalle, Aviva Kapitkovsky, Alfred Gorea, Itamar Shalit, and Mati Fridkin. All-D-Magainin: chirality, antimicrobial activity and proteolytic resistance. *FEBS Letters*, 274(12):151–155, 1990.

[133] A. J Verkleij, R. F. A Zwaal, B Roelofsen, P Comfurius, D Kastelijn, and L. L. M van Deenen. The asymmetric distribution of phospholipids in the human red cell membrane. A combined study using phospholipases and freeze-etch electron microscopy. *Biochimica et Biophysica Acta, Biomembranes*, 323(2):178–193, 1973.

[134] Colin Ratledge. Microbial lipids. In *Biotechnology Set*, chapter 4, pages 133–197. Wiley-VCH Verlag GmbH, 2001.

[135] Sven Morein, Ann-Sofie Andersson, Leif Rilfors, and Göran Lindblom. Wild-type *Escherichia coli* cells regulate the membrane lipid composition in a win-

dow between gel and non-lamellar structures. *Journal of Biological Chemistry*, 271(12):6801–6809, 1996.

[136] Judith M. White, Sue E. Delos, Matthew Brecher, and Kathryn Schornberg. Structures and mechanisms of viral membrane fusion proteins: Multiple variations on a common theme. *Critical Reviews in Biochemistry and Molecular Biology*, 43(3):189–219, 2008.

[137] Richard M. Epand. Fusion peptides and the mechanism of viral fusion. *Biochimica et Biophysica Acta, Biomembranes*, 1614(1):116–121, 2003.

[138] P. Joanne, P. Nicolas, and C. El Amri. Antimicrobial peptides and viral fusion peptides: How different they are? *Protein and Peptide Letters*, 16(7):743–750, 2009.

[139] Beatriz Apellániz, Nerea Huarte, Eneko Largo, and José L. Nieva. The three lives of viral fusion peptides. *Chemistry and Physics of Lipids*, 181:40–55, 2014.

[140] Alex L. Lai, Heather Park, Judith M. White, and Lukas K. Tamm. Fusion peptide of influenza hemagglutinin requires a fixed angle boomerang structure for activity. *Journal of Biological Chemistry*, 281(9):5760–5770, 2006.

[141] Fernando Porcelli, Ayyalusamy Ramamoorthy, George Barany, and Gianluigi Veglia. On the role of NMR spectroscopy for characterization of antimicrobial peptides. *Methods in Molecular Biology*, 1063:159–180, 2013.

[142] Yongchao Su, Shenhui Li, and Mei Hong. Cationic membrane peptides: Atomic-level insight of structure-activity relationships from solid-state NMR. *Amino Acids*, 44(3):821–833, 2013.

[143] Lena Mäler. Solution NMR studies of cell-penetrating peptides in model membrane systems. *Advanced Drug Delivery Reviews*, 65(8):1002–1011, 2013.

[144] Jennifer Gesell, Michael Zasloff, and Stanley J. Opella. Two-dimensional ^{1}H NMR experiments show that the 23-residue Magainin antibiotic peptide is an α-helix in dodecylphosphocholine micelles, sodium dodecylsulfate micelles, and trifluoroethanol/water solution. *Journal of Biomolecular NMR*, 9(2):127–135, 1997.

[145] Periathamby Antony Raj, Emil Marcus, and Dinesh K. Sukumaran. Structure of human salivary histatin 5 in aqueous and nonaqueous solutions. *Biopolymers*, 45(1):5167, 1998.

[146] Alex L. Lai, Anna Eswara Moorthy, Yinling Li, and Lukas K. Tamm. Fusion activity of HIV gp41 fusion domain is related to its secondary structure and depth of membrane insertion in a cholesterol-dependent fashion. *Journal of Molecular Biology*, 418(12):3–15, 2012.

[147] Evelyne Schrank, Gabriel E. Wagner, and Klaus Zangger. Solution NMR studies on the orientation of membrane-bound peptides and proteins by paramagnetic probes. *Molecules*, 18(7):7407–7435, 2013.

[148] Walter Hohlweg, Simone Kosol, and Klaus Zangger. Determining the orientation

and localization of membrane-bound peptides. *Current Protein and Peptide Science*, 13(3):267–279, 2012.

[149] N. Dautin and H. D. Bernstein. Protein secretion in Gram-negative bacteria via the autotransporter pathway. *Annual Review of Microbiology*, 61:89–112, 2007.

[150] M. Kostakioti, C. L. Newman, D. G. Thanassi, and C. Stathopoulos. Mechanisms of protein export across the bacterial outer membrane. *Journal of Bacteriology*, 187:4306–4314, 2005.

[151] David C. Oliver, George Huang, and Rachel C. Fernandez. Identification of secretion determinants of the *Bordetella pertussis* BrkA autotransporter. *Journal of Bacteriology*, 185(2):489–495, 2003.

[152] E. Marin, G. Bodelon, and L. A. Fernández. A comparative analysis of the biochemical and functional properties of C-terminal domains of autotransporters. *Journal of Bacteriology*, 192(21):5588–5601, 2010.

[153] P. van Ulsen, L. van Alphen, J. ten Hove, F. Fransen, P. van der Ley, and J. Tommassen. A Neisserial autotransporter NalP modulating the processing of other autotransporters. *Molecular Microbiology*, 50:1017–30, 2003.

[154] Michael P Malakhov, Michael R Mattern, Oxana A Malakhova, Mark Drinker, Stephen D Weeks, and Tauseef R Butt. SUMO fusions and SUMO-specific protease for efficient expression and purification of proteins. *Journal of Structural and Functional Genomics*, 5(1-2):75–86, 2004.

[155] G. W. Vuister and A. Bax. Quantitative j correlation : a new approach for measuring homonuclear 3-bond J($H^N H^\alpha$) coupling constants in ^{15}N enriched proteins. *Journal of the American Chemical Society*, 115:7772–7777, 1993.

[156] T. Herrmann, P. Güntert, and K. Wüthrich. Protein NMR structure determination with automated NOE assignment using the new software CANDID and the torsion angle dynamics algorithm DYANA. *Journal of Molecular Biology*, 319:209–227, 2002.

[157] P. Güntert, C. Mumenthaler, and K. Wüthrich. Torsion angle dynamics for NMR structure calculation with the new program DYANA. *Journal of Molecular Biology*, 273:283–298, 1997.

[158] LLC Schrödinger. The PyMOL molecular graphics system, version 1.3r1. 2010.

[159] J. Martin Scholtz, Hong Qian, Eunice J. York, John M. Stewart, and Robert L. Baldwin. Parameters of helix-coil transition theory for alanine-based peptides of varying chain lengths in water. *Biopolymers*, 31(13):1463–1470, 1991.

[160] Yee-Hsiung Chen, Jen Tsi Yang, and Kue Hung Chau. Determination of the helix and β form of proteins in aqueous solution by circular dichroism. *Biochemistry*, 13(16):3350–3359, 1974.

[161] P. Luginbühl, T. Szyperski, and K. Wüthrich. Statistical basis for the use of $^{13}C^\alpha$ chemical-shifts in protein-structure determination. *Journal of Magnetic Resonance. Series B*, 109:229–233, 1995.

[162] S. Spera and A. Bax. Empirical correlation between protein backbone conformation and Cα and Cβ ^{13}C nuclear magnetic resonance chemical shifts. *Journal of the American Chemical Society*, 113:5490–5492, 1991.

[163] D. S. Wishart, B. D. Sykes, and F. M. Richards. The chemical shift index: a fast and simple method for the assignment of protein secondary structure through NMR spectroscopy. *Biochemistry*, 31(6):1647–1651, 1992.

[164] Antonio Demarco, Miguel Llinas, and Kurt Wüthrich. Analysis of the ^{1}H-NMR spectra of ferrichrome peptides. I. The non-amide protons. *Biopolymers*, 17(3):617–636, 1978.

[165] Andy C. Wang and Ad Bax. Reparametrization of the karplus relation for ^{3}J(H$^{\alpha}$-N) and ^{3}J(H^{N}-C$'$) in peptides from uniformly ^{13}C/^{15}N-enriched human ubiquitin. *Journal of the American Chemical Society*, 117(6):1810–1813, 1995.

[166] Lindsay M. McMorran, Alice I. Bartlett, Gerard H. M. Huysmans, Sheena E. Radford, and David J. Brockwell. Dissecting the effects of periplasmic chaperones on the in vitro folding of the outer membrane protein PagP. *Journal of Molecular Biology*, 425(17):3178–3191, 2013.

[167] Jorge J. Velarde and James P. Nataro. Hydrophobic residues of the autotransporter EspP linker domain are important for outer membrane translocation of its passenger. *Journal of Biological Chemistry*, 279(30):31495–31504, 2004.

[168] Charles R. Cantor and Paul R. Schimmel. *Techniques for the Study of Biological*

Structure and Function, volume 2 of *Biophysical chemistry*. W. H. Freeman, San Francisco, 1980.

[169] Danilo Roccatano, Giorgio Colombo, Marco Fioroni, and Alan E. Mark. Mechanism by which 2,2,2-trifluoroethanol/water mixtures stabilize secondary-structure formation in peptides: A molecular dynamics study. *Proceedings of the National Academy of Sciences of the United States of America*, 99(19):12179–12184, 2002.

[170] B. H. Zimm and J. K. Bragg. Theory of the phase transition between helix and random coil in polypeptide chains. *Journal of Chemical Physics*, 31(2):526–535, 1959.

[171] Shneior Lifson and A. Roig. On the theory of helix-coil transition in polypeptides. *Journal of Chemical Physics*, 34(6):1963–1974, 1961.

[172] Tomasz Cierpicki and Jacek Otlewski. Amide proton temperature coefficients as hydrogen bond indicators in proteins. *Journal of Biomolecular NMR*, 21(3):249–261, 2001.

[173] Soyoun Hwang and Christian Hilty. Folding of a tryptophan zipper peptide investigated on the basis of the nuclear Overhauser effect and thermal denaturation. *Journal of Physical Chemistry B*, 115(51):15355–15361, 2011.

[174] Rochus Keller. *The Computer Aided Resonance Assignment Tutorial*. CANTINA Verlag, 2004.

[175] S. Rothemund, H. Weisshoff, M. Beyermann, E. Krause, M. Bienert, C. Mügge, B. D. Sykes, and F. D. Sönnichsen. Temperature coefficients of amide proton NMR resonance frequencies in trifluoroethanol: a monitor of intramolecular hydrogen bonds in helical peptides. *Journal of Biomolecular NMR*, 8(1):93–97, 1996.

[176] N. J. Baxter and M. P. Williamson. Temperature dependence of ^{1}H chemical shifts in proteins. *Journal of Biomolecular NMR*, 9(4):359–369, 1997.

[177] Frans A. A. Mulder, Dick Schipper, Richard Bott, and Rolf Boelens. Altered flexibility in the substrate-binding site of related native and engineered high-alkaline *Bacillus* subtilisins. *Journal of Molecular Biology*, 292(1):111–123, 1999.

[178] Johan Evenäs, Vitali Tugarinov, Nikolai R Skrynnikov, Natalie K Goto, Ranjith Muhandiram, and Lewis E Kay. Ligand-induced structural changes to maltodextrin-binding protein as studied by solution NMR spectroscopy. *Journal of Molecular Biology*, 309(4):961–974, 2001.

[179] Bennett T. Farmer, Keith L. Constantine, Valentina Goldfarb, Mark S. Friedrichs, Michael Wittekind, Joseph Yanchunas, James G. Robertson, and Luciano Mueller. Localizing the $NADP^{+}$ binding site on the MurB enzyme by NMR. *Nature Structural and Molecular Biology*, 3(12):995–997, 1996.

[180] Michael Zasloff. Antimicrobial peptides of multicellular organisms. *Nature*, 415(6870):389–395, 2002.

[181] Lois M. Yin, Michelle A. Edwards, Jessica Li, Christopher M. Yip, and Charles M.

Deber. Roles of hydrophobicity and charge distribution of cationic antimicrobial peptides in peptide-membrane interactions. *Journal of Biological Chemistry*, 287(10):7738–7745, 2012.

[182] Ziqing Jiang, Adriana I. Vasil, John D. Hale, Robert E. W. Hancock, Michael L. Vasil, and Robert S. Hodges. Effects of net charge and the number of positively charged residues on the biological activity of amphipathic α-helical cationic antimicrobial peptides. *Peptide Science*, 90(3):369–383, 2008.

[183] Fabiana A. Carneiro, Guy Vandenbussche, Maria A. Juliano, Luiz Juliano, Jean-Marie Ruysschaert, and Andrea T. Da Poian. Charged residues are involved in membrane fusion mediated by a hydrophilic peptide located in vesicular stomatitis virus G protein. *Molecular Membrane Biology*, 23(5):396–406, 2006.

[184] R. A. Cruciani, J. L. Barker, S. R. Durell, G. Raghunathan, H. R. Guy, M. Zasloff, and E. F. Stanley. Magainin 2, a natural antibiotic from frog skin, forms ion channels in lipid bilayer membranes. *European Journal of Pharmacology*, 226(4):287–296, 1992.

[185] B. Bechinger, M. Zasloff, and S. J. Opella. Structure and orientation of the antibiotic peptide Magainin in membranes by solid-state nuclear magnetic resonance spectroscopy. *Protein Science*, 2(12):2077–2084, 1993.

[186] Dominik Leitz, Beat Vögeli, Jason Greenwald, and Roland Riek. Temperature dependence of $^{1}H_{N}$-$^{1}H_{N}$ distances in ubiquitin as studied by exact measurements of NOEs. *Journal of Physical Chemistry B*, 115(23):7648–7660, 2011.